REPUBLIQUE ALGERIENNE DEMOCRATIQUE EPOPULAIRE
MINISTERE DE L'ENSEIGNEMENT SUPERIEUR
ET DE LA RECHERCHE SCIENTIFIQUE
UNIVERSITÉ KASDI MERBAH OUARGLA
Faculté des sciences appliquées
Département : Génie Civil et hydraulique

Mémoire

MASTER ACADEMIQUE

Domaine : Sciences et Technologies

Filière : Hydraulique

Spécialité : Ressources en eau

Présenté Par :

KOUSKOUS Idris

DERADJI Kheireddine

Thème

HYDRAULIC TRANSIENT MODELING IN URBAN WATER DISTRIBUTION SYSTEMS : COMPARATIVE AND APPLIED STUDY

Soutenu publiquement le: 07/06/2026

Devant le jury composé de :

Dr. MECHERI Laid	**MCA**	**UKM Ouargla**	**Présidente**
Pr. KATEB Samir	**Pr**	**UKM Ouargla**	**Examinateur**
Dr. ZEGAIT Rachid	**MCA**	**UKM Ouargla**	**Encadreur**

Année Universitaire : 2025/2026

ملخص

يهدف هذا العمل إلى تأمين البنية التحتية لنقل المياه تحت الضغط من خلال تحسين التحكم في الظواهر العابرة هيدروليكياً، والتي غالباً ما تكون مدمرة للشبكات. ومن خلال الجمع بين الدقة النظرية وأدوات المحاكاة الرقمية، تقدم هذه الدراسة تحليلاً مقارناً معمقاً لبرمجيات مرجعية، مثل Bentley HAMMER و AFT Impulse، لتحديد الأساليب الأكثر فعالية. وفي النهاية، يوفر هذا العمل منهجية تشغيلية قوية تسمح بتشخيص دقيق لمخاطر الضغط الزائد والكهف (التكهف) في حالات واقعية، مع التحقق تقنياً من حلول تخفيف عملية لتعزيز ديمومة وكفاءة المنشآت الهيدروليكية.

الكلمات المفتاحية: ظواهر عابرة، مطرقة مائية ، Bentley HAMMER، AFT Impulse، حماية هيدروليكية، نمذجة رقمية

Abstract

This work aims to secure pressurized water transport infrastructure by optimizing the control of hydraulic transients, which are often destructive phenomena for networks. By articulating theoretical rigor and numerical simulation tools, the study proposes an in-depth comparative analysis of reference software, such as Bentley HAMMER and AFT Impulse, to determine the most effective approaches. Ultimately, this work offers a robust operational methodology allowing for the precise diagnosis of overpressure and cavitation risks in real-world cases, while technically validating concrete mitigation solutions to enhance the durability and efficiency of hydraulic installations.

Key words : Transient Phenomena, Water Hammer, Bentley HAMMER, AFT Impulse, Hydraulic Protection, Numerical Modeling.

Résumé

Ce travail a pour but de sécuriser les infrastructures de transport d'eau sous pression en optimisant la maîtrise des transitoires hydrauliques, phénomènes souvent destructeurs pour les réseaux. En articulant rigueur théorique et outils de simulation numérique, l'étude propose une analyse comparative approfondie des logiciels de référence, tels que Bentley HAMMER et AFT Impulse, afin de déterminer les approches les plus performantes. Finalement, ce travail offre une méthodologie opérationnelle robuste permettant de diagnostiquer avec précision les risques de surpression et de cavitation sur des cas réels, tout en validant techniquement des solutions d'atténuation concrètes pour renforcer la durabilité et l'efficacité des installations hydrauliques.

Mots Clés : Phénomènes Transitoires, Coup de bélier, Bentley HAMMER, AFT impuls, Protection hydraulique, Modélisation numérique.

Keyword Cloud

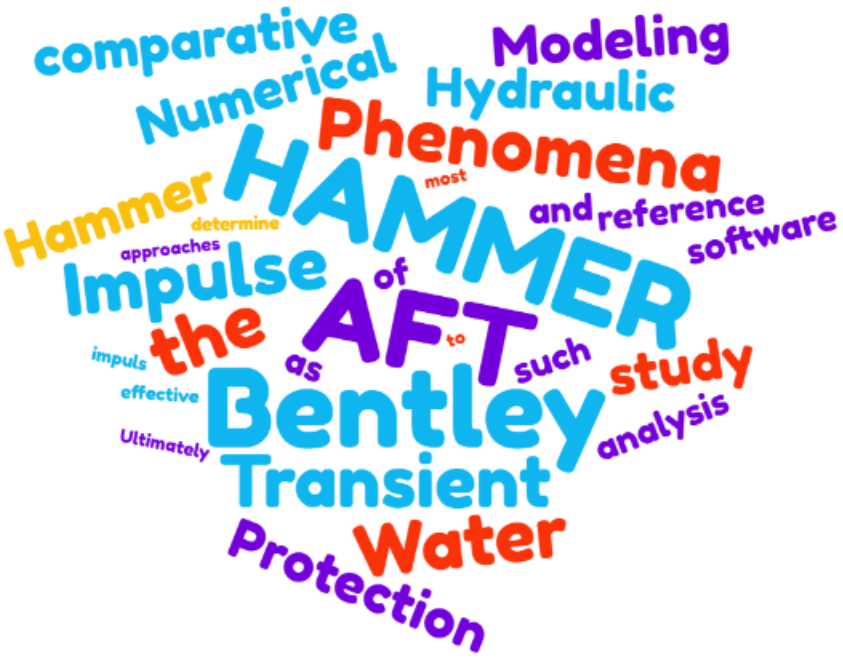

DÉDICACES

To my my beloved parents, who supported me every step of the way.

To my friends, whose presence made the hard days easier.

To my professors, especially Professor Zegait Rachid, for his valuable guidance throughout this research.

To my classmate and friend Deradji Kheireddine, who shared this journey with me.

And to everyone who contributed in any way to the completion of this work, near or far in completing this thesis.

thank you.

Kouskous Idris

DÉDICACES

To all those who have contributed to my journey...

To my dear and beloved mother, who stayed up for me and toiled for my sake — words fall short of describing her grace.

To my dear family, my unwavering support, who raised me and brought me to where I am today.

To my professors who stood by me throughout my academic journey, and especially Professor Zegait Rachid, who guided me and illuminated my path.

And finally, to my companion and brother kouskous Idris, with whom I faced this experience together, through all its hardships.

To all of you, I dedicate this humble work.

Deradji Kheireddine

Remerciement

Praise be to Allah, who granted us the strength and success to complete this work, and peace and blessings be upon our noble Prophet, peace be upon him.

We extend our sincerest gratitude and appreciation to our supervising professor, ***Zegait Rachid****, for his continuous support, valuable guidance, and patience throughout all stages of this research.*

We would also like to thank ***the members of the jury*** *for accepting to evaluate our work.*

We also thank all the professors of the Department of Water Resources and Hydraulics at Kasdi Merbah University – Ouargla, for the knowledge they shared with us throughout our academic journey.

Special thanks go to my beloved parents and my dear family, who never stopped encouraging me and stood by my side every step of the way.

I would also like to thank my classmate and friend, for his cooperation and dedication throughout all stages of completing this work.

Finally, we thank everyone who helped us in any way, near or far, with a word or a gesture your contribution did not go unnoticed.

Kouskous Idris
Deradji Kheireddine

TABLE OF CONTENTS

Abstract / Résumé ii
Dedications iv
Acknowledgements v
Keyword Cloud iii
General Introduction 1
Chapter I – Background and Literature Review 3
I.1 Background and General Context 4
I.2 Literature Review 4
I.2.1 Historical Development 4
I.2.2 Evolution of Numerical Solution Methods 6
I.2.4 Applied Studies and Notable Cases 8
I.3 Research Objectives 9
Chapter I Conclusion 9
Chapter II – Theoretical Background and Mathematical Formulation 11
II.1 Fundamentals of the Water Hammer Phenomenon 12
II.1.1 Physical Definition and Basic Terminology 12
II.1.2 Causes and Triggering Events 14
II.1.3 Mechanism of Pressure Wave Propagation 15
II.1.4 Historical Development of the Theory 18
II.2 Mathematical Derivation of the Governing Equations 20
II.2.1 The Continuity Equation 20
II.2.2 The Momentum Equation 23
II.2.3 Pressure Wave Celerity 25
II.2.4 Joukowsky's Equation and Allievi's Parameter 27
II.2.5 Steady-State as the Initial Condition 29
II.3 Numerical Solution Methods 33
II.3.1 The Method of Characteristics (MOC) 33
II.3.2 Alternative Numerical Methods 38
II.3.3 Boundary Conditions 42
II.3.4 Bergeron's Graphical Method 46
II.3.5 The Michaud Formula for Slow Closure 49
II.3.6 Optimal Valve Closure Laws 51
II.4 Water Hammer Protection Devices 53
II.4.1 Classification of Protection Measures 53
II.4.2 Pressurized Air Vessels 54
II.4.3 Surge Tanks 56
II.4.4 Supplementary Protection Measures 57
II.5 Advanced Considerations 59
II.5.1 Cavitation and Column Separation 59
II.5.2 Unsteady Friction – The Brunone–Vítkovský Model 62
II.5.3 Fluid-Structure Interaction 64
Chapter II Conclusion 57

Chapter III – Transient Simulation Software 58
III.1 Introduction 59
III.2 Overview of Transient Simulation Software 59
III.2.1 The Current Landscape and the Dominance of MOC 59
III.2.2 Software Classification and Selection Criteria 60
III.2.3 Comprehensive Comparative Table 61
III.3 Bentley HAMMER 62
III.3.1 Historical Background and Numerical Foundation 62

III.3.2 Hydraulic Modeling 64
III.3.3 Integration with Other Engineering Environments 65
III.3.4 Strengths and Limitations 66
III.3.5 Version Used 66
III.4 AFT Impulse 67
III.4.1 Historical Background and Numerical Foundation 67
III.4.2 Hydraulic Modeling – Friction, Cavitation, and Boundary Conditions 68
III.4.3 Operational Flexibility and Industrial Applications 69
III.4.4 Strengths and Limitations 70
III.4.5 Version Used 70
III.5 Structural Comparison Between the Two Programs 70
III.5.1 Similarities and Shared Assumptions 70
III.6 Justification of Selection and Transition to the Case Study 71
III.6.1 Grounds for Selecting the Two Programs 71
III.6.2 Their Application in the Case Study 71
III.7 Conclusion 71
Chapter IV – Case Study: Simulation and Analysis 72
IV.1 System Description and Model Construction 73
IV.1.1 Presentation of the Study Area 73
IV.1.2 Data and Assumptions 76
IV.1.3 Steady-State Calibration 77
IV.2 Scenarios and Simulation Setup 79
IV.2.1 Scenario One – Sudden Power Failure 79
IV.2.3 Simulation Parameters 79
IV.3 Results and Protection Device Evaluation 80
IV.3.1 Pre-Protection Results – Pressure Envelopes 80
IV.3.2 Protection Device Selection and Design 81
IV.4 Comparison 82
IV.4.1 Maximum Pressure Peaks 82
IV.4.2 Minimum Pressure and Cavitation 83
IV.4.3 Recommendations and Conclusions 83
IV.5 Supplementary Case: Closed-End Boundary Condition 84
Chapter IV Conclusion 85

Conclusions and Recommendations 91
Bibliographical References 98

LIST OF TABLES

Table No.	Title	Page
Table I.1	Major Historical Milestones in Water Hammer Theory	5
Table I.3	Key Applied Studies Referenced in the Literature Review	8
Table II.1	Fundamental Parameters and Variables – Water Hammer	21
Table II.2	The Three Pressure Regimes – Threshold and Consequence	21
Table II.4	Axial Restraint Coefficient ψ for Different Installation Conditions	19
Table II.5	Pipe Material Coefficient κ and Typical Wave Celerity Range	26
Table II.5b	Absolute Roughness ε for Common Pipe Materials	33
Table II.6	Comparative Overview of Four Numerical Methods for Water Hammer	40
Table II.7	Applicable Formula by Valve Closure Regime	49
Table II.8	Engineering Criteria for Selecting a Water Hammer Protection Device	53
Table II.9	Classification of Main Water Hammer Protection Devices	54
Table II.10	Polytropic Exponent n – Air Cushion in Hydropneumatic Vessel	55
Table II.11	Air Vessel vs. Surge Tank – Comparative Assessment	56
Table II.12	Supplementary Water Hammer Protection Devices	57
Table II.17	Comparison of Three Friction Models for Water Hammer Analysis	63
Table III.1	Survey of Commercial Transient Flow Simulation Software	60
Table III.2	Technical Specifications of Bentley HAMMER	61
Table IV-1	Actual Current Consumption of Existing Units	74
Table IV-2	Inventory of Current and Planned Consumers	74
Table 4-3	Geometric Characteristics of Segment SR2–SR3	76
Table 4-4	Simulation Results at the Node Level (SR2–SR3)	78
Table 4-5	Simulation Results at the Section Level (SR2–SR3)	78
Table V.1	Comprehensive Comparative Assessment: Bentley HAMMER vs. AFT Impulse	93 – 94

LIST OF FIGURES

Figure No.	Caption	Page
Fig. III.1	Main Interface of Bentley HAMMER	62
Fig. III.2	Pump Definition Window – Grundfos CR 95-6 Properties in Bentley HAMMER	63
Fig. III.3	Wave Speed Calculation Window in Bentley HAMMER	63
Fig. III.4	Pipe Properties Table in Bentley HAMMER – SR2–SR3 Network	64
Fig. III.5	Main Interface of AFT Impulse	67
Fig. III.6	Analysis Setup Screen – AFT Impulse	68
Fig. III.7	Solution Window – AFT Impulse	68
Fig. IV-1	Administrative Location of the Study Area	73
Fig. IV-2	Location of the Tin Sériрine Basin	74
Fig. IV-3	Hydrogeological Diagram of the Tassilis	75
Fig. IV-4	Existing Boreholes	75
Fig. IV-5	Location of Existing and Planned Boreholes (In Guezzam Region)	75
Fig. IV-6	Water Supply Mode within the Units	76
Fig. VI-6	Route Map of the Abalkan–Djebel Hadid Transmission Pipeline (SR1 to SR4)	76
Fig. IV-7	Steady-State Pressure Distribution along the SR2–SR3 Pipeline	77
Fig. IV-8	Steady-State Velocity Distribution along the SR2–SR3 Pipeline	77
Fig. IV-9	Vertical Water Transfer Diagram (SR2–SR3) – Elevation Profiles	78
Fig. IV-10	Vertical Water Transfer Diagram (SR2–SR3) – Pressure Profiles	78
Fig. IV-11	Vertical Water Transfer Diagram (SR2–SR3) – Head Profiles	78
Fig. IV-12	Hydraulic Model Diagram in Bentley HAMMER (SR2–SR3)	79
Fig. IV-13	Pressure Envelope – Scenario 1 (Sudden Power Failure) – Ductile Iron – Pre-Protection – Bentley HAMMER	80
Fig. IV-14	Pressure Envelope – Scenario 1 (Sudden Power Failure) – Ductile Iron – Pre-Protection – AFT Impulse	80
Fig. IV-15	Pressure Envelope – Scenario 1 (Sudden Power Failure) – Ductile Iron – Post-Protection – Bentley HAMMER	81
Fig. IV-16	Pressure Envelope – Scenario 1 (Sudden Power Failure) – Ductile Iron – Post-Protection – AFT Impulse	81

LIST OF NOMENCLATURE

Symbol	Definition	SI Unit
a	Pressure wave celerity	m/s
A	Cross-sectional area of the pipe	m^2
C	Pressure wave celerity (general notation)	m/s
Cd	Discharge coefficient	–
D	Internal pipe diameter	m
e	Pipe wall thickness	m
E	Young's modulus of the pipe material	GPa
f	Darcy–Weisbach friction factor	–
g	Gravitational acceleration	m/s^2
H	Piezometric head	m
H_o	Initial (steady-state) piezometric head	m
ΔH	Transient piezometric head rise or drop	m
Kf	Bulk modulus of water	GPa
L	Pipe length between two analysis nodes	m
n	Polytropic exponent (air cushion)	–
P	Pressure	Pa
Pv	Vapour pressure of water	Pa
Q	Volumetric flow rate	m^3/s
R	Hydraulic resistance coefficient	s/m^2
S	Pipe cross-sectional area	m^2
t	Time	s
Tp	Full oscillation period (Tp = 4L/a)	s
Tr	Wave travel return time (Tr = 2L/a)	s
U_o	Initial air volume in the vessel	m^3
V	Cross-sectional mean flow velocity	m/s
V_o	Initial (steady-state) flow velocity	m/s
ΔV	Sudden change in flow velocity	m/s
x	Spatial coordinate along the pipe axis	m
z	Elevation head (datum reference)	m
α	Celerity coefficient / Joukowsky factor	–
ε	Absolute wall roughness	mm
κ	Pipe material coefficient for wave celerity	–
ν	Poisson's ratio of the pipe material	–
ρ	Water density	kg/m^3
ψ	Axial restraint coefficient	–
AEP	Alimentation en Eau Potable (Drinking Water Supply)	–
AFT	Applied Flow Technology (AFT Impulse software)	–

General Introduction

General Introduction

Pressurized water transport systems serve as the backbone of modern infrastructure, whether for municipal drinking water supply (AEP), large-scale irrigation, or industrial water transfer. The efficient and safe management of these networks represents a major technical challenge, particularly due to the inherent vulnerability of hydraulic systems to transient phenomena. Among these, the "water hammer" effect remains a persistent threat, capable of generating extreme pressure variations that can lead to pipe bursts, pump failures, and irreversible structural damage.

In a context where requirements for sustainability, optimization of maintenance costs, and infrastructure safety have become paramount, traditional empirical approaches are no longer sufficient. Engineers must now rely on advanced modeling methods to anticipate these shock waves and design appropriate protection systems. This is where numerical simulation becomes essential: by accurately simulating network behavior during critical phases ;such as pump start-ups or sudden power failures ; it becomes possible to mitigate risks before they occur.

This thesis is part of this preventive engineering approach. Its objective is to explore the theoretical foundations of hydraulic transients and to evaluate current simulation tools against the requirements of real-world networks. Through a comparative analysis of the reference software packages Bentley HAMMER and AFT Impulse, we aim to assess their reliability and respective contributions to technical decision-making.

The work is structured as follows:

- **Chapter 1** establishes the theoretical foundations of the water hammer phenomenon, detailing the physical principles and fundamental equations that govern wave propagation in pressurized pipelines.
- **Chapter 2** focuses on the numerical modeling of hydraulic transients, explaining the Method of Characteristics and the importance of numerical approaches in preventing hydraulic shocks.
- **Chapter 3** presents a technical comparative study of the software Bentley HAMMER and AFT Impulse, evaluating their criteria for precision and flexibility to justify their use in our case study.
- **Chapter 4** describes the practical application of this methodology to a real-world network, including data collection, simulation setup, and the technical validation of proposed mitigation measures.
- **Finally,** Summarizes the results obtained, while discussing the study's limitations and future perspectives related to the integration of new technologies in hydraulic network management.

Chapter I
Background and Literature Review

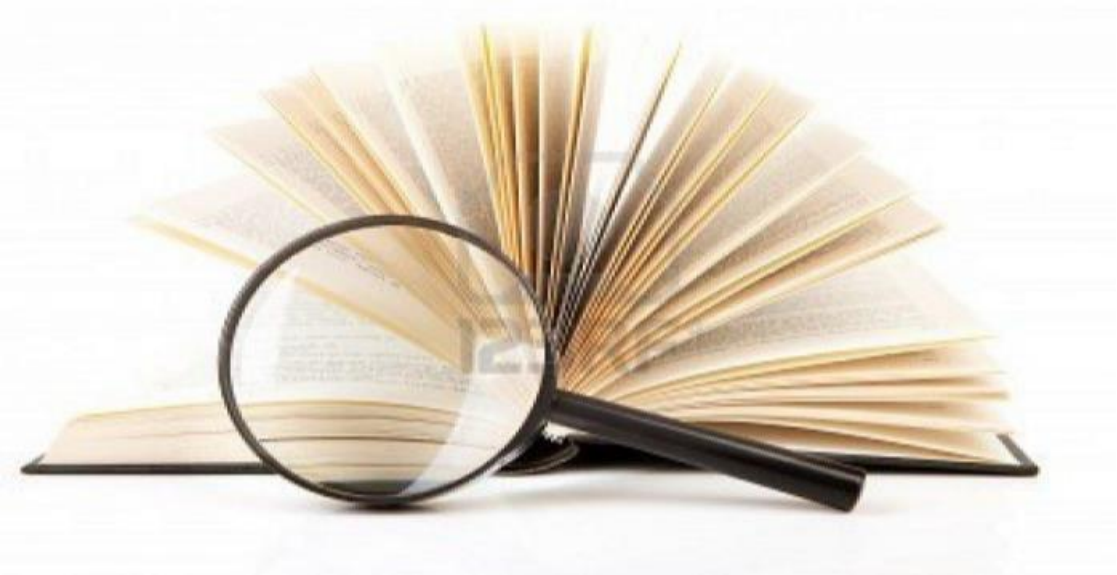

Background and Literature Review

I.1 Background and General Context

Pressurized water distribution networks are far more than a collection of pipes and pumps. They constitute the hydraulic backbone of any urban center linking water sources to end consumers through pumping stations, main transmission lines, and balancing reservoirs. As cities expand and demand continues to grow, these networks increasingly operate under hydraulic conditions that leave virtually no margin for error.

Yet regardless of how precise and robust the design may be, these networks remain inherently vulnerable to disturbances. Any abrupt change in flow velocity a valve maneuver, a pump shutdown, a sudden power outage triggers pressure waves that propagate through the network at speeds approaching the speed of sound in water. Within fractions of a second, pressure may exceed the structural capacity of the pipe, or drop below the vapor pressure of water, leading to column separation and cavitation along the pipeline. This phenomenon is known as water hammer, or the transient state.

The consequences extend well beyond the pipe itself. The repeated occurrence of these pressure surges fatigues pipe walls and deteriorates joints, shortens service life, and drives up maintenance and replacement costs, while also damaging pumping equipment and instrumentation. A major transmission line failure means an immediate disruption of water supply to thousands of residents at once. Yet more hazardous than any of this is what remains invisible: sub-vapor-pressure conditions during the negative phase of a transient event are capable of drawing contaminants directly from the surrounding soil into the drinking water network — a public health risk that only becomes apparent once it is too late.

I.2 Literature Review

I.2.1 Historical Development

Science is not born all at once. What we refer to today as water hammer theory did not originate in hydraulics it began in the medical examination room, where researchers were questioning why blood pulsates in such a particular manner through the arteries.

In **1878**, the Dutch scientist **Korteweg** established the first mathematical framework unifying fluid compressibility and pipe elasticity into a single expression for computing pressure wave celerity [1]. Five years later, the German physiologist **Johannes von Kries** (**1883**) who was studying blood pulse propagation in arteries became the first to derive and experimentally validate the fundamental relationship between pressure change and velocity change, the very relationship that would later bear the name of **Joukowsky's** equation [2]. Yet his work remained confined to the medical domain, never reaching the infrastructure engineers of his era.

In **1898**, and in complete independence from one another, the Russian scientist **Joukowsky** and the American **Frizell** derived the same equation separately [2]. Yet what distinguished

Joukowsky's standing was not the derivation itself it was the fieldwork. He traveled to Moscow, constructed long steel pipelines, measured the waves, and documented their reflections, the effects of air chambers, and the behavior of safety valves. It was this that elevated his paper to the status of an indispensable reference document, rather than a mere theoretical derivation [3].

Four years later, the Italian engineer **Allievi** (**1902**, **1913**) formulated the general theory from first principles, accompanied by graphical charts for estimating pressure under conditions of gradual valve closure [3].

Contributions continued to accumulate throughout the twentieth century at the hands of **Jaeger**, **Parmakian**, and others. **Jaeger** (**1933**) produced the first systematic treatment of the phenomenon in hydroelectric power stations, while **Parmakian** (**1955**) developed computational tables and methods that gained widespread adoption. It was not until Wylie and Streeter (**1978**, **1993**) that the classical form of the one-dimensional continuity and momentum equations was definitively established the two governing equations that underpin every transient simulation to this day [4]. **Ghidaoui** and colleagues (**2005**) subsequently reviewed and critically assessed this entire body of development, and their paper has since remained the most comprehensive in the field [1].

Table I.1 — Major Historical Milestones in Water Hammer Theory

Year	Scientist / Author	Country	Key Contribution	Ref.
Foundations (1788–1883)				
1788	Lagrange	France	First wave celerity formula for open channels: $c = \sqrt{(g \cdot h)}$	[2]
1808	Young, T.	UK	First to include pipe-wall elasticity in wave propagation	[2]
1848	Helmholtz	Germany	Qualitative explanation of reduced celerity in elastic pipes	[2]
1878	Korteweg	Netherlands	Unified formula combining fluid compressibility and wall elasticity	[4]
1883	von Kries	Germany	First derivation and experimental validation of $\Delta H = (a/g) \cdot \Delta V$	[2]
Classical Theory (1897–1955)				
1898	Joukowsky	Russia	Field validation of pressure equation; documented reflections and air chambers	[3]
1898	Frizell	USA	Independent derivation of the same equation (dual discovery)	[3]
1902–13	Allievi	Italy	Complete analytical theory; graphical charts for gradual valve closure	[4]
1931	Bergeron	France	Graphical H–Q method; primary design tool until digital computing era	[3]
1960–93	Wylie& Streeter	USA	MOC formulation as programmable algorithm; foundational reference for all modern software	[4]
2005	Ghidaoui et al.	International	Comprehensive critical review of water hammer theory and practice	[1]
2021	Wéber & Hős	Hungary	Comparison of unsteady friction models in engineering software	[8]
2024	Zhang et al.	China	Quantified friction model effect on wave damping in pipelines	[13]

I.2.2 Evolution of Numerical Solution Methods

When the system is simple a reservoir, a single pipe, a valve closed-form analytical solutions suffice. However, when the network branches, boundary conditions multiply, and components diversify, numerical solution becomes unavoidable. Four methods have historically shared this role, each distinguished by fundamental differences in accuracy, computational cost, and suitability.

The Method of Characteristics (MOC) is the oldest and most widely adopted approach. **Gray** introduced it in **1953** for a frictionless system [5], after which **Lister** (**1960**) developed the fixed-grid scheme, rendering its computational implementation feasible. **Lai** incorporated friction effects, while **Streeter** introduced valve boundary conditions; together, in **1965**, the two achieved experimental validation across varying closure time intervals. The method operates by transforming the continuity and momentum partial differential equations into ordinary differential equations solved along the characteristic lines $\mathbf{C^+}$ and $\mathbf{C^-}$, subject to the **Courant–Friedrichs–Lewy** stability condition [4]. Today, the majority of commercially available simulation software is built upon this method.

The Finite Difference Method (FDM) approximates partial differential equations using finite differences on a regular spatial-temporal grid. Its principal advantage lies in its implicit formulation: it circumvents the **Courant number** constraint that restricts the time step in explicit schemes, thereby permitting larger time steps in large-scale systems [6]. Its most notable application in water hammer analysis is the **MacCormack** scheme, which combines a predictor and a corrector step to achieve second-order accuracy, and has demonstrated effectiveness in studies of valve closure laws [12].

The Finite Element Method (FEM) despite its power in structural mechanics — has not found a prominent place in one-dimensional transient pipe flow analysis, owing to its higher computational cost relative to **MOC** and the difficulty it faces in handling time-varying boundary conditions such as valves and pumps. Nevertheless, it imposes itself in two- and three-dimensional modeling of junction zones and branching regions, as well as in fluid-structure interaction (**FSI**) analysis where dynamic stresses in pipe walls are evaluated. **Kochupillai** and colleagues (**2005**) developed a specialized **FEM** formulation based on the flow velocity variable, specifically addressing water hammer problems.

The Finite Volume Method (FVM) inherently conserves mass and momentum within each computational cell, making it the logical choice when pressure wave celerity varies with time as encountered in systems involving trapped air and vapor cavitation [5]. Godunov-type schemes built upon this framework handle shock waves and water column separation with greater flexibility than **MOC**, and conserve mass and momentum fluxes across cell faces without requiring additional assumptions.

Bentley HAMMER built on **MOC**, its true strength lies not in its algorithm but in its integration: it operates seamlessly with **WaterCAD** and **EPANET**, making it the natural choice for those already working within the Bentley ecosystem. It implements the **Vítkovský** unsteady friction model, which offers greater accuracy under conditions of sudden acceleration and deceleration.

AFT Impulse also **MOC**-based, yet distinguished by greater flexibility in modeling fluid properties and networks with varying pipe diameters. In its standard configurations, it employs quasi-steady friction, and has demonstrated satisfactory accuracy when benchmarked against documented references across a range of engineering contexts.

This is precisely where the paradox lies the one that makes the comparison between the two a genuinely substantive question rather than a mere technical footnote: quasi-steady friction tends to amplify pressure oscillations over longer time horizons, whereas the **Vítkovský** model describes wave damping with considerably greater fidelity. This means that the choice of software is not an administrative decision it is a decision that directly bears on the reliability of the numerical results it will produce.

1.2.4 Applied Studies and Notable Cases

Theory alone is insufficient without confrontation with field reality. What truly validates any model is its application to a real network, a real pump, and a valve closing in real time.

Comparative Studies Between Simulation Software: **Gasiaa** (**2009**) is among the few who brought **Bentley HAMMER** and **AFT Impulse** under the same roof: applying both to documented reference networks, he concluded that both programs yielded good agreement with field data, and recommended their adoption as validation benchmarks in future studies [9].

Vargas and colleagues (**2025**) went further, evaluating five software packages against a six-criterion decision matrix, and found that **AFT Impulse** and **ALLIEVI** performed more straightforwardly in systems where wave celerity exceeds 1000 m/s, while **HAMMER** required additional technical calibration in such cases [10].

Wéber and **Hős** (**2021**) added what others had not explicitly stated: the difference in friction modeling between software packages generates a notable disparity in wave damping accuracy, and neglecting unsteady friction leads to a systematic overestimation of pressure oscillations over longer time horizons [8].

Real Urban Networks **Meniconi** and colleagues (**Water Resources Research, 2024**) combined low- and high-frequency pressure measurements in real urban networks, revealing that network branching and pipe material diversity generate additional wave reflections that complicate interpretation and accumulate structural stresses over time.

In the context of long-distance networks, **Tang** and colleagues (**Water**, **2024**) applied **MOC** to a multi-pump water supply project and demonstrated that combining an air vessel with a hydraulically controlled butterfly valve reduces peak pressure by more than 30 Pipe Material and Environmental Conditions: Recent research clearly indicates that pipe material exerts a measurable effect on transient wave behavior.

A comparative experimental and modeling study (**Scientific Reports, 2024**) demonstrated that plastic pipes such as **HDPE** and **GRP** absorb a portion of the wave energy through their viscoelastic relaxation meaning that any simulation model neglecting damping and relaxation coefficients will produce inaccurate predictions [15].

This finding complements what **Urbanowicz** and colleagues (**Water**, **2022**) established, confirming that neglecting frequency-dependent skin friction in rigid pipes constitutes an unavoidable source of error in high-fidelity modeling [14].

Emerging Applications: Leak detection has become a field in its own right; a study (**Frontiers in Water, 2025**) demonstrated that inverse transient analysis in the frequency domain achieves twice the computational efficiency of its time-domain counterpart, with equivalent accuracy in localizing and quantifying leaks [18]. More remarkably, **Yan** and colleagues (**Water Resources Research, 2025**) explored the deployment of Physics-Informed Neural Networks (**PINNs**) to solve water hammer equations in branched networks an horizon that transcends all classical numerical methods [19].

Table I.3 — Key Applied Studies Referenced in the Literature Review

Author(s) / Year	Network / System	Software / Method	Key Finding	Ref.
A — Software Comparison Studies				
Gasiaa (2009)	Reference networks	HAMMER & AFT Impulse	Both programs agree with field data; comparison limited to simplified cases	[9]
Wéber & Hős (2021)	Laboratory pipe	WANDA (IAB vs. Q-S)	IAB model reduces damping overestimation by up to 40% vs. quasi-steady	[8]
Vargas et al. (2025)	Multi-scenario network	5 software packages	AFT Impulse and ALLIEVI perform better for a > 1000 m/s; HAMMER needs celerity calibration	[10]
Zhang et al. (2024)	Steel pipeline	MOC (IAB vs. Q-S)	Quasi-steady overestimates oscillation amplitude 25–40% after 10+ cycles	[13]
Tang et al. (2024)	Long-distance supply main	MOC	Air vessel + butterfly valve reduces peak pressure by > 30%	[17]
C — Urban Networks & Pipe Materials				
Meniconi et al. (2024)	Real urban network	Field + low/high-freq. data	Branching and material diversity generate additional reflections accumulating structural stress	[16]
Neyestanaki et al. (2024)	HDPE & steel pipes	Experimental + MOC	Plastic pipes absorb wave energy via viscoelastic relaxation; models without damping coefficients are inaccurate	[15]
Urbanowicz et al. (2022)	Rigid pipe	MOC + convolution	Neglecting frequency-dependent skin friction is an unavoidable error source in high-fidelity modelling	[14]
D — Emerging Applications				
Bakhshipour et al. (2025)	Water supply network	Inverse transient analysis	Frequency-domain ITA achieves 2× CPU efficiency vs. time-domain with equivalent accuracy	[18]
Yan et al. (2025)	Branched network	Physics-Informed Neural Net (PINN)	Hybrid PINN–MOC surpasses classical methods in speed for complex topologies	[19]

I.3 Research Objectives

The gaps identified through the literature review precisely define what this research must accomplish: not to re-document a well-documented phenomenon, but to place **Bentley HAMMER** and **AFT Impulse** within the same network, under the same conditions, and determine what differs between them where, and why.

The primary objective is to conduct a systematic comparison between the two programs by applying them simultaneously to a real urban water distribution network under unified and controlled conditions, in order to assess the effect of their modeling differences on the accuracy of water hammer prediction, and to deliver evidence-based recommendations that guide the practicing engineer in selecting the appropriate tool.

Achieving this objective requires beginning from the theoretical foundation a thorough understanding of the one-dimensional **continuity** and **momentum** equations, **Joukowsky's** equation for peak pressure estimation, and the constraints and assumptions that define the validity domain of the models embedded in commercial simulation software.

Mastering these foundations is not a standalone theoretical objective it is a prerequisite for interpreting output discrepancies at a later stage, since passing judgment on differing results is impossible without knowing the source of the theoretical divergence.

From this foundation, the next step follows: constructing the computational models of the network in both programs according to a unified methodology that fixes the same modeling parameters pipe diameters - friction coefficients - wave celerities and valve characteristics so that the essential difference remains confined to the computational scheme and friction model rather than to any discrepancy in input data.

On this basis the quantitative analysis of results is carried out with focus on the governing engineering indicators: peak and minimum pressures at critical nodes, wave damping duration and pressure oscillation frequency.

The fundamental question driving this analysis is: under which conditions does the difference between the **Vítkovský** model in **HAMMER** and the **quasi-steady friction** in **AFT Impulse** produce a divergence significant enough to alter a design decision or elevate the estimated risk level?

The answer to this question is what ultimately translates into practical recommendations addressed to designers who require clear guidance on tool selection for each scenario, and to network operators who rely on simulation results for valve operation decisions, protection device specification, and emergency protocol preparation.

This study does not seek an absolute verdict declaring one program superior to the other. What it seeks is an objective, evidence-supported characterization of the differences between them under specific application conditions one that enables the engineer to make an informed decision that balances modeling accuracy, computational complexity, and the demands of the project at hand.

Conclusion

Pressurized water distribution networks are not merely pipes and pumps they are a system that tolerates no margin for error. Any abrupt disturbance in flow velocity a valve maneuver, a pump shutdown, a power outage triggers pressure waves that propagate at speeds approaching the speed of sound in water, and their consequences extend far beyond the pipe itself: from wall fatigue, equipment damage, and service disruption, to the most hazardous of all sub-atmospheric pressures during the negative phase of a transient event are capable of drawing contaminants directly into the drinking water network.

Through a literature review spanning from the contributions of **Joukowsky** and **Allievi** to the most recent studies published between **2022** and **2025**, the chapter identified three knowledge gaps, all converging on the absence of a unified systematic comparison between commercial simulation software applied to real urban distribution networks. It is this absence that motivated the formulation of the primary objective and its four sub-objectives, and the definition of the methodology adopted for the comparison between **Bentley HAMMER** and **AFT Impulse** and the criteria for evaluating its results.

Chapter II

Theoretical Background and Mathematical Formulation



II.1 Fundamentals of the Water Hammer Phenomenon

II.1.1 Physical Definition and Basic Terminology

Water in a pressurized pipe does not come to rest quietly when forced to do so. Any abrupt change in the velocity of the fluid column converts its kinetic energy into latent elastic energy stored simultaneously in the compressed fluid and in the radially expanding pipe wall then released in the form of a pressure wave that propagates longitudinally at a finite celerity ***a.*** This is water hammer **Water Hammer** or **Hydraulic Transient** depending on context and it is the most severe form of unsteady flow in pressurized pipe systems.

The distinction between the two flow regimes defines when the phenomenon arises. In steady flow, hydraulic variables remain constant at every point with respect to time, and the fluid column maintains full dynamic equilibrium with pressure, friction, and gravitational forces:

$$\frac{\partial V}{\partial t} = 0, \qquad \frac{\partial P}{\partial t} = 0$$

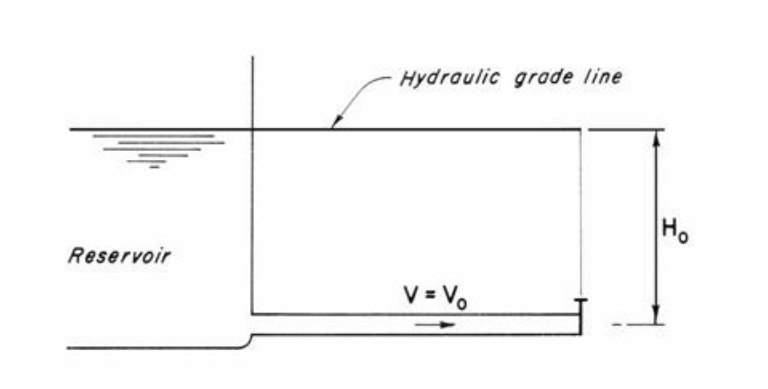

In unsteady flow, temporal and spatial variation of pressure occur simultaneously:

$$\frac{\partial P}{\partial x} \neq 0, \qquad \frac{\partial P}{\partial t} \neq 0$$

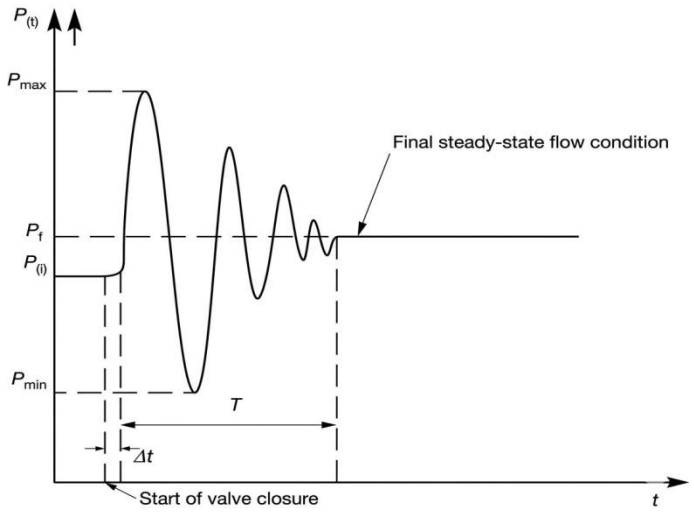

Within this general condition, water hammer is distinguished specifically by the fact that the change in hydraulic momentum is nearly instantaneous which is precisely what makes it the most violent form of unsteady flow.

Here lies what surprises many engineers: conventional engineering treats water as an incompressible fluid, which is entirely valid under steady flow conditions. However, this assumption becomes a source of error in transient analysis, because the finite bulk modulus of water $\boldsymbol{K_f \approx 2.1 \times 10^9 Pa}$ is precisely the property that governs the intensity of the pressure wave and the speed of its propagation. Likewise the elasticity of the pipe wall expressed through Young's modulus $\boldsymbol{E}$ enters the determination of $\boldsymbol{a}$ via the **Korteweg** formula [1][4]:

$$a = \frac{\sqrt{K_f/\rho}}{\sqrt{1 + \psi \cdot \frac{K_f}{E} \cdot \frac{D}{e}}}$$

Where:

- K_f: bulk modulus of water ($\approx 2.1 \times 10^9$ Pa)

- ρ: fluid density (kg/m³)

- E: Young's modulus of the pipe material (Pa)

- D: internal pipe diameter (m)

- e: pipe wall thickness (m)

- ψ: axial restraint coefficient takes different values depending on installation conditions, and will be derived in full in Section II.2.3

Wave celerity a is always lower than the speed of sound in free water (~1440 m/s at 20°C) because wall elasticity provides an additional energy storage pathway that slows wave propagation. The distinction between $\boldsymbol{a}$ and $\boldsymbol{V}$ is fundamental and frequently misunderstood: in steel pipes $\boldsymbol{a}$ is of the order of 1000 m/s whereas flow velocity $\boldsymbol{V}$ rarely exceeds 3 m/s in water distribution networks.

Table II.1 Fundamental Parameters and Variables Water Hammer

Symbol	Variable / Parameter	Definition	SI Unit	Typical Range
a	Pressure wave celerity	Propagation speed of the pressure wave in the pipe	m/s	200 – 1400
ΔH	Piezometric head change	Head rise or drop during the transient event	m	10 – 1500
V_0	Initial flow velocity	Mean velocity before the disturbance	m/s	0.5 – 3.0
H_0	Initial piezometric head	Static hydraulic head before transient begins	m	10 – 500
L	Pipe length	Distance between two analysis nodes	m	10 – 50 000
Tr	Wave travel time	Tr = 2L/a return time of the pressure wave	s	0.01 – 200
Tp	Full oscillation period	Tp = 4L/a duration of one complete wave cycle	s	0.02 – 400
Kf	Bulk modulus of water	Fluid compressibility; controls wave intensity	GPa	2.1 (constant)
E	Young's modulus (pipe)	Pipe wall stiffness; controls wave celerity via Korteweg	GPa	0.2 – 210

II.1.2 Causes and Triggering Events

Every event that imposes a non-gradual change on the velocity of the fluid column is a potential transient event. The fundamental distinction between causes lies not in the effect which is identical in both cases but in its origin: was it intentional or accidental?

Operational events originate from direct or indirect human intervention: rapid or instantaneous closure of isolation valves, sudden shutdown or startup of pump sets, rapid fluctuations in reservoir water levels, and the operation of variable-speed drives under unstable control conditions. In all such cases, the event imposes a change ΔV in fluid column velocity, generating a pressure change that propagates in both directions from the point of disturbance according to Joukowsky's equation:

$$\Delta H = \pm \frac{a}{g} \cdot \Delta V$$

Where:

- ΔH: change in piezometric head (m)
- a: pressure wave celerity (m/s)
- g: gravitational acceleration (m/s²)
- ΔV: sudden change in flow velocity (m/s)

Accidental events are more hazardous precisely because they occur without preparation. The most severe among them is power failure at pumping stations along long transmission mains the pump set stops instantaneously, generating a sharp pressure gradient along the entire pipeline with no prior protective measure in place.

Added to this are mechanical failures and pump impeller vibration, and the involuntary closure of check valves upon flow reversal.

In buried pipelines, the interaction between the pressure wave and the surrounding soil modifies the effective stiffness of the pipe wall, thereby influencing both wave celerity and the amplitude of the transient phenomenon [3][4].

What the event produces depends on the sign and magnitude of the pressure deviation. Three possible pressure regimes exist, summarized in Table II.2:

Table II.2 The Three Pressure Regimes Threshold and Consequence

| Pv = 2 340 Pa abs. (20 °C) | Regimes may alternate within a single event

Regime	Condition	Physical Threshold	Primary Risk
Overpressure (Positive Surge)	P > Pmax,op	ΔH = +(a/g)·V₀ exceeds maximum allowable operating pressure	Pipe rupture; joint failure; fitting blowout
Normal Range	Pv < P ≤ Pmax,op	Pressure within safe hydraulic envelope	None system operating normally
Sub-Atmospheric (Negative Surge)	P ≤ Pv ≈ −10.2 m gauge	Local pressure reaches vapour pressure of water	Column separation; vapour cavity; violent secondary shock on collapse

The first and second regimes frequently alternate within a single transient event the initial positive wave drives pressure above the maximum allowable limit, followed by a negative wave that plunges pressure below vapor pressure, giving rise to the cavitation phenomenon that will be treated in detail in Section II.5.1 [3][6].

II.1.3 Mechanism of Pressure Wave Propagation

The simplest scenario fully reveals the mechanism: a horizontal pipe of length L connecting an upstream reservoir to a valve at its downstream end which is then instantaneously closed. What follows is a complete cycle of four phases.

Phase One $(0 \leq t \leq L/a)$ At the moment of closure $t = 0$, the fluid layer immediately adjacent to the valve decelerates to complete rest. Since the fluid is slightly compressible, this layer compresses locally, raising the pressure by $\boldsymbol{\Delta H}$, after which each successive upstream layer compresses in turn advancing a positive pressure wave front toward the reservoir at celerity $\boldsymbol{a}$, leaving behind stationary fluid under elevated pressure, while the fluid ahead of it continues to flow at its initial velocity $\boldsymbol{V_0}$. The magnitude of the piezometric head rise generated according to Joukowsky's equation [2][4]:

$$\Delta H = \frac{a}{g} \cdot V_0$$

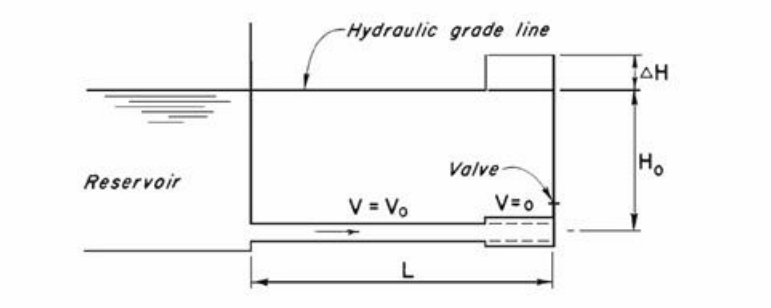

(a) Time, $t = \epsilon$

Where:

- ΔH: transient piezometric head rise at instantaneous closure (m)
- a: pressure wave celerity (m/s)
- g: gravitational acceleration (m/s²)
- V_0: initial flow velocity prior to closure (m/s)

Phase Two $(L/a \leq t \leq 2L/a)$ Upon the positive wave reaching the constant-head reservoir boundary, the reservoir cannot sustain the elevated pressure, and the disturbance reflects as a negative wave of equal magnitude traveling back toward the valve, restoring pressure to its original value $\boldsymbol{H_0}$ and returning the fluid to flow in the reverse direction at velocity $-\boldsymbol{V_0}$.

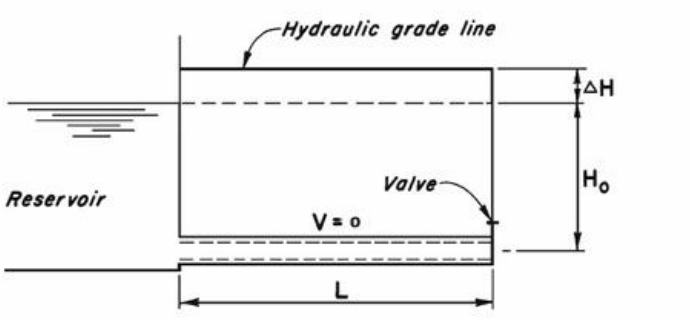

(b) Time, $t = \frac{L}{a}$

Phase Three $(2L/a \leq t \leq 3L/a)$ When the negative wave reaches the closed valve, it reflects as another negative wave propagating back toward the reservoir, causing pressure at the valve to drop to:

$$H_{min} = H_0 - \frac{a}{g} \cdot V_0$$

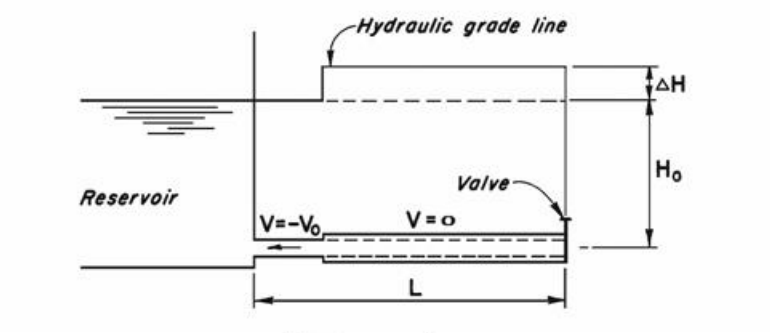

(c) Time, $t = \frac{L}{a} + \epsilon$

Where:

- H_{min}: minimum piezometric head at the valve (m)

- H_0: initial static piezometric head (m)

If H_{min} falls below the vapor pressure head H_v, localized vapor cavities form the sub-atmospheric pressure phase that poses the greatest threat to system integrity.

Phase Four $(3L/a \leq t \leq 4L/a)$ The negative wave returns from the reservoir as a positive wave, restoring pressure $\boldsymbol{H_0}$ and velocity $\boldsymbol{V_0}$ completing one full oscillation cycle of duration:

$$T_p = \frac{4L}{a}$$

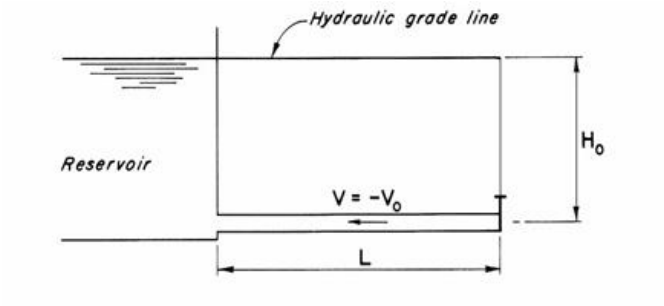

(d) Time, $t = \frac{2L}{a}$

Where:

- T_p: full oscillation cycle period (s)

- L: pipe length (m) - a: pressure wave celerity (m/s)

In the absence of friction, this cycle repeats indefinitely in reality, however, viscosity progressively damps the wave amplitude across successive cycles until the system returns to steady flow.

What determines whether the full Joukowsky head rise is achieved or a lesser value is the ratio of closure time T_c to the wave travel time $T_r = 2L/a$ the decisive criterion separating the rapid and slow closure regimes [4][6]:

$$\text{Rapid closure} \quad T_c \leq \frac{2L}{a} \longrightarrow \Delta H = \frac{a}{g} \cdot V_0$$

$$\text{Slow closure} \quad T_c > \frac{2L}{a} \longrightarrow \Delta H < \frac{a}{g} \cdot V_0$$

In rapid closure, the reflected wave returns to the valve after closure is complete, and the full Joukowsky head rise is realized. In slow closure, the reflected wave begins to cancel the generated pressure wave before closure is complete, so the actual head rise falls below the theoretical maximum with Michaud's approximate formula providing its preliminary estimate, as will be shown in Section II.3.5 [4].

II.1.4 Historical Development of the Theory

What distinguishes the history of this subject is that it did not follow a straight line. Parallel discoveries in different countries, scientific priorities that remained contested well into the late twentieth century, and equations bearing the names of those who published them rather than necessarily those who derived them these are the hallmarks of a remarkably rich history spanning more than two centuries.

The mathematical foundation began in an unexpected place: **Lagrange** (**1788**) derived the first correct formula for wave propagation celerity but in an open channel, not a pressurized pipe:

$$c = \sqrt{g \cdot h}$$

Where:

- c: wave celerity in an open channel (m/s)
- g: gravitational acceleration (m/s²)
- h: flow depth (m)

The formula is far removed from pressurized pipes, yet it established the mathematical structure upon which those who followed would build. **Thomas Young** (**1808**) was the first to recognize that the pipe wall is not merely a passive container its elasticity participates actively in the propagation of pressure disturbances, and he incorporated it into the celerity equation for the first time. **Helmholtz** (**1848**) offered a qualitative explanation of why wave celerity in elastic pipes falls below that in free water but did not complete the mathematical treatment [2].

The unified formulation came with **Korteweg** (**1878**), who presented the first comprehensive mathematical treatment combining fluid compressibility and wall elasticity into a single equation the formula that bears his name to this day and from which Section 2.2.3 will be derived in full. Five years later, **Von Kries** (**1883**) derived the first explicit mathematical relationship linking pressure change to flow velocity change and validated it experimentally.

Tijsseling and **Anderson** (**2007**), in their comprehensive review, established that true priority in this derivation belongs to **Von Kries** rather than **Joukowsky** one of the priority disputes alluded to earlier [2].

The decisive experimental validation was accomplished by **Joukowsky** between **1897** and **1898** in **Moscow**: a series of precise field experiments on pipes of varying lengths and diameters, conclusively documenting the relationship between flow velocity change and the resulting transient pressure rise entirely independently of **Von Kries**.

His results were published in **1898** in Russian, then translated into English by **Simin** in **1904**, whereupon they spread through the Western literature and his name became permanently associated with the fundamental equation. In that same year, **Frizell** independently derived the same relationship in the English-language literature [2][4] yet another dual discovery in the history of this subject.

Between **1902** and **1913**, **Allievi** presented the complete analytical solution in the form of partial differential equations, and his pressure peak estimation charts remained an engineering reference used for decades before the advent of the computer [4].

The graphical method that bridged the gap between theory and field application came with **Bergeron** (**1931**) an elegant approach in the H-Q plane that exploits the structure of characteristic lines to track the hydraulic state at every cross-section and time instant without algebraic solution. This method remained the primary currency of practicing engineers until the **1960s**, and will be presented in Section II.3.4 [3][4].

Computing changed everything. **Streeter** and **Wylie**, between **1960** and **1993**, developed the modern formulation of the Method of Characteristics as a directly programmable algorithm, and their book ***Fluid Transients in Systems*** [4] became the foundational reference upon which most commercial simulation software relies to this day including the two programs that are the subject of comparison in this study.

In the decades that followed, contributions accumulated in the modeling of unsteady friction, fluid-structure interaction, and vapor cavitation, most recently **Wéber** and **Hős's** (**2021**) comprehensive comparison of unsteady friction models in simulation software each of which will be given a dedicated section in this chapter [1][5][8].

II.2 Mathematical Derivation of the Governing

II.2.1 The Continuity Equation

The continuity equation is the mathematical expression of the principle of mass conservation in unsteady flow within pressurized pipes. It answers a single question: where does the mass go when the fluid compresses and the pipe walls expand? The answer requires tracking three physical variables that change during the transient event fluid density $\boldsymbol{\rho}$, pipe cross-sectional area $\boldsymbol{S}$, and the longitudinal length of the element $\boldsymbol{\Delta x}$.

Mass conservation requires that the sum of their relative changes equals zero:

$$\frac{d\rho}{\rho} + \frac{dS}{S} + \frac{d(\Delta x)}{\Delta x} = 0$$

First Term Fluid Compressibility Water is not incompressible in the strict sense its bulk modulus is finite, $K_f \approx 2.1 \times 10^9$Pa. The relative change in density is proportional to the change in pressure:

$$\frac{d\rho}{\rho} = \frac{dP}{K_f}$$

Where:

- K_f: bulk modulus of the fluid (Pa)

- dP: pressure change (Pa)

Second Term Pipe Wall Deformation The oscillating pressure expands the cross-section radially. Applying **Hooke's** law to the pipe wall with consideration of hoop stress and axial restraint:

$$\frac{dS}{S} = \frac{\psi \cdot D}{E \cdot e} \cdot dP$$

Where:

- D: internal pipe diameter (m)
- E: Young's modulus of the pipe material (Pa)
- e: pipe wall thickness (m)
- ψ: axial restraint coefficient values given in Table 2.4 below

Table II.4 Axial Restraint Coefficient ψ for Different Installation Conditions

Case	Installation Condition	ψ Expression	Note
1	Pipe anchored at both ends no expansion joints	**$\psi = 1 - \nu^2$**	Most restrictive; max wall constraint
2	Pipe with expansion joints free axial movement	**$\psi = 1$**	No axial stress; lowest wave celerity for given material
3	Pipe anchored at upstream end only (most common in buried mains)	**$\psi = 1 - \nu/2$**	Intermediate; typical buried transmission main condition

Where ν is Poisson's ratio of the pipe material.

Third Term Longitudinal Deformation of the Element Tracking the element boundaries through the transient event demonstrates that the relative change in length equals the spatial velocity gradient:

$$\frac{d(\Delta x)}{\Delta x} = \frac{\partial V}{\partial x} \cdot dt$$

Substitution and Definition Substituting the three terms into the mass conservation equation and collecting the dPterms, a quantity with the dimensions of velocity squared emerges precisely wave celerity a:

$$\frac{1}{a^2} = \rho\left(\frac{1}{K_f} + \frac{\psi \cdot D}{E \cdot e}\right)$$

Dividing by $\boldsymbol{\rho g}$ and introducing the piezometric head $\boldsymbol{H = P/(\rho g) + z}$ in place of pressure $\boldsymbol{P}$ yields the final compact form the first equation in the Saint-Venant system:

$$\boxed{\frac{\partial H}{\partial t} + \frac{a^2}{g}\frac{\partial V}{\partial x} = 0}$$

Where:
- H: piezometric head (m)
- t: time (s)
- a: pressure wave celerity (m/s)
- g: gravitational acceleration (m/s²)
- V: cross-sectionally averaged flow velocity (m/s)
- x: longitudinal coordinate along the pipe axis (m)

The first term $\boldsymbol{\partial H/\partial t}$ is the rate of change of pressure energy stored within the element. The second term $\boldsymbol{a^2/g \cdot \partial V/\partial x}$ is the net volumetric flux entering or leaving the element. Their balance enforces mass conservation at every instant and every location [1][4].

II.2.2 The Momentum Equation

Newton's second law applied to the fluid element itself mass $\boldsymbol{\rho \cdot S \cdot dx}$ and acceleration $\boldsymbol{DV/Dt}$. Three forces act on it simultaneously along the pipe axis, and their algebraic sum equals mass times acceleration.

Net Pressure Force the pressure difference across the two faces of the element in the longitudinal direction:

$$F_P = -\frac{\partial P}{\partial x} \cdot S \cdot dx$$

Where:

- $\partial P/\partial x$: pressure gradient along the pipe axis (Pa/m)

- S: pipe cross-sectional area (m²)

- dx: infinitesimal element length (m)

Gravity Component the pipe's inclination at angle $\boldsymbol{\alpha}$ to the horizontal accelerates the fluid in the downslope direction or decelerates it in the opposite direction:

$$F_g = -\rho g \sin\alpha \cdot S \cdot dx$$

Where:

- ρ: fluid density (kg/m³)

- α: pipe inclination angle to the horizontal (radians)

Wall Friction Force formulated according to **Darcy–Weisbach**, which will be derived in Section II.2.5:

$$F_f = -\frac{\lambda V|V|}{2D} \cdot \rho \cdot S \cdot dx$$

Where:

- λ: Darcy–Weisbach friction factor (dimensionless)

- V: cross-sectionally averaged flow velocity (m/s)

- D: internal pipe diameter (m)

The notation $\boldsymbol{V|V|}$is not a mere formal convention it is a physically essential condition ensuring that friction always opposes the direction of flow, regardless of the sign of velocity. During a transient event, flow may reverse; had $\boldsymbol{V^2}$alone been used, this property would be lost.

Assembly and Simplification Setting the sum of the three forces equal to $\boldsymbol{\rho \cdot S \cdot dx \cdot DV/Dt}$ and simplifying. In water networks $\boldsymbol{V/a \ll 1}$ at all times the ratio rarely exceeds

0.003 [4][5] which justifies neglecting the convective term $\boldsymbol{V \cdot \partial V/\partial x}$ relative to the temporal term $\boldsymbol{\partial V/\partial t}$.

Expressing pressure in terms of piezometric head $\boldsymbol{P = \rho g(H - z)}$ yields the second equation in the Saint-Venant system:

$$\boxed{\frac{\partial V}{\partial t} + g\frac{\partial H}{\partial x} + \frac{\lambda V|V|}{2D} = 0}$$

Where:

- V: cross-sectionally averaged flow velocity (m/s)

- t: time (s) - g: gravitational acceleration (m/s²)

- H: piezometric head (m)

- x: longitudinal coordinate along the pipe axis (m)

- λ: Darcy–Weisbach friction factor (dimensionless)

- D: internal pipe diameter (m)

The Complete Saint-Venant System The continuity and momentum equations together form the governing framework for all one-dimensional unsteady flow in pressurized pipes:

$$\begin{cases} \dfrac{\partial H}{\partial t} + \dfrac{a^2}{g}\dfrac{\partial V}{\partial x} = 0 \\ \dfrac{\partial V}{\partial t} + g\dfrac{\partial H}{\partial x} + \dfrac{\lambda V|V|}{2D} = 0 \end{cases}$$

The system is hyperbolic the eigenvalues of the Jacobian matrix are real and distinct, $\boldsymbol{\lambda_{1,2} = \pm a}$ which guarantees physically that disturbances propagate at finite celerity in both directions. Were the system parabolic or elliptic, the very concept of a wave would cease to exist [4][5].

The system is mathematically closed: two unknowns $H(x,t)$ and $V(x,t)$ in two equations. Its solution requires only the specification of wave celerity $\boldsymbol{a}$, boundary conditions, and initial conditions. The derivation of $\boldsymbol{a}$ follows in Section II.2.3, and boundary conditions in Section II.3.3 [4].

II.2.3 Pressure Wave Celerity

Korteweg's formula emerged from the derivation of the continuity equation in Section II.2.1 yet its numerical reading reveals more than the derivation alone:

$$a = \frac{\sqrt{K_f/\rho}}{\sqrt{1 + \psi \cdot \frac{K_f}{E} \cdot \frac{D}{e}}}$$

Where:

- a: pressure wave celerity (m/s)

- K_f: bulk modulus of the fluid ($\approx 2.07 \times 10^9$ Pa for water at 20°C)

- ρ: fluid density (≈ 1000 kg/m³ for water)

- ψ: axial restraint coefficient (from Table 2.4 in Section 2.2.1)

- E: Young's modulus of the pipe material (Pa)

- D: internal pipe diameter (m)

- e: pipe wall thickness (m)

The numerator $\sqrt{K_f/\rho} \approx \mathbf{1440 m/s}$ is the speed of sound in free, unconfined water the absolute upper limit that wave celerity in any pipe can never exceed. The denominator is always greater than unity because the pipe elasticity term $\boldsymbol{\psi \cdot K_f D/(Ee)}$ is invariably positive mathematically confirming that wall elasticity reduces propagation celerity below this limit under all conditions.

The Practical Formula for Water Networks Substituting the fixed water properties at 20°C **Korteweg's** formula reduces to a direct applied expression that determines $a$from the $\boldsymbol{D/e}$ ratio and the pipe material property alone:

$$a = \frac{9900}{\sqrt{48.3 + \kappa \cdot \frac{D}{e}}}$$

Where:

- κ: pipe material coefficient from Table 2.5

- D: internal pipe diameter (m)

- e: pipe wall thickness (m)

The constant 9900 in the numerator is $\sqrt{K_f/\rho}$ scaled to appropriate units, and the constant 48.3 in the denominator is K_f/E_{water} the bulk modulus of water scaled by an effective Young's modulus.

Table 2.5 lists $\kappa$and the typical $a$range for the most commonly used pipe materials [4][6]:

Table II.5 Pipe Material Coefficient κ and Typical Wave Celerity Range

Pipe Material	κ ()	E (GPa)	a Range (m/s)	Wave Speed Class
Steel	0.5	200	1 000 – 1 400	Very High
Cast Iron	0.5	170	1 000 – 1 300	Very High
Asbestos Cement	1.0	~24	900 – 1 200	High
Concrete	5.0	16	400 – 600	Moderate
PVC	33	2.7	300 – 500	Low
HDPE	83	0.8	200 – 400	Very Low
LDPE	300	0.2	100 – 200	Ultra Low

The difference between **LDPE** and **steel** from 150 m/s to 1200 m/s represents an eightfold difference in Joukowsky head rise for the same system. Material selection alone determines a substantial portion of the phenomenon's severity.

What the Formula Alone Does Not Reveal Three factors beyond material and geometry influence a and are overlooked in many calculations:

Temperature affects both $\boldsymbol{K_f}$ and $\boldsymbol{\rho}$ simultaneously $\boldsymbol{K_f}$ rises with increasing temperature up to approximately 50°C, then declines, and $\boldsymbol{a}$ follows the same behavior. In hot water transmission mains, neglecting this effect leads to estimation errors.

Dissolved gas content is the most influential factor and the one that most frequently surprises engineers: an air fraction of the order of $10^{-4}$is sufficient to reduce $\boldsymbol{a}$ by a full order of magnitude. Trapped air in the network is invisible, yet its effect is considerable this will be treated in detail in Section II.5.1 [1].

The type of axial restraint through $\boldsymbol{\psi}$ which ranges between 0.75 and 1.0 in practical applications a difference that translates to up to 12% variation in $\boldsymbol{a}$ for the same pipe under different installation conditions [4]. At the preliminary design stage, neglecting this effect is acceptable, but it becomes consequential when verifying peak values.

2.2.4 Joukowsky's Equation and Allievi's Parameter

Joukowsky's equation is one of the fundamental equations in water hammer theory, directly determining the transient piezometric head rise $\boldsymbol{\Delta H}$ resulting from a corresponding change in flow velocity $\boldsymbol{\Delta V}$. It is derived by applying the principles of mass and momentum conservation to the propagating wave front in an ideal horizontal, frictionless pipe.

Consider the following: a valve closes. Within fractions of a second, a water column that had been moving at 1.5 m/s is forced to complete rest. Where does its kinetic energy go? It does not dissipate it is instantaneously converted into a pressure wave propagating in both directions at a celerity three times greater than the speed of sound in air. This is the essence of water hammer and **Joukowsky's** equation is the precise mathematical expression of this conversion.

Derivation from the Momentum Principle The key lies in selecting the correct reference frame one attached to the wave front propagating at celerity a. In this frame, the stationary fluid enters at velocity $\boldsymbol{a}$ and exits at velocity $\boldsymbol{a - \Delta V}$. Applying the momentum equation under the assumption that invariably holds in water networks

$\boldsymbol{V \ll a}$ yields the equation in its two forms [2][4]:

$$\Delta P = \pm \rho \cdot a \cdot \Delta V$$

$$\boxed{\Delta H = \pm \frac{a}{g} \cdot \Delta V}$$

Where:

- ΔH: change in piezometric head (m)
- ΔP: change in pressure (Pa)
- ρ: fluid density (kg/m³)
- a: pressure wave celerity (m/s)
- g: gravitational acceleration (m/s²)
- ΔV: sudden change in flow velocity (m/s)

The positive sign applies to waves propagating upstream, the negative to those propagating downstream. For complete instantaneous closure from $\boldsymbol{V_0}$ to full rest the piezometric head reaches its peak:

$$\Delta H_{max} = \frac{a}{g} \cdot V_0$$

The magnitude of this equation becomes clear through a numerical example: for a typical steel transmission main with wave celerity $\boldsymbol{a \approx 1000\,\text{m/s}}$ and initial flow velocity $\boldsymbol{V_0 = 1.5\,\text{m/s}}$ the resulting pressure head rise is:

$$\Delta H_{max} = \frac{1000}{9.81} \times 1.5 \approx 153\,\text{m}$$

This is precisely what makes $\boldsymbol{a}$ the decisive parameter in every application of Joukowsky's equation: wave celerity is not merely a propagation coefficient it is the direct multiplier that links the hydraulic disturbance to the structural load imposed on the pipe [4][2].

Limits of Applicability of Joukowsky's Equation Joukowsky's equation holds with full rigor only in two cases: complete instantaneous closure ($\boldsymbol{T_c = 0}$), or any closure satisfying $\boldsymbol{T_c \leq 2L/a}$. Beyond this condition, the equation transitions from an actual value to a theoretical upper bound useful for worst-case verification, but an overestimate when closure is slower. In such cases, full transient analysis or Michaud's approximate formula presented in Section II.3.5 must be used [4][6].

Allievi's Parameter A Diagnostic Tool Before Simulation Allievi proposed a dimensionless parameter that assesses the relative sensitivity of a system to transient phenomena. Before running any simulation software, there is a preliminary question the engineer cannot afford to skip: is this system inherently sensitive to water hammer, or are its effects marginal? Allievi quantified this question:

$$\rho_A = \frac{a \cdot V_0}{2g \cdot H_0}$$

Where:

- ρ_A: Allievi's parameter (dimensionless)
- V_0: initial flow velocity (m/s)
- H_0: initial static piezometric head (m)

The definition of $\boldsymbol{\rho_A}$ makes clear that the systems most susceptible to water hammer are those combining three simultaneous factors: high wave celerity (rigid steel pipes), high flow velocity (transmission mains with small diameters), and low static piezometric head (systems with limited operating pressure). This parameter is the first tool the engineer reaches for in a rapid preliminary assessment of the phenomenon's severity in any given system, before proceeding to detailed simulation [4][6].

II.2.5 Steady-State as the Initial Condition for Simulation

No transient simulation begins from a void it always departs from a preceding steady hydraulic state that constitutes the initial condition upon which the values of $H(x,0)$and $V(x,0)$are determined at every point in the system.

The validity and accuracy of this initial condition directly reflect on the reliability of the entire transient results, since any error in characterizing the steady state is amplified through the subsequent transient phases [4][6].

Bernoulli's Equation Energy Conservation Between Two Points

$$\frac{P_1}{\rho g}+\frac{V_1^2}{2g}+z_1=\frac{P_2}{\rho g}+\frac{V_2^2}{2g}+z_2+h_f+h_m$$

Where:

- P_1, P_2: pressure at the two points (Pa)

- V_1, V_2: flow velocity at the two points (m/s)

- z_1, z_2: elevation head at the two points (m)

- h_f: friction head loss along the pipe (m)

- h_m: minor losses at fittings, valves, and bends (m)

This equation is reformulated in terms of piezometric head $\boldsymbol{H=P/(\rho g)+z}$ to render it more suitable for application within the Saint-Venant system:

$$H_1=H_2+\frac{V_2^2-V_1^2}{2g}+h_f+h_m$$

In pipes of uniform diameter where $V_1=V_2$, this reduces to a direct balance between piezometric head and pressure losses along the line [4].

Darcy–Weisbach Equation Friction Head Loss

The friction head loss along a pipe of length $L$and diameter $\boldsymbol{D}$ is given by the Darcy–Weisbach equation:

$$h_f=\lambda\cdot\frac{L}{D}\cdot\frac{V^2}{2g}$$

Where:

- h_f: friction head loss (m)

- λ: Darcy–Weisbach friction factor (dimensionless)

- L: pipe length (m)

- D: internal pipe diameter (m)

- V: cross-sectionally averaged flow velocity (m/s)

Expressing velocity in terms of volumetric flow rate $Q=V\cdot A$ yields the hydraulic resistance formulation the most suitable form for pipe network solutions:

$$h_f = \frac{8\lambda L}{\pi^2 g D^5} \cdot Q^2 = R \cdot Q^2$$

Where:

- Q: volumetric flow rate (m^3/s)

- $R = 8\lambda L/(\pi^2 g D^5)$: hydraulic pipe resistance (s^2/m^5)

The expression $h_f = RQ^2$ is the algebraic tool for pipe network solution the entire network is reduced to a system of resistances connected by nodal continuity equations.

The Friction Factor $\boldsymbol{\lambda}$ Not a Constant Its value depends on the flow regime and the relative wall roughness $\boldsymbol{\varepsilon/D}$, and is determined from the **Colebrook–White** equation or the Moody diagram [4][6].

Reynolds number:

$$Re = \frac{V \cdot D}{\nu}$$

Where:

- Re: Reynolds number (dimensionless)

- ν: kinematic viscosity of the fluid (m^2/s)

In laminar flow ($Re < 2000$), an explicit direct formula applies:

Hagen–Poiseuille:

$$\lambda = \frac{64}{Re}$$

In turbulent flow ($Re > 4000$), the most accurate expression is the Colebrook–White equation an implicit formulation recognized as the most accurate for determining λin both rough and smooth pipes alike [4][6]:

$$\frac{1}{\sqrt{\lambda}} = -2\log\left(\frac{\varepsilon}{3.7D} + \frac{2.51}{Re\sqrt{\lambda}}\right)$$

Where:

- ε: absolute pipe wall roughness (m)

- ε/D: relative roughness (dimensionless)

Its implicit nature requires an iterative solution acceptable in computational implementation but costly in manual application. The **Swamee–Jain** equation provides an explicit formula with acceptable accuracy over a wide range of $Re$and pipe roughness values [6]:

$$\lambda = \frac{0.25}{\left[\log\left(\frac{\varepsilon}{3.7D} + \frac{5.74}{Re^{0.9}}\right)\right]^2}$$

Table II.5 Absolute Roughness ε for Common Pipe Materials

Pipe Material	ε (mm)	Surface Class	Typical Application
Steel (new)	0.046	Smooth	Transmission mains; pump discharge lines
Steel (used/corroded)	0.15	Moderately rough	Aging networks; requires field calibration
Cast Iron (new)	0.26	Moderately rough	Urban distribution; older infrastructure
Cast Iron (tuberculated)	0.90	Rough	Old unlined mains; high head-loss penalty
Asbestos Cement	0.046	Smooth	Existing networks in some regions
Concrete (smooth)	0.30	Moderately rough	Large-diameter gravity mains
Concrete (rough cast)	1.50	Rough	Unlined precast; significant uncertainty
PVC	0.0015	Hydraulically smooth	Pressurised distribution; new installations
HDPE	0.007	Hydraulically smooth	Flexible buried mains; trenchless installation

How Simulation Software Uses These Calculations Commercial simulation software including Bentley HAMMER and AFT Impulse, the two programs under comparison in this study operates according to the same logic: a first phase solves the steady state of the complete pipe network using the Hardy–Cross method or the nodal matrix approach, after which a second phase transfers the resulting $\boldsymbol{H(x,0)}$ and $\boldsymbol{V(x,0)}$ values as initial conditions for solving the Saint-Venant system by the Method of Characteristics. The two phases are sequential and the first cannot be bypassed [7][4].

A practical pitfall that many fall into: entering $\boldsymbol{\lambda}$ from textbook tables without calibration. Practitioners consistently recommend calibrating $\boldsymbol{\lambda}$ from actual field measurements wherever possible, rather than relying solely on tabulated values [7].

II.3 Numerical Solution Methods

II.3.1 The Method of Characteristics (MOC)

The Method of Characteristics is the primary mathematical and computational foundation of modern water hammer analysis, upon which most commercially available simulation software is built including the two programs under study [4][5].

The fundamental challenge in solving the Saint-Venant system lies in the fact that the two unknowns $\boldsymbol{H(x,t)}$ and $\boldsymbol{V(x,t)}$ are coupled through partial derivatives in both x and t simultaneously which is precisely what makes them partial differential equations rather than ordinary ones.

Solving such equations directly is computationally expensive and structurally complex. The Method of Characteristics finds an elegant way out: instead of solving across the entire $\boldsymbol{x}$-$\boldsymbol{t}$ plane, it asks are there curves in this plane along which the partial equations reduce to ordinary ones? The answer is yes. And those curves are the characteristic lines.

Derivation of the Characteristic Lines

The Saint-Venant system is written in its simplified form, neglecting the convective terms $\boldsymbol{V \cdot \partial/\partial x}$ whose smallness in water networks has been established [5]:

$$\frac{\partial H}{\partial t} + \frac{a^2}{g}\frac{\partial V}{\partial x} = 0 \qquad \text{(Continuity)}$$

$$\frac{\partial V}{\partial t} + g\frac{\partial H}{\partial x} + \frac{\lambda V|V|}{2D} = 0 \qquad \text{(Momentum)}$$

The approach: the continuity equation is multiplied by an unknown coefficient μ and added to the momentum equation, subject to the condition that the resulting equation constitutes total time derivatives along a curve $\boldsymbol{dx/dt}$ **= constant.** This condition forces μ to take only two values:

$$\mu = \pm\frac{g}{a}$$

yielding two families of straight characteristic lines in the $\boldsymbol{x}$-$\boldsymbol{t}$ plane:

$$C^+: \frac{dx}{dt} = +a$$

$$C^-: \frac{dx}{dt} = -a$$

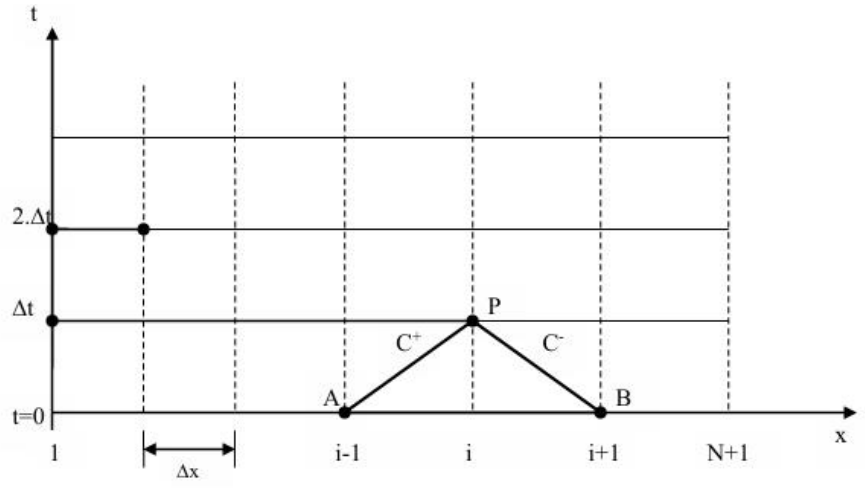

Where:

- C^+: positive characteristic line propagates downstream at celerity $+a$
- C^-: negative characteristic line propagates upstream at celerity $-a$

This is not coincidental it is the hyperbolic character of the Saint-Venant system revealing itself: the eigenvalues of the matrix are $\pm\boldsymbol{a}$, and the straight lines of slope $\pm\boldsymbol{a}$ in the $\boldsymbol{x}$-$\boldsymbol{t}$ plane are precisely the wave propagation paths through the network.

The Compatibility Equations Partial Equations Become Ordinary

Along $\boldsymbol{C^+}$ and $\boldsymbol{C^-}$, time and space cease to be separate independent variables time alone remains. The two partial differential equations transform into two ordinary differential equations:

$$\text{along} \qquad C^+: \frac{dV}{dt} + \frac{g}{a}\frac{dH}{dt} + \frac{\lambda V|V|}{2D} = 0$$

$$\text{along} \qquad C^-: \frac{dV}{dt} - \frac{g}{a}\frac{dH}{dt} + \frac{\lambda V|V|}{2D} = 0$$

The physical meaning requires no equation: along $\boldsymbol{C^+}$, a hydraulic signal propagates downstream; along $\boldsymbol{C^-}$, upstream. This means that the state at any interior point $\boldsymbol{P}$ is governed by the state at two neighboring points from the previous time step, one from each side [4]. No information beyond that is needed.

Finite Differences The Programmable Algorithm

Applying finite differences to the two compatibility equations, constants are defined that are computed from the previous time step data:

$$C_P = H_R + \frac{a}{g}V_R - R_f \cdot Q_R|Q_R|$$

$$C_M = H_S - \frac{a}{g}V_S + R_f \cdot Q_S|Q_S|$$

Where:

- C_P: compatibility constant for line C^+(m)
- C_M: compatibility constant for line C^-(m)
- H_R, H_S: piezometric head at points $R$and $S$from the previous time step (m)
- V_R, V_S: flow velocity at points $R$and $S$from the previous time step (m/s)
- $R_f = \lambda\Delta x/(2gDA^2)$: estimated friction coefficient (s²/m⁵)

Once $\boldsymbol{C_P}$ and $\boldsymbol{C_M}$ are known, the solution at interior point $\boldsymbol{P}$ in the new time step is extracted explicitly and directly [4]:

$$\boxed{H_P = \frac{C_P + C_M}{2}}$$

$$\boxed{V_P = \frac{g}{a} \cdot \frac{C_P - C_M}{2}}$$

Where:

- H_P: piezometric head at point Pin the new time step (m)

- V_P: flow velocity at point Pin the new time step (m/s)

This is the core of the Method of Characteristics and the reason for its dominance: a partial differential problem with two unknowns in two dimensions becomes two equations of addition and subtraction. Each time step is solved in a single sweep across the grid explicit, parallelizable, and implementable in dozens of lines of code.

The Courant Stability Condition (CFL

For the characteristic lines to pass precisely through grid points from the previous time step, the stability condition known as the Courant–Friedrichs–Lewy condition must be satisfied:

$$\boxed{\Delta t \leq \frac{\Delta x}{a}}$$

Where:

- Δt: simulation time step (s)

- Δx: distance between two adjacent spatial grid points (m)

- a: pressure wave celerity (m/s)

The optimal case is at exact equality $\boldsymbol{\Delta t = \Delta x / a}$, where characteristic lines pass precisely through grid points and interpolation errors vanish entirely. In branched networks containing pipes with different wave celerities, satisfying this condition for all pipes simultaneously becomes impractical, and one of two approaches is adopted:

adjusting wave celerities by no more than 15 % to align with the grid, or applying linear interpolation between grid points the latter introducing numerical dispersion that artificially smooths the wave front and reduces the accuracy of pressure peaks [5][4].

The Complete Algorithm Its Logic, Not Its Steps

MOC does not solve the entire equation at once it marches through time step by step. At each step: $\boldsymbol{C_P}$ and $\boldsymbol{C_M}$ are computed for every interior point from the known values of the previous step; $\boldsymbol{H_P}$ and $\boldsymbol{V_P}$ are extracted using the two explicit expressions; boundary conditions are then applied at pipe ends and junction nodes these will be detailed in Section II.3.3. The new values become the "previous step" for the next iteration, and the loop repeats until the end of the simulation time [4][5].

Boundary conditions are not an addition to the method they are what closes the problem. An interior point receives signals from both sides. A boundary point receives a signal from one side only and requires an additional equation from the boundary condition to close the system.

II.3.2 Alternative Numerical Methods

The Method of Characteristics is not the only option for solving the Saint-Venant system three alternative categories exist, each with its own mathematical structure and domain of applicability. Understanding these differences is essential for evaluating modeling choices across different simulation software [5].

The Finite Difference Method MacCormack Scheme

The core idea: the partial derivatives in the Saint-Venant system are replaced by finite difference approximations on a regular grid in the $\boldsymbol{x\text{-}t}$ plane. The most widely used scheme in water hammer analysis is the **MacCormack scheme** two steps per time step, second-order accurate in both time and space [12][5].

Predictor Step forward differences to compute intermediate values:

$$\tilde{H}_i = H_i^n - \frac{a^2}{g} \cdot \frac{\Delta t}{\Delta x} \cdot (V_{i+1}^n - V_i^n)$$

$$\tilde{V}_i = V_i^n - g \cdot \frac{\Delta t}{\Delta x} \cdot (H_{i+1}^n - H_i^n) - \frac{\lambda \Delta t}{2D} \cdot V_i^n |V_i^n|$$

Corrector Step backward differences applied to the intermediate values to obtain the final values at step $n+1$:

$$H_i^{n+1} = \frac{1}{2}\left[H_i^n + \tilde{H}_i - \frac{a^2}{g}\cdot\frac{\Delta t}{\Delta x}\cdot\left(\tilde{V}_i - \tilde{V}_{i-1}\right)\right]$$

$$V_i^{n+1} = \frac{1}{2}\left[V_i^n + \tilde{V}_i - g\cdot\frac{\Delta t}{\Delta x}\cdot\left(\tilde{H}_i - \tilde{H}_{i-1}\right) - \frac{\lambda\Delta t}{2D}\cdot\tilde{V}_i|\tilde{V}_i|\right]$$

Where:

- H_i^n, V_i^n: piezometric head and flow velocity at node $i$and time step n
- $\tilde{H}_i, \tilde{V}_i$: intermediate values from the predictor step
- Δt: time step (s)
- Δx: spatial discretization (m)
- λ: Darcy–Weisbach friction factor (dimensionless)

The practical advantage of this scheme is that the spatial grid is uniform and requires no alignment with characteristic lines which simplifies its application to branched pipe networks. **Toumi and Remini** (**2024**) demonstrated that the scheme yields results comparable to MOC for pressure peaks without requiring such alignment [12]. It remains, however, subject to the CFL condition:

$$\Delta t \leq \frac{\Delta x}{a}$$

The Finite Element Method (FEM)

Rather than working directly with the differential equations, FEM begins by multiplying the Saint-Venant system by test functions $\boldsymbol{\phi_j(x)}$ and integrating over the full domain $[\mathbf{0}, \boldsymbol{L}]$, which relaxes continuity requirements and enables high-precision treatment of boundary conditions [5] this is the so-called *Weak Formulation*.

The weak formulation of the continuity term takes the form:

$$\int_0^L \frac{\partial H}{\partial t}\phi_j dx + \frac{a^2}{g}\int_0^L \frac{\partial V}{\partial x}\phi_j dx = 0 \forall \phi_j$$

Integration by parts on the second term, followed by element-wise approximation:

$$H(x,t) \approx \sum_k N_k\,(x) H_k(t)$$

Where:

N_k are *shape functions*. The system transforms into a set of ordinary differential equations in time alone:

$$\mathrm{MH} + \mathrm{KV} = \mathrm{f}_H$$

$$\mathrm{MV} + g\mathrm{K}^T\mathrm{H} + \mathrm{F(V)} = \mathrm{f}_V$$

Where:

- M: element mass matrix
- K: element stiffness matrix
- F(V): nonlinear friction vector
- f_H, f_V: boundary load vectors

Where it excels and where it falls short: The weak formulation handles irregular geometries and spatially varying properties with a fidelity that MOC cannot match. However, at every time step, element matrices must be assembled and a large linear system solved a computational cost that renders FEM rarely used in commercial simulation software for water networks [5].

The Finite Volume Method (FVM) Godunov Scheme

Rather than approximating derivatives at points, FVM integrates the governing equations over volumetric cells and tracks fluxes across cell boundaries. The first step is writing the Saint-Venant system in conservation law form [5]:

$$\frac{\partial U}{\partial t} + \frac{\partial F(U)}{\partial x} + S(U) = 0$$

$$U = \begin{pmatrix} H \\ V \end{pmatrix}, F(U) = \begin{pmatrix} \frac{a^2}{g} V \\ gH \end{pmatrix}, S(U) = \begin{pmatrix} 0 \\ \frac{\lambda V|V|}{2D} \end{pmatrix}$$

Where:

- U: vector of conserved variables
- F(U): vector of flux densities
- S(U): source term vector (friction)

Integrating this equation over the cell $[x_{i-1/2}, x_{i+1/2}]$and applying Gauss's theorem yields the first-order Godunov scheme:

$$U_i^{n+1} = U_i^n - \frac{\Delta t}{\Delta x}\left[F_{i+1/2}^n - F_{i-1/2}^n\right] - \Delta t \cdot S(U_i^n)$$

Where:

- $F_{i+1/2}^n$: numerical flux at the right boundary of cell i
- $F_{i-1/2}^n$: numerical flux at the left boundary of cell i

The pivotal question: how is the flux $\mathbf{F}_{i+1/2}$computed at each boundary? By solving the local Riemann problem between the two values of **U**on either side of the boundary. The exact expression for the linear system:

$$F_{i+1/2} = \frac{1}{2}[F(U_i) + F(U_{i+1})] - \frac{1}{2}|A|[U_{i+1} - U_i]$$

Where:

$|A| = R|\Lambda|R^{-1}$is derived from the eigenvalue decomposition of the Jacobian matrix

$A = \partial \mathrm{F}/\partial \mathrm{U}$. The two eigenvalues

$\lambda_{1,2} = \pm a$ the same hyperbolic character upon which MOC built its characteristic lines.

Where it excels and where it falls short: Conservation properties are preserved here in the strict sense mass and momentum are conserved at the level of every individual cell, not merely pointwise. This makes FVM the most suitable method for modeling sharp discontinuities such as pressure shocks and wave reflections. However, computing the Riemann problem at every cell boundary at every time step imposes a cost that commercial water network simulation software cannot sustain which is why its use remains largely confined to research environments [12][5].

Table II.6 Comparative Overview of Four Numerical Methods for Water Hammer

Criterion	MOC	FDM MacCormack	FEM Galerkin	FVM Godunov
Mathematical basis	Characteristic line transformation of hyperbolic PDE	Finite-difference approximation (MacCormack predictor–corrector)	Weak formulation via test functions (Galerkin)	Conservation-law flux balance across cell boundaries (Godunov)
Accuracy	2nd order; exact on grid points	2nd order in space and time	High-order possible; element-dependent	1st order; 2nd with MUSCL reconstruction
CFL stability	$\Delta t = \Delta x/a$ (exact equality required)	$\Delta t \leq \Delta x/a$ (required; flexible)	Implicit schemes can relax CFL	$\Delta t \leq \Delta x/a$ (explicit Godunov)
Computational cost	Very low single explicit sweep	Low two sweeps per step	High global matrix inversion	Moderate Riemann problem per face
Primary advantage	Exact wave-front tracking; dominant in engineering practice	Simple implementation; no grid-celerity coupling	Highest geometric flexibility; rigorous error control	Conservative; handles shocks and column separation naturally
Primary limitation	Celerity rounding in multi-pipe networks	Numerical dispersion smooths pressure peaks	High cost prohibits real-time simulation	Lower accuracy for smooth transients without reconstruction
Used in software	HAMMER · AFT Impulse · WANDA	RELAP; research codes	Rarely in commercial WH tools	Research & CFD-coupled tools

The conclusion is that each method finds its advantage in a specific context: MOC remains the optimal choice for standard engineering applications by virtue of its efficiency, simplicity, and accuracy; the MacCormack scheme constitutes a competitive alternative when a uniformly discretized grid is required; Finite Volumes excel in modeling sharp discontinuities and shock phenomena; while Finite Elements retain their niche in problems involving complex geometries and demanding boundary conditions [5].

II.3.3 Boundary Conditions

An interior point receives two compatibility equations one from each side completing the system in the two unknowns $\boldsymbol{H_P}$ and $\boldsymbol{V_P}$. At a boundary, however, only one compatibility equation is available, and the missing second equation is supplied by an expression that captures the physical condition at that location. Any simplification of this condition reflects directly on the computed pressure peaks and their timing [4].

First Constant-Head Reservoir Boundary

A large reservoir imposes a fixed piezometric head regardless of the transient event:

$$H_P = H_{res} = \text{constant}$$

Where:

- H_P: piezometric head at the reservoir boundary (m)

- H_{res}: water level in the reservoir above the reference datum (m)

This assumption holds whenever the reservoir surface area is large enough to render fluctuations in its water level negligible. $\boldsymbol{H_P}$ is known it is substituted into the available compatibility equation ($\boldsymbol{C^-}$ at the upstream boundary or $\boldsymbol{C^+}$at the downstream boundary) to extract $\boldsymbol{Q_P}$ directly [4].

Second Valve

The valve is characterized by its dimensionless opening ratio τranging between zero (fully closed) and unity (fully open), and its flow rate follows the hydraulic orifice equation:

$$Q_P = \tau^2 \cdot Q_0 \sqrt{\frac{H_P}{H_0}}$$

Where:

- Q_P: volumetric flow rate through the valve at the new time step (m³/s)

- τ: valve opening ratio at the current step (dimensionless)

- Q_0: initial flow rate under steady-state conditions (m³/s)

- H_0: static piezometric head at the valve (m)

The equation is nonlinear in $\boldsymbol{H_P}$ it is solved in conjunction with the available compatibility equation at the node. For instantaneous closure ($\tau = 0$), $Q_P = 0$, and Joukowsky's equation is recovered directly from C^+in its compact form [4]:

$$H_P = C_P \Rightarrow \Delta H = H_P - H_0 = \frac{a}{g} \cdot V_0$$

Third Pump

The pump boundary is the most complex it requires characterizing the machine across four operating quadrants. The equation of rotational motion of the pump-motor set is coupled with the two compatibility equations at the node:

$$I \frac{d\omega}{dt} = T_m - T_h$$

Where:

- I: polar moment of inertia of the pump-motor set (kg·m²)

- ω: angular velocity of the set (rad/s)

- T_m: electric motor torque (N·m)

- T_h: resisting hydraulic torque (N·m)

The complete four-quadrant characteristic curves of the pump covering normal pumping, turbine operation, reverse rotation, and dissipation are represented by dimensionless

curves scaled to the rated speed, head, and flow rate. The rotational equation and the two compatibility equations are solved simultaneously at every time step [7][4].

At power failure the most hazardous scenario in long transmission mains $\boldsymbol{T_m}$ vanishes instantaneously and the set decelerates under $\boldsymbol{T_h}$ alone. A sharp negative pressure wave propagates downstream, and in the absence of adequate protection measures, water column separation becomes unavoidable.

Fourth Multi-Pipe Junction Node

At a node where n pipes converge, two physical conditions jointly govern the solution:

Piezometric head continuity all pipes connected to the node share the same $\boldsymbol{H_P}$, in the absence of any added hydraulic element:

$$H_{P,1} = H_{P,2} = \cdots = H_{P,n} = H_P$$

Flow rate conservation the algebraic sum of flow rates at the node equals zero:

$$\sum_{i=1}^{n} Q_{P,i} = 0$$

Where:

- $Q_{P,i}$: flow rate in pipe i positive for inflow, negative for outflow

With $n$compatibility equations one for each pipe in the direction toward the node a system of $\boldsymbol{n+1}$ equations in $\boldsymbol{n+1}$ unknowns ($\boldsymbol{H_P}$ and $\boldsymbol{n}$ flow rates) is formed. The solution proceeds by determining $\boldsymbol{H_P}$ first, then extracting each $\boldsymbol{Q_{P,i}}$ directly from it [4].

Fifth Vapor Cavitation

When the computed pressure at a node drops below vapor pressure $\boldsymbol{P_v}$, the single-phase flow model loses its validity. The Discrete Vapor Cavity Model (DVCM) caps the local pressure at its minimum bound:

$$H_P \geq H_v = \frac{P_v}{\rho g}$$

Where:

- H_v: piezometric head corresponding to vapor pressure (m) ≈ -10m water column at 20°C

Once this condition is satisfied, a localized vapor cavity forms and its volume $\boldsymbol{V_{cav}}$ is tracked through an independent continuity equation until collapse. Full details are provided in Section II.5.1 [3][4].

II.3.4 Bergeron's Graphical Method

Before the advent of the computer, Bergeron (1931) observed something elegant: the two compatibility equations which in the $\boldsymbol{x}$-$\boldsymbol{t}$ plane represent characteristic lines propagating at celerities $\pm\boldsymbol{a}$ transform in the $\boldsymbol{H}$-$\boldsymbol{Q}$ plane into two straight lines with slopes of opposite sign. The transient solution at every time step is nothing more than the intersection point

of these two lines [3][4] no computer, no system of equations to solve, just paper, a pencil, and a ruler.

Mathematical Formulation in the H-Q Plane

Expressing the two compatibility equations in terms of flow rate $\boldsymbol{Q = V \cdot A}$ rather than velocity $\boldsymbol{V}$, they take the form:

$$\text{along} \qquad C^+ : H = C_P - \frac{a}{gA} \cdot Q$$

$$\text{along} \qquad C^- : H = C_M + \frac{a}{gA} \cdot Q$$

Where:

- H: piezometric head (m)
- Q: volumetric flow rate (m³/s)
- C_P: compatibility constant for line C^+computed from the previous step (m)
- C_M: compatibility constant for line C^-computed from the previous step (m)
- $a/(gA)$: characteristic pipe resistance (m·s/m³)

Line $\boldsymbol{C^+}$ descends with negative slope $\boldsymbol{-a/(gA)}$ from left to right in the $\boldsymbol{H}$-$\boldsymbol{Q}$ plane, while line $\boldsymbol{C^-}$ ascends with positive slope $\boldsymbol{+a/(gA)}$. The quantity $\boldsymbol{a/(gA)}$ is identical in both cases and is termed the characteristic pipe resistance directly analogous to electrical resistance in AC circuits: it relates pressure change to flow rate change, and varies from pipe to pipe according to its diameter and wave celerity.

The Graphical Construction Procedure

At every time step $\boldsymbol{\Delta t = \Delta x / a}$, the same procedure repeats. The hydraulic state at the previous step for each cross-section is represented by a point in the $\boldsymbol{H}$-$\boldsymbol{Q}$ plane the intersection of $\boldsymbol{C^+}$ and $\boldsymbol{C^-}$ from that step. From this point, two new lines are drawn: a $\boldsymbol{C^+}$ line of slope $\boldsymbol{-a/(gA)}$ propagating downstream, and a $\boldsymbol{C^-}$ line of slope $\boldsymbol{+a/(gA)}$ propagating upstream. The new state at any interior cross-section is simply the intersection of the $\boldsymbol{C^+}$ line arriving from upstream with the $\boldsymbol{C^-}$ line arriving from downstream.

At boundary points, the single available characteristic line intersects the boundary condition curve instead of the second characteristic. At a constant-head reservoir with head $\boldsymbol{H_{res}}$, the boundary condition is a horizontal line at $\boldsymbol{H = H_{res}}$in the $\boldsymbol{H}$-$\boldsymbol{Q}$ plane, and its intersection with the available characteristic line directly yields the new flow rate. At a valve, the boundary condition is a quadratic curve:

$$H = \left(\frac{Q}{\tau Q_0}\right)^2 \cdot H_0$$

As the valve closes progressively, the value of τchanges step by step, the quadratic curve narrows toward the H-axis, and the intersection point with the characteristic line traces a path that can be followed by eye on the page. This is what numerical tables cannot achieve the engineer watches the wave propagate; he does not merely read its numbers.

Graphical Application of Boundary Conditions

Bergeron's method is distinguished by exceptional visual clarity in applying boundary conditions. At a constant-head reservoir boundary $\boldsymbol{H_{res}}$, the condition is represented by a horizontal line at $\boldsymbol{H = H_{res}}$ in the $\boldsymbol{H\text{-}Q}$ plane, and the new state is identified at the intersection of this horizontal line with the available characteristic. At a valve boundary, the valve characteristic curve $\boldsymbol{H = (Q/\tau Q_0)^2 \cdot H_0}$ is represented as a quadratic curve in the $\boldsymbol{H\text{-}Q}$ plane, and the state is determined at its intersection with the incoming characteristic line [4].

Educational Value and Practical Limitations

Bergeron's method retains its enduring educational value for two fundamental reasons: first, it renders the physics of wave propagation visually immediate in a way that numerical tables cannot replicate the engineer observes with his own eyes how the hydraulic signal advances from section to section and interacts with boundary conditions. Second, it enables rapid verification of numerical software results in simple cases without any programming whatsoever.

However, the method becomes impractical when the network branches, wave celerities vary, or boundary conditions grow complex, because manual line drawing becomes unmanageable as the number of pipes and nodes increases; friction transforms the straight lines into curves, complicating the construction; and branched networks with multiple junctions cannot be represented in a single $\boldsymbol{H\text{-}Q}$ plane. These very limitations were what drove the development of MOC as a programmable numerical formulation of the same physical principles [3][4].

II.3.5 The Michaud Formula for Slow Closure

The Joukowsky equation assumes instantaneous closure and instantaneous closure is, in practice, rare. Most valves close over a span of seconds or minutes, and when the closure time $\boldsymbol{T_c}$ exceeds the wave travel time $\boldsymbol{2L/a}$, the wave reflected from the reservoir begins to cancel part of the pressure surge generated before closure is complete and the full Joukowsky head rise is never realized. Michaud (1878) derived an approximate formula for this regime that remains in use today for preliminary estimation, owing entirely to its simplicity no simulation, no software required [4][6].

The Formula:

The derivation rests on two assumptions: that flow velocity varies linearly with time, and that reflected waves superpose in a simple linear fashion. Applying these two assumptions to a closure that brings velocity from $\boldsymbol{V_0}$ to zero over time $\boldsymbol{T_c}$:

$$\boxed{\Delta H_{Michaud} = \frac{2LV_0}{gT_c}}$$

Where:

- $\Delta H_{Michaud}$: approximate pressure head rise under slow closure (m)
- L: pipe length from valve to reservoir (m)
- V_0: initial steady-state flow velocity (m/s)
- g: gravitational acceleration (m/s²)
- T_c: total closure time (s)

The formula says something remarkably direct: doubling the closure time halves the pressure peak. This inverse relationship is precisely what the engineer seeks when determining the minimum closure time permissible for a given maximum allowable line pressure.

Consistency with Joukowsky:

At $\boldsymbol{T_c = 2L/a}$ the boundary between rapid and slow closure the Michaud formula yields:

$$\Delta H_{Michaud}|_{T_c=2L/a} = \frac{2LV_0}{g \cdot (2L/a)} = \frac{aV_0}{g} = \Delta H_{Joukowsky}$$

The two formulas converge at the same point Michaud is a consistent extension of Joukowsky into the slow-closure regime, not an independent expression [4].

Limitations and Scope of Application:

The Michaud formula neglects actual valve characteristics and does not account for friction in wave attenuation its accuracy is approximate within ±15%

Table II.7 Applicable Formula by Valve Closure Regime

Closure Regime	Condition	Applicable Formula	Accuracy	Expression
Rapid Closure	Tc ≤ 2L/a	Joukowsky's Equation	Exact	ΔH = (a/g) · V₀
Intermediate Closure (most common)	2L/a < Tc < 10×(2L/a)	Numerical MOC (full simulation)	Required	HP=(CP+CM)/2 VP=(g/a)·(CP−CM)/2
Slow Closure	Tc ≥ 10×(2L/a)	Michaud's Formula	Approximate ±15%	ΔH = 2·L·V₀ / (g·Tc)

The intermediate zone between the two bounds is the most common in real-world applications valves are deliberately designed to close more slowly than the rapid-closure threshold, yet rarely reach ten times the wave travel period. Neither Joukowsky nor Michaud is adequate here and this is precisely the essential justification for numerical simulation [4][6].

Numerical Example:

A steel transmission main: $L = 2000$m, $a = 1000$m/s, $V_0 = 1.2$m/s. Wave travel period: $2L/a = 4$s. The valve closes over $T_c = 60$s more than ten times the travel period; the Michaud condition is satisfied.

$$\Delta H_{Michaud} = \frac{2 \times 2000 \times 1.2}{9.81 \times 60} \approx 8.2 \text{ m}$$

For comparison, the Joukowsky head rise under instantaneous closure:

$$\Delta H_{Joukowsky} = \frac{1000 \times 1.2}{9.81} \approx 122 \text{ m}$$

From 122 m down to 8.2 m slow closure reduced the pressure peak to less than 7

II.3.6 Optimal Valve Closure Laws

Closure time alone is not sufficient. The choice of valve closure law is no less consequential than the choice of closure time itself, as it exerts a direct influence on the shape, peak, and timing of the resulting pressure wave. For the same $\boldsymbol{T_c}$, two different closure laws can produce pressure peaks that differ by as much as 40 % [4][12]. These laws may be classified into three categories.

The Linear Law:

In this law, the valve opening coefficient τdecreases uniformly and linearly with time from unity to zero:

$$\tau(t) = 1 - \frac{t}{T_c}, 0 \leq t \leq T_c$$

Where:

- τ: valve opening ratio (dimensionless)

- t: time elapsed from the start of closure (s)

- T_c: total closure time (s)

A linear decrease in τdoes not imply a linear decrease in flow rate since $\boldsymbol{Q \propto \tau^2}$. The bulk of the flow reduction is concentrated in the final stages, when $\tau$is small, producing a sharp pressure gradient at the end of closure. This makes the linear law ill-suited for pressure-sensitive systems [4].

The Quadratic Law:

In this law, the square of the opening ratio $\boldsymbol{\tau^2}$decreases linearly with time, which is equivalent to a linear decrease in flow rate itself:

$$\tau^2(t) = 1 - \frac{t}{T_c}, 0 \leq t \leq T_c$$

- τ^2: square of the valve opening ratio (dimensionless)

Here $\boldsymbol{\tau^2}$decreases linearly and since $\boldsymbol{Q \propto \tau^2}$, the flow rate decreases linearly as well. The pressure disturbance is distributed uniformly across the entire closure duration rather than concentrated at its end. A study by Toumi and Remini (2024) demonstrated that the resulting pressure peak is lower than that of the linear law by a margin of 15% to 25% depending on network characteristics [12].

The Optimal Two-Stage Law:

The two-stage law is considered the best-performing of the three from an engineering standpoint. It combines two phases with distinct closure rates.

The governing principle: the pressure peak is determined primarily by the change in flow rate during the *final* phase of closure, not the first. The two-stage law exploits this fact directly:

$$\tau(t) = \begin{cases} 1 - \dfrac{(1-\tau^*)}{t_1} \cdot t & 0 \leq t \leq t_1 \\ \tau^* \cdot \left(1 - \dfrac{t - t_1}{T_c - t_1}\right) & t_1 < t \leq T_c \end{cases}$$

Where:

- τ^*: opening ratio at the end of the first phase (dimensionless)

- t_1: duration of the first phase (s)

The first phase reduces τrapidly from 1 to τ^* the majority of the flow is arrested here at the lowest possible pressure rise. The second phase eliminates the remaining velocity slowly, within the Michaud regime the sharp gradient at closure's end is kept under control. The trade-off is the speed of initial closure; the reward is a significantly attenuated final pressure peak [4].

The optimal pair (τ^*, t_1) is the solution to an optimization problem that maximizes pressure peak reduction subject to the constraint of total closure time T_c. In engineering practice, the following values constitute a reliable starting point:

$$\tau^* \approx 0.2 \text{ to } 0.3, t_1 \approx 0.3 \cdot T_c \text{ to } 0.5 \cdot T_c$$

This strategy is considered the optimal practical solution for most pumping installations, and the two-stage law is the default recommended choice in commercial simulation software [4][7].

Practical Warning:

These three laws are theoretical models. A real valve does not necessarily conform to any of them the relationship between opening angle and discharge coefficient depends on the valve type (ball, butterfly, gate) and its specific design. Accurate simulation requires the input of the experimentally measured τ-versus-angle curve supplied by the manufacturer, not the theoretical law alone [4][7].

II.4 Water Hammer Protection Devices

II.4.1 Classification of Protection Measures

Protection measures against water hammer operate by one of two mechanisms and only two: either preventing the wave from reaching its full magnitude by controlling the triggering event itself, or absorbing its energy after generation and limiting its propagation. This functional distinction is the foundation of the classification [4][7].

Category One Passive Measures

These are operational and design-level measures that require no addition of independent hydraulic equipment they function by controlling the nature of the triggering event itself:

- Slow valve closure programs following optimal closure laws (Section II.3.5) - Staged start-up and shutdown procedures for pump sets - Check valve closure laws designed to prevent sudden snap-shut upon flow reversal - Flywheels that extend the deceleration time of the pump set upon power failure - Variable frequency drives (VFD) that convert an abrupt shutdown into a programmed, extended deceleration

Category Two Active Measures

These are independent hydraulic components added to the system that respond automatically to the pressure disturbance after it has occurred and operate regardless of the nature of the triggering event. They include:

- Pressurized air vessels
- Surge towers
- Pressure relief valves
- Vacuum-breaking valves

Each is addressed in a dedicated subsection of this chapter.

Why Both Categories Are Needed:

Passive measures alone are insufficient in long transmission mains with complex topography they attenuate the initial wave intensity but cannot prevent the sub-atmospheric pressure phase that follows. Active measures alone are costly and must be sized for worst-case scenarios. Combining both is the sound engineering logic: passive measures reduce the wave's magnitude, and active measures treat what remains [4][7].

Selection Criteria

The selection of an appropriate protection measure for a given system is governed by a set of interrelated criteria summarized in the following table:

Table II.8 Engineering Criteria for Selecting a Water Hammer Protection Device

Selection Criterion	Recommended Device / Action	Key Constraint
Nature of transient event	Pump trip → Air vessel or flywheel Valve closure → PRV or controlled actuator	No single device covers all cause types simultaneously
System operating pressure	Pmax exceeded → PRV (Pset = 1.05–1.10 × Pmax)	PRV alone cannot prevent sub-atmospheric pressure
Risk of sub-atmospheric P / cavitation	Hmin < Hv = −10.2 m → Air inlet valve or air vessel with P_0 control	PRV is ineffective against negative-pressure events
Pipeline profile high points	Vulnerable high points → Air inlet valve at each point	Single centralised device may not protect distant high points
Available head & site constraints	Low H_0 + available space → Surge tank (standpipe)	Surge tank impractical at high operating pressure
Transient frequency	Frequent stop-start cycles → VFD ramp or flywheel	Air vessel volume must be re-verified after each cycle if gas leaks
Maintenance & reliability	Minimal maintenance → Passive devices (air vessel, flywheel)	PRV requires periodic calibration; VFD requires electrical maintenance
Site footprint & civil constraints	Limited space → VFD or flywheel within pump station	Surge tank and large air vessel require significant civil structure

Integrated Design Procedure

The design follows three sequential stages, none of which may be bypassed:

First compute the Allievi parameter $\boldsymbol{\rho_A}$ to assess the severity of the phenomenon and determine whether passive measures alone are sufficient.

Second run a full MOC simulation to extract the maximum and minimum pressure envelopes along the entire pipeline and identify the critical points knowing the peak at the valve is not enough; the real problem is often located elsewhere along the line.

Third select the protection measures and determine their design parameters, then re-run the simulation to verify that both criteria are met: a maximum pressure not exceeding 1.1 times the maximum operating pressure, and a minimum pressure no lower than 3 m absolute to prevent cavitation [4][7].

Table II.9 Classification of Main Water Hammer Protection Devices

Device	Category	Primary Protection	Typical Application	Key Limitation
Air Vessel (Hydropneumatic Tank)	Passive Hydraulic	Both positive surge & negative (sub-atmospheric) phases	Long transmission mains; pump-trip scenarios	Gas leakage → periodic recharging; critical volume sizing
Surge Tank (Standpipe)	Passive Hydraulic	Positive pressure surge; slow oscillations	Low-pressure systems ($H_0 < 30$ m)	Tower height ≥ max piezometric head; impractical at high pressure
Restricted-Orifice Surge Tank	Passive Hydraulic	Pressure surge with enhanced damping	Systems prone to sustained oscillations	Orifice sizing requires careful calibration to avoid instability
Pressure Relief Valve (PRV)	Passive Valve	Positive pressure surge only (opens at Pset = 1.05–1.10 × Pmax)	Distribution networks; pump discharge lines	No protection against sub-atmospheric pressure
Air Inlet Valve (Vacuum Breaker)	Passive Valve	Negative pressure prevents vapour cavity at high points	Pipeline high points in long-distance mains	Must be paired with slow-release vent to avoid secondary surge
Flywheel	Passive Mechanical	Slows pump deceleration; reduces initial ΔV	Pump stations with frequent trip risk	Added rotational inertia increases shaft stress; maintenance required
Variable Frequency Drive (VFD)	Active Electrical	Controlled deceleration ramp → reduces ΔV	Pump stations with programmable control	Electrical maintenance; fails under power outage

II.4.2 Pressurized Air Vessels

A sealed vessel compressed air above, water below, connected to the pipeline through an orifice throttle. This deceptively simple configuration is what makes the pressurized air vessel (*Air Vessel* / *Hydropneumatic Tank*) the most versatile active protection measure in pumping line applications, owing to its unique capacity to simultaneously counter both positive and negative pressure waves.



Operating Principle:

Under steady pumping conditions the vessel remains pressure-neutral, its air pressure in equilibrium with line pressure. When the pump trips suddenly, a negative pressure wave propagates downstream. As line pressure drops below the vessel's air pressure, the air

expands and drives water into the pipe the vessel acts as an instantaneous standby pump, preventing pressure from falling below the safe threshold. When a subsequent positive wave returns, water is pushed back into the vessel, re-compressing the air and capping the excess head rise. The throttle orifice slows this exchange and damps the oscillations without it, the abrupt response would itself generate secondary waves [4][7].

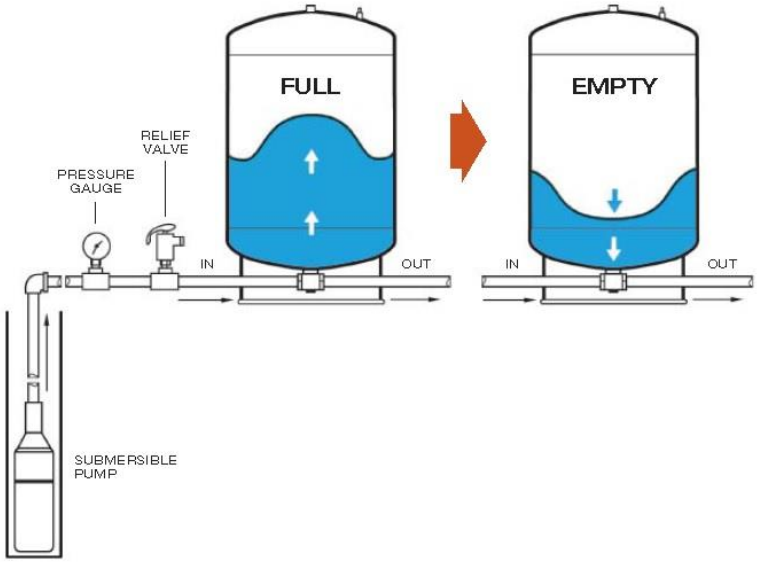

Thermodynamics of the Air Cushion:

The air in the vessel follows a polytropic process during the transient event:

$$P_0 \cdot V_0^n = P_1 \cdot V_1^n$$

Where:

- P_0: initial absolute air pressure (Pa)
- V_0: initial air volume (m³)
- P_1: absolute air pressure during the transient (Pa)
- V_1: air volume during the transient (m³)
- n: polytropic exponent (dimensionless)

The value of $n$depends on the speed and nature of the transient event [4]:

Table II.10 Polytropic Exponent n Air Cushion in Hydropneumatic Vessel

n Value	Process Type	Transient Condition	Design Guidance
n = 1.0	Isothermal	Very slow transient; high heat exchange with surroundings	Smallest vessel volume conservative only in sizing; rarely achievable in practice
1.0 < n < 1.2	Polytropic (slow event)	Moderate duration; partial heat exchange	Suitable for slow pump trips on long mains; requires field calibration
n = 1.2	**Polytropic (design)**	**Standard engineering design value for all scenarios**	**Recommended default; safety margin without excessive conservatism**
n = 1.4	Adiabatic	Very rapid transient; no heat exchange	Most conservative largest vessel volume; use when event duration < 0.1 s

In standard engineering design, $n = 1.2$ is adopted a conservative value that provides an acceptable safety margin without excessive vessel oversizing [4][7].

Sizing Procedure Bouch-Monier Method:

The objective: the initial air volume U_0 must be sufficient to feed the pipeline throughout the deceleration phase without allowing pressure to fall below $P_{min} \approx 3$m absolute. Three dimensionless parameters are defined [4]:

$$K = \frac{H_{abs} - H_0}{H_0}$$

$$A_p = \frac{C \cdot V_0}{g \cdot H_0}$$

$$B = \frac{V_0^2 \cdot L \cdot S}{g \cdot H_{abs} \cdot U_0}$$

Where:

- H_{abs}: initial absolute pressure at the vessel location (m water column)
- H_0: static piezometric head at the vessel location (m)
- C: pressure wave celerity in the line (m/s)
- V_0: initial flow velocity (m/s)
- L: line length from pump to vessel (m)
- S: pipe cross-sectional area (m²)
- U_0: initial air volume the unknown (m³)

Once B is read from standard design charts at a guaranteed pressure margin of ≥ 3m absolute:

$$U_0 = \frac{V_0^2 \cdot L \cdot S}{g \cdot H_{abs} \cdot B}$$

The maximum air volume at minimum pressure P_{min}, derived from the polytropic state equation:

$$U_{max} = U_0 \cdot \left(\frac{H_{abs}}{P_{min}}\right)^{1/n}$$

Where:

- U_{max}: maximum air volume at minimum pressure (m³)
- P_{min}: minimum allowable absolute pressure (m water column)

The actual vessel volume is set 20

$$\boxed{U_{real} = (1.2 \text{ to } 1.3) \cdot U_{max}}$$

- U_{real}: total actual vessel volume (m³)

The Throttle Equation:

Flow through the throttle orifice follows the standard orifice flow equation:

$$Q_{vessel} = C_d \cdot A_{or} \cdot \text{sign}(\Delta H) \cdot \sqrt{2g|\Delta H|}$$

Where:

- Q_{vessel}: flow rate through the throttle orifice (m³/s)

- C_d: discharge coefficient (dimensionless, typically 0.6 – 0.8)

- A_{or}: throttle orifice area (m²)

- ΔH: piezometric head difference between vessel and line (m)

The ratio of orifice area to main pipe area is set within the range of 0.3 to 0.7 to balance response speed against oscillation damping. A full MOC simulation is required to verify that both the maximum and minimum pressure envelopes satisfy design criteria along the entire pipeline not at the vessel location alone [4][7].

Vessel Placement:

The optimal location is immediately at the pump outlet, or within a distance no greater than $L/10$ from it this ensures the vessel intercepts the negative wave before it accumulates along the line. In pipelines with complex topography and multiple high points, more than one vessel may be required. The critical points warranting an additional vessel are not guessed they are identified from the minimum pressure envelope produced by simulation, before any hardware is installed [4][7][10].

II.4.3 Surge Tanks

The operating principle is fundamentally different from that of the pressurized air vessel: no air, no compression, no mechanical equipment. A surge tank designated as a *Surge Tank* or *Standpipe* is a vertical open or semi-open cylinder connected to the pipeline at a strategic location. When pressure rises, water enters the tower; when it falls, water exits. The restoring force is gravity alone, acting on the oscillating water column. This is what makes it mechanically simpler, longer-lasting, and less costly to maintain [4].



The Simple Surge Tank:

The basic tower is a cylinder of horizontal cross-sectional area A_s, connected to the line via a connecting tunnel of length L_t and cross-sectional area A_t. Its behavior is governed by two coupled differential equations [4]:

Momentum equation in the connecting tunnel:

$$\frac{L_t}{gA_t} \cdot \frac{dQ_t}{dt} = H_{res} - Z_s - h_{f,t}$$

Continuity equation in the tower:

$$A_s \cdot \frac{dZ_s}{dt} = Q_t - Q_{turbine}$$

Where:

- Q_t: flow rate in the connecting tunnel (m³/s)
- H_{res}: water level in the main reservoir (m)
- Z_s: water level in the tower above the reference datum (m)
- $h_{f,t}$: friction loss in the connecting tunnel (m)
- L_t: connecting tunnel length (m)
- A_s: horizontal cross-sectional area of the tower (m²)
- $Q_{turbine}$: flow rate withdrawn from the system (m³/s)

Neglecting friction under constant discharge, the two equations reduce to simple harmonic oscillation with period:

$$T_s = 2\pi \sqrt{\frac{L_t \cdot A_s}{g \cdot A_t}}$$

Where:

- T_s: oscillation period of the surge tank (s)

$T_s$is proportional to $\sqrt{A_s/A_t}$ a wider tower oscillates with a longer period and smaller amplitude. The design trade-off is straightforward: greater volume means a calmer but slower response.

The Thoma Stability Criterion:

For the tank to perform its stabilizing function and not become a source of disturbance rather than a damper its cross-sectional area must satisfy the minimum condition first derived by Thoma (1910):

$$A_s \geq A_{s,Thoma} = \frac{f \cdot Q_0^2 \cdot L_t}{2g \cdot A_t \cdot H_0 \cdot h_{f0}}$$

Where:

- $A_{s,Thoma}$: minimum required cross-sectional area of the tower (m²)
- f: Darcy–Weisbach friction factor in the connecting tunnel (dimensionless)
- Q_0: initial steady-state discharge (m³/s)
- H_0: static piezometric head at the tower location (m)
- h_{f0}: static friction loss in the connecting tunnel at Q_0(m)

The criterion ensures that the energy dissipated by friction is sufficient to damp the oscillations rather than amplify them. This is a non-negotiable constraint any design falling below $A_{s,Thoma}$ is inadmissible, regardless of all other considerations [4].

Types of Surge Tanks:

Surge tanks take several forms depending on site requirements and system characteristics, of which four are most prominent:

The Simple Open Tank the basic type described above. Used where sufficient space is available and structural height poses no constraint. No equipment, no complex maintenance.

The Restricted Orifice Surge Tank incorporates a throttle in the connecting tunnel that adds hydraulic resistance, damping oscillations more rapidly and allowing A_s to be reduced below the Thoma limit while maintaining stability. The modified momentum equation:

$$\frac{L_t}{gA_t} \cdot \frac{dQ_t}{dt} = H_{res} - Z_s - h_{f,t} - h_{or}$$

$$h_{or} = \frac{Q_t^2}{2g \cdot C_d^2 \cdot A_{or}^2} \cdot \text{sign}(Q_t)$$

Where:

- h_{or}: head loss at the throttle (m) sign changes with flow direction
- C_d: throttle discharge coefficient (dimensionless)
- A_{or}: throttle orifice area (m²)

The Differential Surge Tank two concentric cylinders: a narrow inner one that responds rapidly to the initial disturbance, and a wider outer one that attenuates oscillations over the longer term. The inner provides response speed; the outer provides storage capacity in a single structure rather than two separate tanks.

The Closed Surge Tank a sealed vessel with compressed air above the water surface. Structurally lower than an open tower, but requires a periodic air repressurization system placing it between the open tank and the pressurized air vessel in terms of maintenance requirements and cost [4].

Table II.11 Air Vessel vs. Surge Tank Comparative Assessment

Criterion	Air Vessel (Hydropneumatic Tank)	Surge Tank (Standpipe)	Advantage
Protection type	Both positive surge AND sub-atmospheric (negative) phases	Positive pressure surge only; effective when H_0 is low	Air Vessel
Operating pressure	Any pressure range; pre-charge adjustable to match system	Practical limit ≈ 30 m head; tower height ≥ max piezometric	Air Vessel
Response speed	Near-instantaneous via throttle orifice	Slow water column inertia delays response	Air Vessel
Maintenance	Periodic gas recharging; orifice and gauge inspection	Minimal no pressurised components; periodic visual check	Surge Tank
Civil requirement	Compact; fits within pump station footprint	Large reinforced concrete tower; significant land area	Air Vessel
Typical application	Long-distance pressurised mains; pump-trip protection	Low-pressure penstocks; gravity mains $H_0 < 30$ m	Context-Dependent

II.4.4 Supplementary Protection Measures

Air vessels and surge tanks address the major scenarios but some systems require additional measures, either to handle what the primary devices cannot, or to reduce their required size by delegating residual conditions to supporting means. These four measures operate at distinct levels: two at the valve, one on the rotational shaft, and one in the control program.

Pressure Relief Valves (PRV):

When local pressure exceeds a pre-set threshold, the valve opens automatically and diverts a portion of the flow to a safe discharge point a collection tank or watercourse until the peak retreats below the maximum allowable limit.

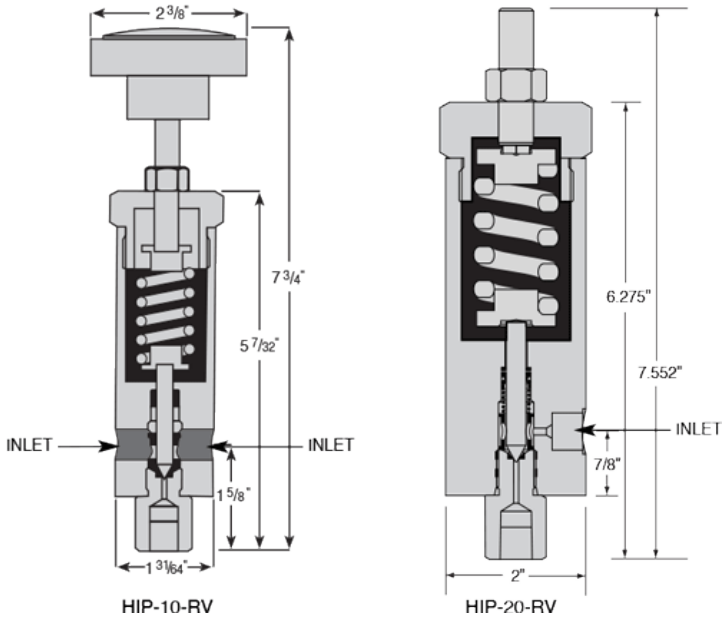

The opening threshold is set at:

$$P_{set} = (1.05 \text{ to } 1.10) \cdot P_{max,op}$$

Where:

- P_{set}: valve opening pressure (Pa)

- $P_{max,op}$: maximum system operating pressure (Pa)

The discharged flow rate upon opening is given by:

$$Q_{PRV} = C_v \cdot \sqrt{P - P_{set}}$$

Where:

- Q_{PRV}: flow rate through the valve (m^3/s)

- C_v: valve flow coefficient (specified by the manufacturer)

- P: instantaneous pressure at the valve location (Pa)

A fundamental constraint: the PRV operates in one direction only it protects exclusively against overpressure, and sub-atmospheric pressure lies entirely outside its scope. It also

requires an appropriate discharge point and periodic maintenance to guarantee response under emergency conditions [4][7].

Vacuum-Breaking Valves (*Air Inlet Valves / Vacuum Breakers*):

When absolute pressure approaches the opening threshold typically between 0.2 and 0.5 bar absolute the one-way valve admits atmospheric air into the line, forming an air pocket that locally arrests the pressure drop and prevents column separation.

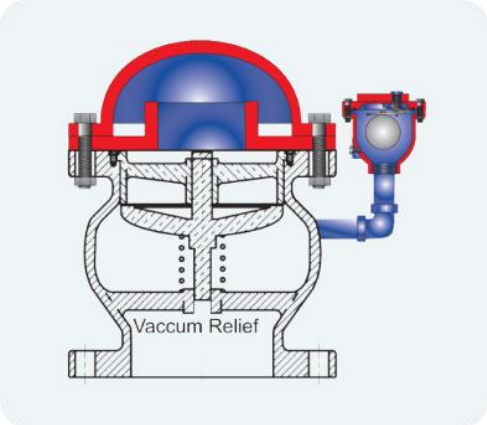

The problem lies not with the air entering but with the air leaving. As water advances, compresses the pocket, and closes it, a secondary pressure wave is generated, expressed mathematically by the air cavity collapse equation [3][4]:

$$\Delta H_{collapse} = \frac{a}{g} \cdot \frac{Q_{final} - Q_{initial}}{A}$$

Where:

- $\Delta H_{collapse}$: pressure head rise resulting from air cavity collapse (m)
- Q_{final}: flow rate after cavity closure (m³/s) - $Q_{initial}$: flow rate at the moment of cavity collapse (m³/s)
- A: pipe cross-sectional area (m²)

This is why a vacuum-breaking valve is never installed alone it is always paired with a slow-release air vent that decelerates air expulsion and attenuates the secondary closure wave [4][7].

The Flywheel (*Flywheel*):

A pump that stops suddenly releases an immediate negative wave. The flywheel prevents the "sudden" it adds rotational inertia to the unit, converting an abrupt halt into a gradual deceleration.



The governing rotation equation:

$$I_{total}\frac{d\omega}{dt} = -T_h(\omega, Q)$$

$$I_{total} = I_{pump} + I_{flywheel}$$

Where:

- I_{total}: total moment of inertia (kg·m²)

- I_{pump}: original moment of inertia of the pump and motor (kg·m²)

- $I_{flywheel}$: added moment of inertia of the flywheel (kg·m²)

- ω: angular velocity (rad/s)

- T_h: resisting hydraulic torque a function of $\omega$and Q(N·m)

The effective deceleration time which determines how much the initial negative wave is reduced:

$$T_{eff} = \frac{I_{total} \cdot \omega_0}{T_{h,0}}$$

Where:

- ω_0: rated angular velocity (rad/s)

- $T_{h,0}$: hydraulic torque at the rated operating point (N·m)

The first negative wave is the most dangerous in polymer pipelines and long transmission mains extending T_{eff} directly reduces the required size of any supplementary protection device. The cost: additional mechanical mass and a higher starting torque that necessitate reassessment of motor capacity and couplings [4][7].

Variable Frequency Drives (*VFD*):

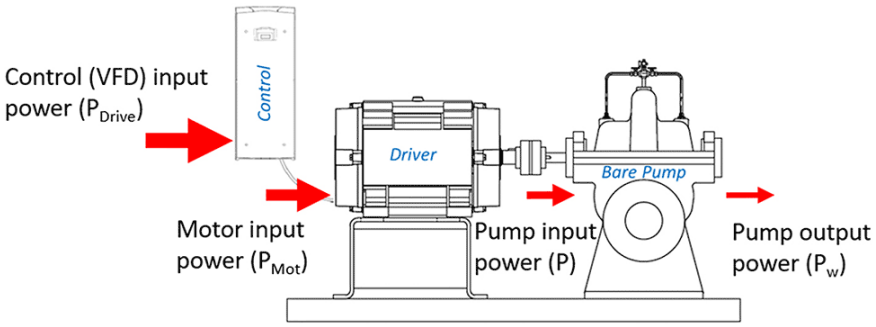

The VFD solves the same problem as the flywheel but in software, not steel. Rather than adding a rotating mass, it converts the instantaneous speed change into a programmed deceleration curve. Pump speed during shutdown:

$$\omega(t) = \omega_0 \cdot \left(1 - \frac{t}{T_{ramp}}\right)^m$$

Where:

- $\omega(t)$: instantaneous angular velocity (rad/s)

- ω_0: rated angular velocity (rad/s)

- T_{ramp}: programmed deceleration time (s)

- m: deceleration curve shape index $m = 1$linear, $m > 1$end-accelerated

Field measurements at VFD-equipped stations have demonstrated reductions of 30

The distinction from the flywheel rests on three points: no added mechanical mass, a deceleration curve adjustable in software at any time, and energy savings during partial-load operation. The trade-offs are a higher initial cost and specialized electrical maintenance [7].

Table II.12 Supplementary Water Hammer Protection Devices

Device	Mechanism	Protects Against	Optimal Application	Key Limitation
Pressure Relief Valve (PRV)	Opens at Pset = 1.05–1.10 × Pmax; diverts excess flow	Overpressure only (positive surge)	Distribution networks; pump discharge lines	No protection against sub-atmospheric pressure
Air Inlet Valve (Vacuum Breaker)	Admits air at P ≤ 0.2–0.5 bar abs.; arrests column separation	Sub-atmospheric pressure; negative surge at high points	Topographic high points on long-distance mains	Must be paired with slow-release vent to avoid secondary surge
Flywheel	Adds rotational inertia to shaft; extends pump deceleration time	Initial negative wave (pump trip reduces first ΔH)	Medium-head single-pump stations; polymer pipelines	Ineffective for valve-induced transients; increases starting torque
Variable Frequency Drive (VFD)	Replaces instantaneous shutdown with controlled ω(t) ramp	Initial negative wave (planned shutdown reduces surge 30–60%)	Pump stations with regular controlled shutdowns	No protection for uncontrolled power-failure unless UPS fitted

II.5 Advanced Considerations

II.5.1 Cavitation and Column Separation

When pressure drops during a transient event to the vapor pressure of water P_v, the liquid locally vaporizes and a vapor cavity forms, splitting the water column into two separate segments that move with relative independence.

The collapse of the vapor cavity sometimes generates a secondary shock more severe than the original wave the literature has documented cases in which the secondary pressure peak exceeded twice the Joukowsky head rise [1][3].

This is the most dangerous aspect of the water hammer phenomenon, and it is what makes column separation (*Column Separation*) the dividing line between a troublesome scenario and a catastrophic one.

Physical Mechanism:

When pressure drops to vapor pressure at 20°C:

$$P_v \approx 2340 \text{ Pa} \Leftrightarrow H_v \approx -10.2 \text{ m water column (gauge)}$$

Where:

- P_v: absolute vapor pressure (Pa)

- H_v: piezometric head corresponding to vapor pressure (m)

Water vaporizes locally at the critical node, forming a vapor cavity at constant pressure P_v that separates the water column into two segments. The cavity grows as long as

pressure remains below P_v. When a returning positive wave raises pressure above P_v, the cavity collapses abruptly the two water columns collide violently and release the secondary pressure peak.

The DVCM Model within the MOC Framework:

The standard MOC model assumes single-phase flow. Upon cavity detection, it is extended by the Discrete Vapor Cavity Model (*DVCM*), which tracks the cavity volume $\boldsymbol{\mathcal{V}_{cav}}$ at each critical node:

$$\frac{d\mathcal{V}_{cav}}{dt} = \frac{A}{2} \cdot (V^{+} - V^{-})$$

In discretized numerical form:

$$\mathcal{V}_{cav}^{n+1} = \mathcal{V}_{cav}^{n} + \frac{A \cdot \Delta t}{2} \cdot (V_P^{+} - V_P^{-})$$

Where:

- $\mathcal{V}_{cav}$: instantaneous cavity volume at the node (m³)
- A: pipe cross-sectional area (m²)
- V^{+}: downstream flow velocity (m/s)
- V^{-}: upstream flow velocity (m/s)
- Δt: time step (s)
- V_P^{+}, V_P^{-}: flow velocities in both directions at node P

The algorithm logic at each time step:

- If $H_P < H_v \rightarrow$ impose $H_P = H_v$and compute $\mathcal{V}_{cav}^{n+1}$
- If $\mathcal{V}_{cav}^{n+1} \leq 0 \rightarrow$ cavity has collapsed; the node reverts to single-phase flow and the secondary pressure wave is released [3][4].

Distributed Cavitation and Two-Phase Flow:

DVCM addresses a single point. When pressure drops to $\boldsymbol{P_v}$ along an entire pipe segment, the flow transitions to two-phase (*Two-Phase Flow*) and requires tracking the void fraction $\alpha_g$at every point. Wave celerity in the two-phase mixture is expressed as [1]:

$$\frac{1}{a_m^2} = \frac{\alpha_g \, \rho_m}{\gamma_g \cdot P_a} + \frac{(1 - \alpha_g) \, \rho_m}{K_f}$$

Where:

- a_m: wave celerity in the two-phase mixture (m/s)
- α_g: void fraction ratio of gas volume to total volume (dimensionless)
- γ_g: polytropic ratio of the gas (≈ 1.4 for air)
- P_a: local absolute pressure (Pa)
- ρ_m: mixture density (kg/m³)

The result is counter-intuitive: a void fraction as minute as $\boldsymbol{\alpha_g \sim 10^{-4}}$ is sufficient to reduce wave celerity by a full order of magnitude fundamentally altering the timing of pressure peaks and complicating their prediction. Ghidaoui et al. (2005) confirmed that this effect is one of the most prominent sources of divergence between simulation results and field measurements in systems that have not been carefully subjected to air-release procedures [1].

Critical Locations in the System:

Cavitation does not arise randomly it concentrates at three locations identified from the minimum pressure envelope prior to any design intervention:

- Geometric high points (High Points): elevated elevation *z*narrows the positive pressure margin above P_v

- Locations adjacent to closed valves: generate sharp localized negative waves

- The pump node immediately upon power failure: sudden reversal of the pressure gradient across the pump unit [3][4]

Relevance to This Study:

Both HAMMER and AFT Impulse adopt DVCM as their default model yet they differ in the mechanism by which it is activated, in the identification of critical nodes, and in the management of the transition between the two phases [3][4]. This divergence will be addressed in detail in the applied comparison of Chapter Three.

II.5.2 Unsteady Friction The Brunone–Vítkovský Model

The classical Darcy–Weisbach model assumes that wall shear stress is determined instantaneously by the mean velocity alone an assumption known as *Quasi-Steady Friction*. This is a reasonable approximation under steady flow, but it collapses under sharp transient conditions. The reason: the near-wall region responds to pressure changes far more rapidly than the flow core during acceleration phases, actual wall shear stresses are higher than the model predicts, and during deceleration phases, lower. The consequence: the classical model overestimates long-term pressure oscillations and predicts a slower attenuation than field measurements consistently record [1][8].

The Original Brunone Model (1991):

The idea is straightforward: add to the Darcy–Weisbach formulation a term proportional to the local acceleration $\boldsymbol{\partial V/\partial t}$:

$$\frac{\partial V}{\partial t} + g\frac{\partial H}{\partial x} + \frac{\lambda_q V|V|}{2D} + \frac{k}{2}\frac{\partial V}{\partial t} = 0$$

Where:

- λ_q: quasi-steady Darcy–Weisbach friction factor (dimensionless)

- k: Brunone coefficient (dimensionless)

The formulation carries a twofold weakness: it lacks a rigorous theoretical foundation, and it neglects the spatial propagation of the acceleration front that is, how the acceleration front advances in the direction opposite to wave travel. This omission limits its accuracy specifically under turbulent flow conditions.

The Vítkovský Enhanced Model (2000) IAB:

Vítkovský et al. (2000) extended the original Brunone formulation by incorporating the spatial acceleration derivative $a \cdot \partial V/\partial x$ into the unsteady friction term, establishing what is now known as the *Instantaneous Acceleration-Based* (IAB) model. The complete equation of motion with unsteady friction becomes:

$$\frac{\partial V}{\partial t} + g\frac{\partial H}{\partial x} + \frac{\lambda_q V|V|}{2D} + \frac{k}{2}\left(\frac{\partial V}{\partial t} - a\frac{\partial V}{\partial x}\right)\cdot \text{sign}(V) = 0$$

Where:

- λ_q : quasi-steady Darcy–Weisbach friction factor computed from the steady-state condition (dimensionless)

- k: Brunone coefficient derived from the Vardy–Brown C^* parameter (dimensionless)

- a: pressure wave celerity (m/s)

- sign(V): ensures friction always opposes the flow direction

This additional term not the formulation as a whole is what improves the characterization of wave attenuation under turbulent flow conditions [1][8].

Determining the Brunone Coefficient :

$$k = \frac{\sqrt{C^*}}{2}$$

where C^* is the Vardy–Brown shear decay coefficient, which varies with the flow regime [1][8]:

$$C^* = \begin{cases} 0.00476 & \text{laminar flow } (Re < 2000) \\ \dfrac{7.41}{Re^{\log(14.3/Re^{0.05})}} & \text{smooth turbulent flow } (Re > 4000) \end{cases}$$

- Re: Reynolds number of the initial steady-state flow (dimensionless)

The expression shows that C^* decreases as Re increases meaning that more intensely turbulent flow attenuates pressure waves more rapidly. The physical logic: turbulence enhances momentum exchange between the flow core and the wall, accelerating the re-establishment of the steady velocity profile.

Table 2.17 Comparison of Three Friction Models for Water Hammer Analysis

Friction Model	Expression	Accuracy (wave attenuation)	Comp. Cost	When to Use
Quasi-Steady (Darcy–Weisbach)	f_q = λ·V|V| / (2D)	Low overestimates oscillation amplitude after multiple cycles	Minimal single term per node	Short pipes (L < 500 m); preliminary design; first-peak accuracy sufficient
Brunone–Vítkovský IAB ★	f_u = f_q + (k/2)·[∂V/∂t − a·|∂V/∂x|·sign(V)]	High improved attenuation; validated for turbulent flow	Low-to-moderate two extra derivatives per node	Long mains (L > 1 000 m); high Re; wave damping accuracy required
Convolution-Based (Zielke)	f_u = f_q + (2νA/D²)·∫₀ᵗ W(t−τ)·(∂V/∂τ) dτ	Highest full velocity history; most accurate for laminar flow	High full velocity history storage required	Laminar flow (Re < 2 000); research applications; accuracy paramount

Relevance to This Study:

The study by Wéber and Hős (2021) the pivotal reference here [8] demonstrated that the Vítkovský model is the most accurate among the available formulations, and that its implementation in HAMMER yields a markedly improved description of wave attenuation compared to the quasi-steady friction used in AFT Impulse. This difference will produce a divergence in long-range attenuation accuracy even where first-peak results converge [1][8] and constitutes one of the principal axes of comparison in Chapter Four.

Zhang et al. (2024) [13] added a consequential qualification: the gap between the two models widens with increasing Re, greater line length, and lower λ_q. Long pipelines with high turbulent flow are the domain most sensitive to friction model selection and this is precisely the context in which the system under study is situated.

II.5.3 Fluid-Structure Interaction A Brief Introduction

The Saint-Venant equations assume the pipe to be a rigid boundary: it deforms radially but neither moves axially nor bends. In reality, the pipe wall is an elastic structure that responds to the internal pressure wave with longitudinal, radial, and flexural stress waves propagating through the pipe material with relative independence from the fluid wave. When the natural frequencies of the hydraulic and structural systems converge, the two interact: the actual pressure record diverges from the prediction of the uncoupled model this is Fluid-Structure Interaction (*FSI*) [4].

The Three Coupling Mechanisms:

Poisson Coupling (*Poisson Coupling*): Internal pressure oscillations expand the wall radially and contract it axially from this axial contraction a longitudinal stress wave arises, propagating at celerity:

$$a_s = \sqrt{\frac{E}{\rho_p}}$$

Where:

- a_s: longitudinal stress wave celerity in the pipe material (m/s)

- E: Young's modulus of the pipe material (Pa)

- ρ_p: pipe material density (kg/m³)

In steel pipes $a_s \approx 5100$ m/s five times higher than $a \approx 1000$ m/s. The two waves propagate at different celerities and interact repeatedly along the line.

Junction Coupling (*Junction Coupling*): At bends, valves, and fittings, hydraulic pressure forces are converted into axial structural forces and vice versa a direct energy exchange between the two waves at every transitional node.

Friction Coupling (*Friction Coupling*): Shear forces on the pipe wall feed the longitudinal stress wave with axial stresses distributed along the entire line, not only at junction points a continuous coupling, not a nodal one.

Mathematical Formulation:

The full FSI model augments the Saint-Venant system with two new variables the axial pipe wall velocity $u$and the axial stress σ_x transforming the system from two equations to four:

$$\frac{\partial H}{\partial t} + \frac{a^2}{g}\frac{\partial V}{\partial x} - \frac{2\nu a^2}{gE} \cdot \frac{\partial \sigma_x}{\partial t} = 0$$

$$\frac{\partial V}{\partial t} + g\frac{\partial H}{\partial x} + \frac{\lambda V|V|}{2D} = 0$$

$$\frac{\partial \sigma_x}{\partial t} + \rho_p a_s^2 \frac{\partial \dot{u}}{\partial x} = \nu \frac{D}{2e}\frac{\partial P}{\partial t}$$

$$\frac{\partial \dot{u}}{\partial t} + \frac{1}{\rho_p}\frac{\partial \sigma_x}{\partial x} = 0$$

Where:

- ν: Poisson's ratio of the pipe material (dimensionless)

- σ_x: axial stress in the pipe wall (Pa)

- ρ_p: pipe material density (kg/m³)

- $\dot{u}$: axial pipe wall velocity (m/s)

- e: pipe wall thickness (m)

The four-equation system possesses four characteristic families: $\pm a$ for fluid waves and $\pm a_s$ for structural waves MOC requires four characteristic lines rather than two [4].

Magnitude of the Effect and Its Practical Significance:

In buried or well-anchored water pipelines: the FSI effect modifies wave celerities by less than 5 % and pressure peaks by less than 10% in typical cases [4]. The effect becomes significant in only two situations:

- Axially free pipes suspended or unburied which amplify Poisson coupling

- Pipes with low natural frequencies that approach the transient event frequencies, triggering hydraulic-structural resonance

Why FSI Is Neglected in This Study:

Three interrelated justifications, not one:

First the pipeline is buried or well-anchored: Poisson coupling is suppressed, and the FSI effect falls below the threshold of engineering significance.

Second the objective is to compare HAMMER and AFT Impulse in their standard configurations, both of which adopt the uncoupled model by default incorporating FSI would add no discriminating value to the comparison.

Third the literature consistently affirms the adequacy of the uncoupled model whenever pressure peak modifications remain below 10 % [4].

Accordingly, the error introduced by neglecting FSI in this study is estimated at less than 5 % in wave celerity and less than 8% in pressure peaks an acceptable margin within the applied engineering context of a software comparison.

Conclusion

The phenomenon is, at its core, simple: kinetic energy converts to latent elastic energy at every disturbance. Yet this simple core conceals layers of complexity that accumulate with every approximation lifted and every assumption examined and this is precisely what the chapter revealed, progressively.

From Joukowsky's simple formula $\boldsymbol{\Delta H = \pm(a/g)\Delta V}$, the picture begins clearly: a velocity change produces a linear pressure change. Yet every assumption behind this equation carries its own limits steady friction does not describe actual damping, single-phase flow does not hold at cavitation, and a rigid pipe does not reflect the response of an elastic structure. Each section of the chapter lifted one of these approximations and replaced it with a more refined model, tracing a path of accumulation spanning two centuries: from Lagrange (1788) through Joukowsky (1898) to Streeter and Wylie, and on to Wéber and Hős (2021).

The Saint-Venant system derived from mass and momentum conservation constitutes the backbone of the chapter: two hyperbolic equations that guarantee disturbances propagate at finite celerity, solvable with precision by the Method of Characteristics or by alternative numerical methods (FDM, FEM, FVM), each with its own domain of superiority. Beneath this backbone boundary conditions, closure laws, and Michaud's formula the computational framework is completed.

Chapter III
Transient Simulation Software



III.1 Introduction

Recent decades have witnessed a fundamental transformation in the tools available for transient analysis in pressurized pipe systems. Since Bergeron (1931) established his manual graphical method in the H-Q plane, and Streeter and Wylie (1960–1993) developed the modern computational formulation of the Method of Characteristics, engineers have progressively transitioned from laborious manual calculations to integrated simulation software capable of handling networks with thousands of pipes and nodes within minutes. This transition has enabled transient analysis to extend to systems of extraordinary complexity that would have been impossible to simulate by hand [4, 5].

Yet the multiplicity of commercially available programs and the divergence of their technical philosophies and mathematical models raises a fundamental methodological question that no rigorous engineering study can afford to ignore: do these programs produce identical results when applied to the same system under the same conditions? And if discrepancies exist as recent literature indicates what are their sources, their magnitude, and their effect on engineering decisions in the domain of water hammer protection?

A comprehensive answer to this question remains an active area of research. Wéber and Hős (2021) [8] demonstrated that differences in friction models between programs produce measurable discrepancies in wave damping representation, and that these discrepancies grow with pipe length and Reynolds number. In the same context, Zhang and colleagues (2024) [13] established that the choice of friction model is the single most influential variable in transient simulation accuracy after wave celerity. This is precisely what the present study seeks to quantify and document on a real system.

The chapter follows a three-stage ascending path: it first surveys the general landscape of commercially available transient simulation software, identifying classification criteria and fundamental differences; it then presents a technically detailed characterization of the two selected programs Bentley HAMMER and AFT Impulse focusing on the differences in their mathematical models that constitute the primary axis of comparison; and it concludes by justifying the selection and defining the application framework for Chapter Four.

III.2 Overview of Transient Simulation Software

III.2.1 The Current Landscape and the Dominance of MOC

Since Streeter and Wylie established the modern computational formulation of the Method of Characteristics in the 1960s and refined it through the 1990s, MOC has become the numerical foundation upon which most commercial simulation software available today is built. This dominance stems from three mutually reinforcing factors: its high computational efficiency relative to alternative methods such as finite elements and finite volumes, its ability to handle complex boundary conditions directly, and its rigorously documented accuracy across decades of engineering applications [4, 5].

Urbanowicz and colleagues (2021) conducted a comprehensive survey of numerical methods employed in transient simulation software, concluding that more than 80

However, a shared numerical foundation does not imply identical results. These programs diverge substantially in implementation details particularly the friction model, the vapor

cavitation model, the mechanism for handling wave celerity variation in branched networks, and the method of imposing boundary conditions. These details ultimately determine the quality of predictions for pressure peaks, their timing, and wave damping across successive cycles. Ghidaoui and colleagues (2005), in their comprehensive review of water hammer theory, documented that the friction model constitutes the single most influential source of the gap between simulation results and field measurements [1].

III.2.2 Software Classification and Selection Criteria

The criteria for evaluating transient simulation software are multiple and interrelated, and can be organized into four principal axes summarized in Table 3.1. In the academic context of this study, the mathematical model axis takes precedence over all others, as it is the independent variable whose effect the study seeks to measure.

Table III.1 Survey of Commercial Transient Flow Simulation Software

Software	Developer / Country	Core Method	Friction Model	DVCM	Key Notes
Bentley HAMMER	Bentley Systems / USA	MOC	Vítkovský (IAB)	Yes	Native WaterCAD/WaterGEMS integration; dominant in urban water utilities worldwide
AFT Impulse	Applied Flow Technology / USA	MOC	Quasi-Steady (D–W)	Yes	Companion to AFT Fathom; flexible fluid properties; strong for a > 1000 m/s systems
WANDA	Deltares / Netherlands	MOC	IAB + Vardy–Brown	Yes	Most advanced unsteady friction; widely used in European water utilities
MIKE URBAN	DHI / Denmark	MOC	Quasi-Steady	Yes	Full GIS integration; preferred for urban drainage coupling in Europe
Pipe2000 / KYPIPE	KYPipe LLC / USA	MOC	Quasi-Steady	Yes	Low-cost academic tool; widely used in teaching; limited commercial adoption
InfoWorks WS Pro	Autodesk / UK–USA	MOC	Quasi-Steady	No	Dominant in UK utilities; strong asset management integration
HYTRAN	HyTran Solutions / NZ	MOC + FDM	Q-S + optional IAB	Yes	Specialised transient tool; includes column separation and gas release models
RELAP5 / TRACE	Idaho National Lab / USA	FDM (two-fluid)	Two-phase Q-S	N/A	Nuclear reactor standard; two-phase steam–water; not applicable to urban networks
OpenFOAM	OpenCFD / Open-Source	FVM (CFD)	Turbulence-based	N/A	Research CFD platform; high accuracy for specific junctions; not for full networks

Two additional criteria carry particular importance in the academic context: transparency in mathematical model documentation since no program's results can be assessed if its equations and models are not adequately documented in peer-reviewed literature and extent of use in prior comparative studies, which enables positioning the results of this study within their proper academic context [7, 8].

III.2.3 Comprehensive Comparative Table of Major Software

Table 3.2 lists the most prominent commercially available transient simulation programs currently on the market, along with their principal characteristics and primary application sectors:

Table III.2 Technical Specifications of Bentley HAMMER

Technical Feature	Specification / Value	Ref.
Core Numerical Engine		
Numerical method	MOC fixed-grid explicit (C^+: dx/dt = +a | C^-: dx/dt = −a)	[4]
CFL stability	Δt = Δx/a (exact equality) | Celerity rounding ≤ ±15%	[5]
Interior point solution	HP = (CP+CM)/2 ; VP = (g/a)·(CP−CM)/2	[4]
Friction Modelling		
Default friction model	Vítkovský IAB: f = f_q + (k/2)·[∂V/∂t − a·|∂V/∂x|·sgn(V)]	[8]
Brunone coefficient k	k = √C* | C* = 7.41/Re^0.05 × Re^(−1/log Re) (turbulent)	[8]
IAB accuracy	Wave damping error < 8% for L > 1 000 m; validated against WANDA	[8]
Cavitation (DVCM)		
DVCM criterion	Cavity forms when P < Pv = 2 340 Pa abs. (20 °C) at any node	[3]
Cavity collapse	ΔH_collapse = (a/g)·|ΔV_collapse| instantaneous secondary shock	[4]
Valve & Pump Boundaries		
Valve closure laws	Linear, quadratic, user-defined tabular; instantaneous closure supported	[4]
Pump boundaries	Pump trip, startup, VFD ramp; four-quadrant Suter curves	[7]
Protection devices	Air vessel (n = 1.2 default), surge tank, PRV, air inlet valve, VFD	[4]
Software Environment		
Ecosystem integration	Native interoperability with WaterCAD & WaterGEMS; direct EPANET .inp import	[7]
GIS / reporting	Full GIS via Bentley platform; pressure envelopes, wave animation, tabular reports	[7]

It is evident from the table that the fundamental divergence between programs does not lie in the numerical foundation since most share MOC but in the friction model, which divides programs clearly into two camps: the Brunone–Vítkovský camp adopted by HAMMER, WANDA, and HYTRAN, and the quasi-steady friction camp adopted by AFT Impulse, KYPIPE, and InfoWorks. Wéber and Hős (2021) documented that this division produces measurable discrepancies in damping representation, particularly in long pipes [8].

It should be noted that this table is limited to widely used commercial programs. Specialized research programs such as TransAT and OpenFOAM, which employ alternative numerical methods, fall outside the scope of standard engineering practice.

III.3 Bentley HAMMER

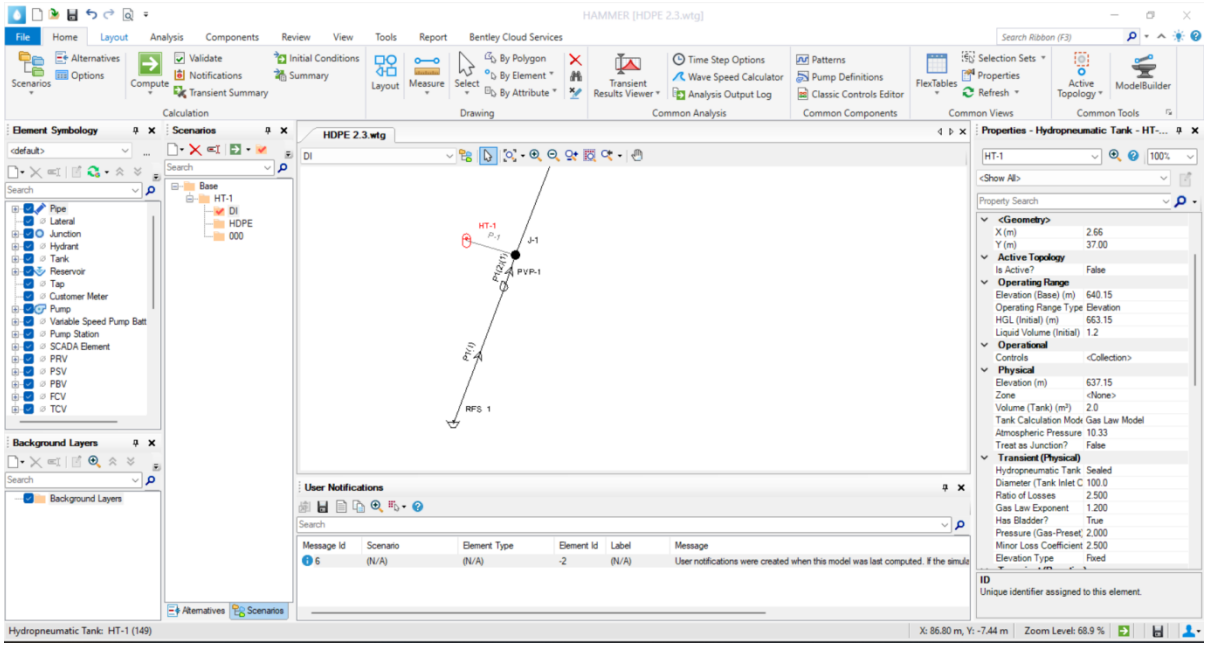

[Figure III 1 Main Interface of— Bently HAMMER]

III.3.1 Historical Background and Numerical Foundation

The origins of the HAMMER program date to the late 1980s, when Haestad Methods developed its first version as a specialized tool for water hammer analysis in water distribution networks, grounding its initial computational structure in the formulation established by Streeter and Wylie for the Method of Characteristics. In 2005, Bentley Systems acquired Haestad Methods, and the program joined Bentley's comprehensive suite of engineering software, retaining its name while its capabilities were expanded through successive releases that added advanced friction models and broader modeling capacities. Today, HAMMER is among the most extensively documented transient analysis programs in the peer-reviewed literature pertaining to water networks, and has been employed in numerous studies as a reference for result verification and model comparison [7, 8].

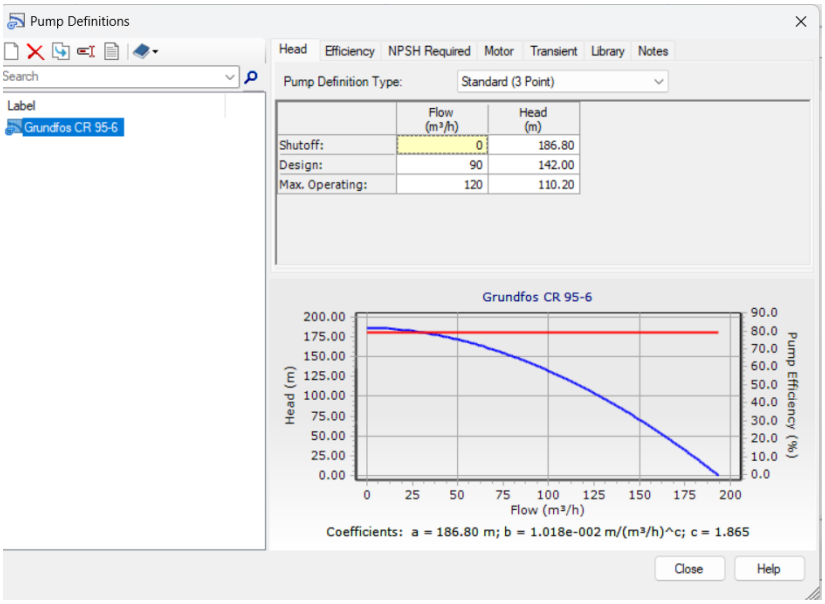

[Figure III 2 Pump Definition Window — Grundfos CR 95-6 Properties in Bentley HAMMER]

HAMMER employs the Method of Characteristics (MOC) as its core computational engine, applying the explicit solution scheme for interior points derived in Section 2.3.1. The spatial-temporal grid is built on a unified time step for the entire system that respects the CFL condition:

$$\Delta t = \frac{\Delta x}{a}$$

Where:

- Δt: unified time step for the entire system (s)
- Δx: spatial discretization of each pipe (m)
- a: pressure wave celerity in the pipe (m/s)

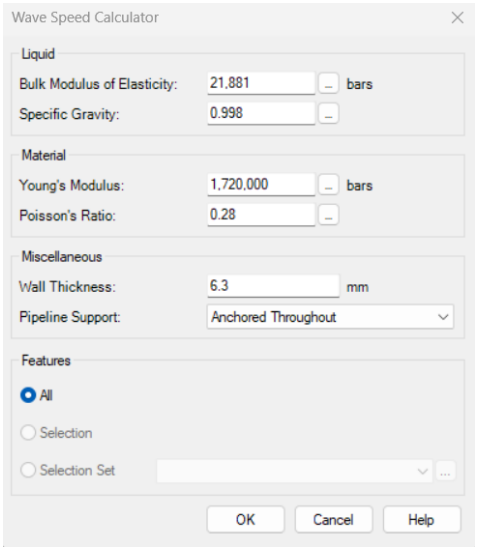

[Figure III 3 Wave Speed Calculation Window in Bentley HAMMER]

When wave celerities vary between pipes which is the common case in real networks the program employs a wave celerity adjustment mechanism of no more than 15% to ensure a unified time step, documenting this adjustment in the simulation report and alerting the user to any pipe whose adjustment exceeds 5% [7][4].

III.3.2 Hydraulic Modeling

The friction model constitutes HAMMER's most prominent technical distinction relative to many of its competitors. The program employs the Brunone–Vítkovský unsteady friction model (IAB), which adds to the classical Darcy–Weisbach term a contribution proportional to both local and convective acceleration as documented in Section 2.5.2. The Brunone coefficient k is computed automatically from the Vardy–Brown decay coefficient C^*according to the flow regime laminar or turbulent without requiring user intervention. Wéber and Hős (2021) demonstrated that this model produces better agreement with experimental measurements, particularly in long pipes and at high Reynolds numbers, and that its implementation in HAMMER improves damping representation considerably relative to quasi-steady friction [8].

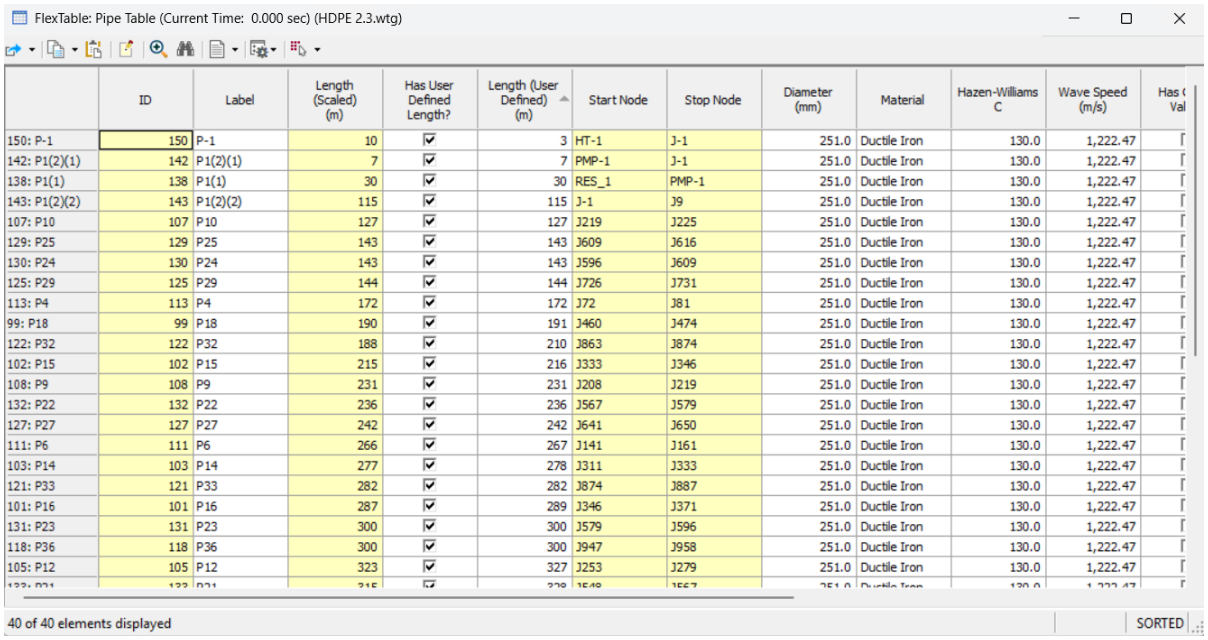
FlexTable: Pipe Table (Current Time: 0.000 sec) (HDPE 2.3.wtg)

	ID	Label	Length (Scaled) (m)	Has User Defined Length?	Length (User Defined) (m)	Start Node	Stop Node	Diameter (mm)	Material	Hazen-Williams C	Wave Speed (m/s)	Has (Val
150: P-1	150	P-1	10	☑	3	HT-1	J-1	251.0	Ductile Iron	130.0	1,222.47	
142: P1(2)(1)	142	P1(2)(1)	7	☑	7	PMP-1	J-1	251.0	Ductile Iron	130.0	1,222.47	
138: P1(1)	138	P1(1)	30	☑	30	RES_1	PMP-1	251.0	Ductile Iron	130.0	1,222.47	
143: P1(2)(2)	143	P1(2)(2)	115	☑	115	J-1	J9	251.0	Ductile Iron	130.0	1,222.47	
107: P10	107	P10	127	☑	127	J219	J225	251.0	Ductile Iron	130.0	1,222.47	
129: P25	129	P25	143	☑	143	J609	J616	251.0	Ductile Iron	130.0	1,222.47	
130: P24	130	P24	143	☑	143	J596	J609	251.0	Ductile Iron	130.0	1,222.47	
125: P29	125	P29	144	☑	144	J726	J731	251.0	Ductile Iron	130.0	1,222.47	
113: P4	113	P4	172	☑	172	J72	J81	251.0	Ductile Iron	130.0	1,222.47	
99: P18	99	P18	190	☑	191	J460	J474	251.0	Ductile Iron	130.0	1,222.47	
122: P32	122	P32	188	☑	210	J863	J874	251.0	Ductile Iron	130.0	1,222.47	
102: P15	102	P15	215	☑	216	J333	J346	251.0	Ductile Iron	130.0	1,222.47	
108: P9	108	P9	231	☑	231	J208	J219	251.0	Ductile Iron	130.0	1,222.47	
132: P22	132	P22	236	☑	236	J567	J579	251.0	Ductile Iron	130.0	1,222.47	
127: P27	127	P27	242	☑	242	J641	J650	251.0	Ductile Iron	130.0	1,222.47	
111: P6	111	P6	266	☑	267	J141	J161	251.0	Ductile Iron	130.0	1,222.47	
103: P14	103	P14	277	☑	278	J311	J333	251.0	Ductile Iron	130.0	1,222.47	
121: P33	121	P33	282	☑	282	J874	J887	251.0	Ductile Iron	130.0	1,222.47	
101: P16	101	P16	287	☑	289	J346	J371	251.0	Ductile Iron	130.0	1,222.47	
131: P23	131	P23	300	☑	300	J579	J596	251.0	Ductile Iron	130.0	1,222.47	
118: P36	118	P36	300	☑	300	J947	J958	251.0	Ductile Iron	130.0	1,222.47	
105: P12	105	P12	323	☑	327	J253	J279	251.0	Ductile Iron	130.0	1,222.47	

40 of 40 elements displayed SORTED

[Figure III 4 Pipe Properties Table in Bentley HAMMER — SR2–SR3 Network]

The vapor cavitation model employs DVCM at every critical node as documented in Section II.5.1, where pressure is capped at the vapor pressure limit and cavity volume is tracked through an independent continuity equation until collapse, at which point the secondary pressure peak is released. The program allows the user to identify critical nodes manually or to rely on automatic detection, with the option to adjust vapor pressure values according to fluid temperature [3, 4].

Boundary conditions: HAMMER supports a broad spectrum of boundary conditions including constant- and variable-head reservoirs; pump sets with four-quadrant curves with support for parallel and series configurations; isolation and control valves with programmable closure laws following the linear, quadratic, and two-phase patterns treated in

Section II.3.6; pressurized air vessels under the polytropic law; surge tanks subject to the Thoma stability criterion; and pressure relief and vacuum-breaking valves.

III.3.3 Integration with Other Engineering Environments

HAMMER is distinguished by its organic integration with Bentley's engineering software suite, particularly WaterCAD and WaterGEMS the most widely used steady-state water distribution network modeling programs. In practice, this integration means that a network model built in WaterCAD is imported directly into HAMMER without re-entering data, retaining all pipe and component properties along with the steady-state results piezometric heads, flow rates, and velocities which constitute the initial conditions for the transient simulation as documented in Section II.2.5. This integration substantially reduces setup time and lowers the probability of data entry errors in large projects, making it the preferred choice for integrated design projects that combine steady-state and transient analysis within a single environment [7].

III.3.4 Strengths and Limitations

HAMMER's strengths center on four principal aspects: the advanced IAB friction model that delivers more accurate damping representation and outperforms quasi-steady friction in long pipes and high-turbulence flow as established by peer-reviewed literature; seamless integration with broader water network modeling environments that reduces simulation preparation effort; a wide academic documentation base in water network literature that makes its results verifiable and comparable; and a user interface oriented toward water resources engineers that simplifies data entry and result interpretation.

Limitations include: the requirement for a WaterCAD or WaterGEMS license to fully benefit from the integration, which raises the total system cost; limited flexibility in modeling non-water industrial systems such as oil and gas pipelines and industrial cooling circuits; and insufficient detailed technical documentation of certain internal implementation algorithms, which can occasionally complicate interpretation of discrepancies with results from other programs.

III.3.5 Version Used

This study employs Bentley openflow HAMMER 2024 The program operates on Windows with standard hardware requirements that do not demand specialized processors for medium-scale networks.

It should be noted that the program's internal technical parameters particularly the mechanism for computing the Brunone coefficient k, time step control, and wave celerity adjustment management are documented in the official user manual and confirmed by peer-reviewed literature including the study of Wéber and Hős (2021) [8], ensuring the verifiability and reproducibility of this study's results.

III.4 AFT Impulse

III.4.1 Historical Background and Numerical Foundation

Applied Flow Technology developed AFT Impulse in the early 1990s as a natural extension of its flagship program AFT Fathom, dedicated to steady-state pipe network analysis. From its inception, the program targeted the process industries sector oil and gas, chemicals, power generation, and cooling systems a focus that shaped its design philosophy and endowed it with broad operational flexibility in handling multiple fluids and diverse operating conditions. Over three decades, the program developed continuously through successive releases and has come to be widely used in large industrial projects worldwide, though its academic documentation in water network literature specifically remains more limited than that of HAMMER and WANDA [7].

It should be noted that applied flow technology was subsequently acquired and rebranded as datacor , thought the aft Impulse product line has retained its original name and continues to be developed and marketed under the aft brand within the datacor portfolio.

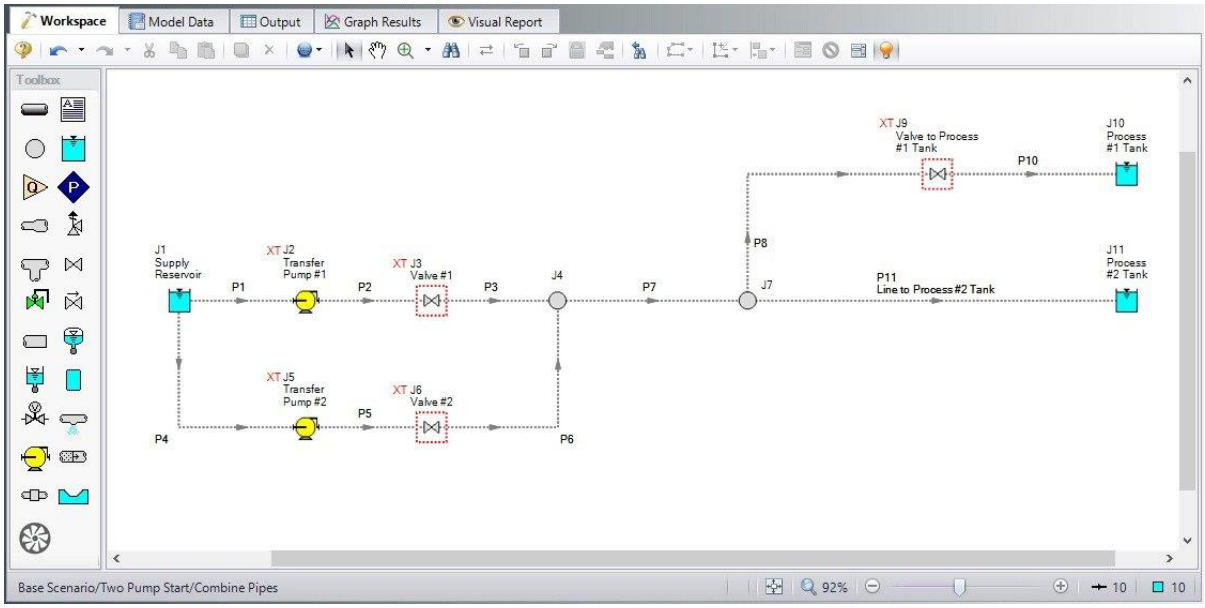

[Figure III 5 Main Interface of— AFT Impulse]

AFT Impulse employs the Method of Characteristics (MOC) as its core computational engine with the same explicit scheme adopted in HAMMER. The spatial-temporal grid is built in compliance with the CFL condition:

$$\Delta t \leq \frac{\Delta x}{a}$$

Where:

- Δt: time step (s)

- Δx: pipe spatial discretization (m)

- a: pressure wave celerity (m/s)

The program handles wave celerity variation in branched networks through linear interpolation between grid points rather than adjusting wave celerities as HAMMER does a mechanism that introduces slight numerical dispersion that artificially smooths the wave front in networks with pipes of heterogeneous properties [5].

III.4.2 Hydraulic Modeling Friction, Cavitation, and Boundary Conditions

The friction model: AFT Impulse employs quasi-steady friction as its default and only integrated model in its standard releases, determining wall shear stress instantaneously from the mean instantaneous velocity alone via the Darcy–Weisbach equation with no acceleration correction. As documented in Section 2.5.2, this choice leads to overestimation of long-term pressure oscillations and exhibits slower damping than field measurements record. The developer justifies this choice on the grounds that quasi-steady friction provides a conservative estimate of pressure peaks overestimating rather than underestimating which furnishes an additional safety margin in engineering design and aligns with the industrial sector's philosophy of preferring caution over precision when structural safety is at stake [7, 8].

The vapor cavitation model employs DVCM in a manner similar in principle to HAMMER, with an implementation difference in the detection mechanism: AFT Impulse applies fully automatic detection of critical nodes without requiring user identification, and allows vapor pressure values to be adjusted by fluid type and temperature from the integrated fluid database [3, 4].

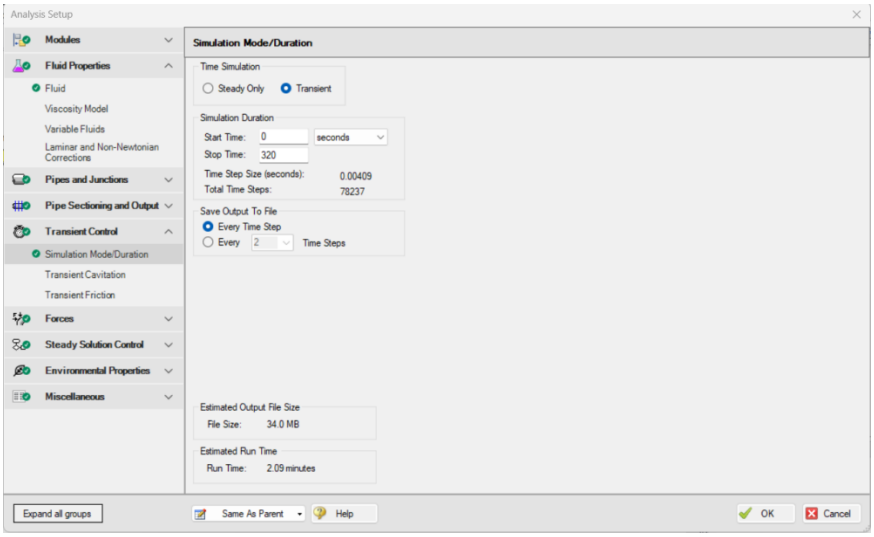

[Figure III 6 Analysis Setup Screen — AFT Impulse]

Boundary conditions: AFT Impulse supports a broad spectrum of boundary conditions including reservoirs and tanks of variable volume; pump sets with four-quadrant curves with support for variable frequency drives (VFD) and programmable deceleration curves; multiple valve types with customizable closure laws; pressurized air vessels, surge tanks, pressure relief valves, and vacuum-breaking valves. The program is distinguished by its extensive

support for multiple fluid types including hydrocarbons, chemicals, and industrial transport fluids through a database encompassing the properties of hundreds of industrial fluids.

III.4.3 Operational Flexibility and Industrial Applications

AFT Impulse surpasses many of its competitors in operational flexibility, enabling the modeling of hydraulic systems of considerable complexity that combine fluids of varying properties and pipes of heterogeneous materials and dimensions within a single integrated network. This flexibility manifests in three principal aspects: a broad fluid database covering the spectrum from water to heavy hydrocarbons through liquefied gases and industrial chemicals; the capacity to model refrigeration, heating, and high-pressure systems common in refineries, power plants, and chemical facilities; and a flexible user interface that allows defining custom components not present in the standard component library through programmable performance equations.

Engineering literature has documented AFT Impulse's application across a wide range of uses that extend beyond water networks to include crude oil pumping systems, petroleum product transmission lines, cooling systems in power plants, and industrial steam distribution networks. It should be noted that this application diversity while an advantage in industrial contexts makes the program less specialized in the requirements of municipal water networks than HAMMER, which was originally built for that specific purpose [7].

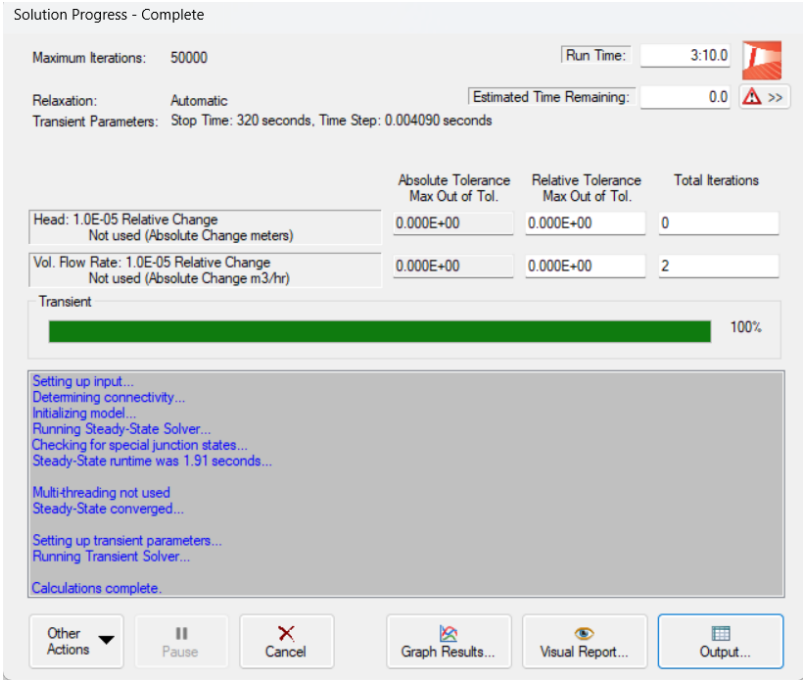

[Figure III 7 Solution window — AFT Impulse]

III.4.4 Strengths and Limitations

AFT Impulse's strengths center on four aspects: exceptional flexibility in modeling diverse fluids and systems that makes it the most suitable choice for industrial applications outside the water sector; seamless integration with AFT Fathom for steady-state calculations ensuring accurate transition to transient simulation; conservative estimation of pressure peaks

that aligns with the philosophy of safe design in the industrial sector; and a flexible user interface oriented toward industrial engineers that permits extensive customization of components and parameters.

Limitations include: the quasi-steady friction model that overestimates long-term oscillations and reduces accuracy in predicting progressive wave damping as established by peer-reviewed literature; limited integration with specialized water network modeling environments compared to HAMMER; and relatively sparse peer-reviewed academic documentation in water network applications specifically, which can occasionally complicate reliance on independent references to verify its results in this context.

III.4.5 Version Used

This study employs AFT Impulse Version 9 the version documented by Wéber and Hős (2021) [8] in their comprehensive friction model comparison is 6

III.5 Structural Comparison Between the Two Programs

III.5.1 Similarities Shared Assumptions

Despite differences in each program's philosophy, original application sector, and development history, HAMMER and AFT Impulse share a set of foundational assumptions and methodologies that render the comparison between them methodologically meaningful for if the two programs diverged in their major numerical foundations, the comparison would be a comparison of methods rather than a comparison of implementations of the same method.

The two programs share the use of one-dimensional MOC as their computational engine; the neglect of fluid-structure interaction (FSI) as a justified assumption for standard engineering applications as documented in Section II.5.3 where its effect modifies wave celerities by less than 5

These shared elements collectively establish a solid methodological common ground, ensuring that any discrepancy in results between the two programs is attributable to specific implementation differences rather than to any difference in theoretical foundation.

III.6 Justification of Selection and Transition to the Case Study

III.6.1 Grounds for Selecting the Two Programs

The selection of Bentley HAMMER and AFT Impulse was not arbitrary it rested on a set of interrelated methodological and technical grounds that make this particular selection capable of answering the central research question of this study.

First Genuine Representation of Two Distinct Camps

The two programs clearly represent two philosophically distinct camps in transient friction modeling IAB versus quasi-steady which is precisely the variable whose effect on simulation accuracy this study seeks to measure. Had two programs sharing the same model been selected, the comparison would have lost its essential methodological value and degenerated into a comparison of interfaces rather than models. More importantly, both

camps are present in the actual engineering software market and applied daily in real projects, making the comparison between them of immediate practical value rather than merely academic interest.

Second Substantial Presence in Peer-Reviewed Literature

Both programs are sufficiently documented in peer-reviewed scientific literature to permit comparison and verification. HAMMER's use is documented in numerous water network studies, foremost among them Boulos and colleagues (2005) [7] and Vargas and colleagues (2025) [10]. AFT Impulse has attracted growing academic attention in comparative friction model studies, notably Wéber and Hős (2021) [8], which constitutes one of the pivotal references in this study. This dual presence in the literature ensures the independent verifiability of this study's results.

Third Reliable Integration with Steady-State Calculations

Each program integrates with an established steady-state modeling environment HAMMER with WaterCAD and AFT Impulse with AFT Fathom ensuring accurate and reliable transition from initial conditions to transient simulation. As documented in Section 2.2.5, the validity of the initial conditions is a fundamental prerequisite for the validity of the comparison since any error in the steady state amplifies through the subsequent transient phases and makes it difficult to isolate the effect of the friction model.

Fourth Availability and Technical Transparency

Both programs are available under licensed academic versions and supported by technical documentation that permits verification of modeling parameters and assumptions. This requirement is indispensable in any objective scientific comparison since result discrepancies cannot be interpreted without knowledge of each program's internal implementation details.

III.6.2 Their Application in the Case Study Chapter Four

The two programs are applied in Chapter Four to a real pumping system that constitutes the central case study of this thesis. The application follows a strictly unified methodological path that ensures all result discrepancies are attributable to modeling differences rather than to any difference in inputs, conditions, or procedures.

The same system with its complete engineering and hydraulic properties is entered into both programs; initial conditions are determined from identical steady-state calculations; the same transient scenarios are applied to both programs under unified conditions; and results are compared according to the criteria defined in Section 3.5.3 pressure peaks, damping, timing, and pressure envelopes along the pipeline.

Chapter Four will address the pivotal question that has framed this study from its outset: do the two programs produce sufficiently convergent results to be used interchangeably in engineering practice, or do the differences in friction modeling lead to discrepancies that warrant attention when selecting a simulation tool? Answering this question with quantitative evidence from a real system is the original scientific contribution this study offers to the specialized literature.

III.7 Conclusion

This chapter surveyed the general landscape of commercially available water hammer simulation software, then progressively narrowed its focus toward the two programs selected for the applied study, establishing the reference framework upon which the comparison in Chapter Four rests.

The survey revealed that MOC's dominance in the transient simulation software market does not imply homogeneity in results on the contrary, the fundamental divergence between programs lies in implementation details rather than in the numerical foundation. Most prominent among these details is the friction model, which divides programs clearly into two camps: unsteady friction models led by Brunone–Vítkovský, and quasi-steady friction models more prevalent in industrial applications. Wéber and Hős (2021) [8] and Zhang and colleagues (2024) [13] both demonstrated that this division produces measurable discrepancies in damping accuracy that grow with pipe length and Reynolds number.

The two selected programs genuinely represent these two camps, supported by interrelated methodological and technical grounds: HAMMER with the Brunone–Vítkovský model that is more accurate in damping characterization and more widely documented in water network literature; and AFT Impulse with quasi-steady friction that is more prevalent in industrial applications and more conservative in peak estimation. Their shared use of one-dimensional MOC, the DVCM cavitation model, and the neglect of FSI makes the comparison between them a clean comparison in which the effect of the friction model is isolated in a methodologically sound manner.

This study occupies a distinctive position in the current academic landscape by applying both programs simultaneously to a single real system under unified conditions, going beyond theoretical comparative studies that evaluate model differences without direct field application. Chapter Four will translate the theoretical framework established in Chapters Two and Three into direct quantitative evidence from a real pumping system, delivering a documented answer to the central question of this thesis.

Chapter IV
Case Study: Simulation & Analysis

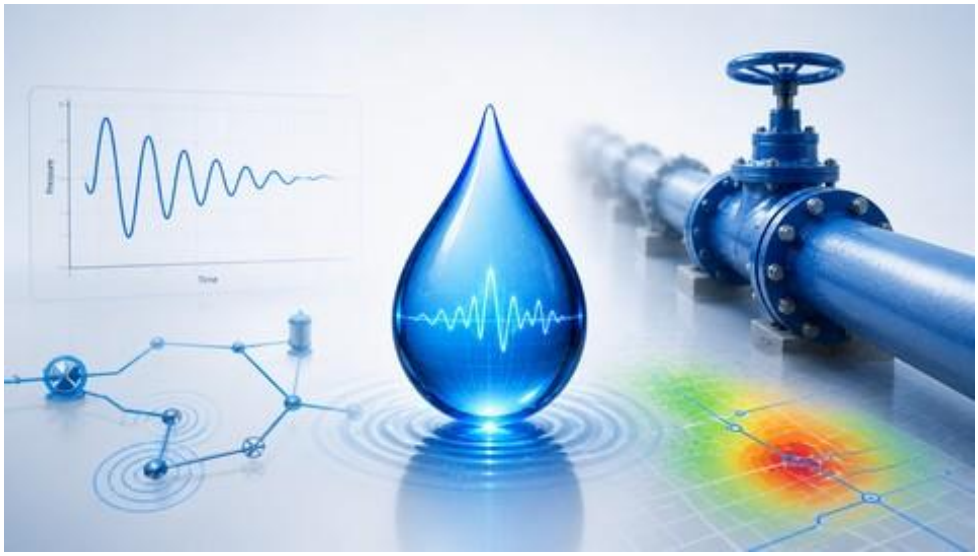

IV.1 System Description and Model Construction

IV.1.1 Presentation of the Study Area

Our study area is part of the territory of the wilaya of In Guezzam created in 2019 and officially recognized in 2021, it is one of the oldest settlements in the Algerian deep South. This wilaya has been ranked among the wilayas of the country since 2021. It is located approximately **400 km** south of the wilaya of Tamanrasset, **2330 km** from the capital Algiers, on the border between Algeria and Niger. It is bounded by:

- To the north by the wilaya of Tamanrasset;
- To the west by the wilaya of Bordj Badji Mokhtar;
- To the south by Mali and Niger.

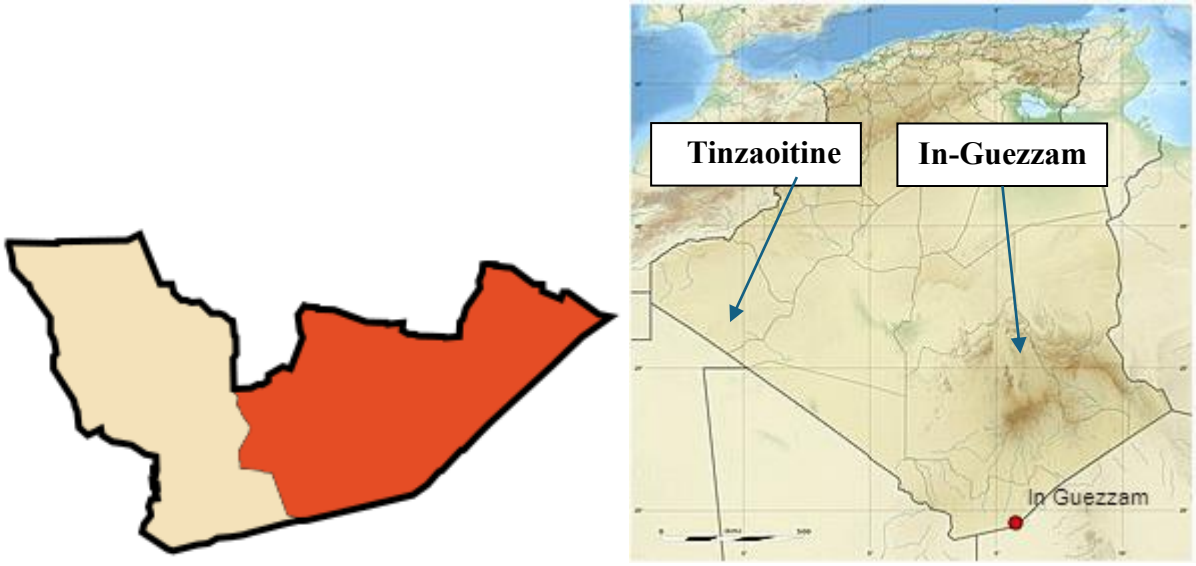

Figure IV-1 : Administrative location of the study area

II.1. Boundaries of the Study Area

Our project involves a transfer from the Abalekan area to the Djbal Lahdid area, which is part of the **Tin séririne** basin, located in the south-eastern part of the central Hoggar, between coordinates 20° and 22° North latitude and 6° and 8° East longitude. The region consists of plateaus and hills of varying elevation, notably the Djebel Amaskor, which forms an impassable barrier toward the interior of the basin.

The hydrographic network is of low density; the Oued Tin Tarabine and the Oued Tinsseghirine occasionally provide makeshift access to the interior zones of the basin.

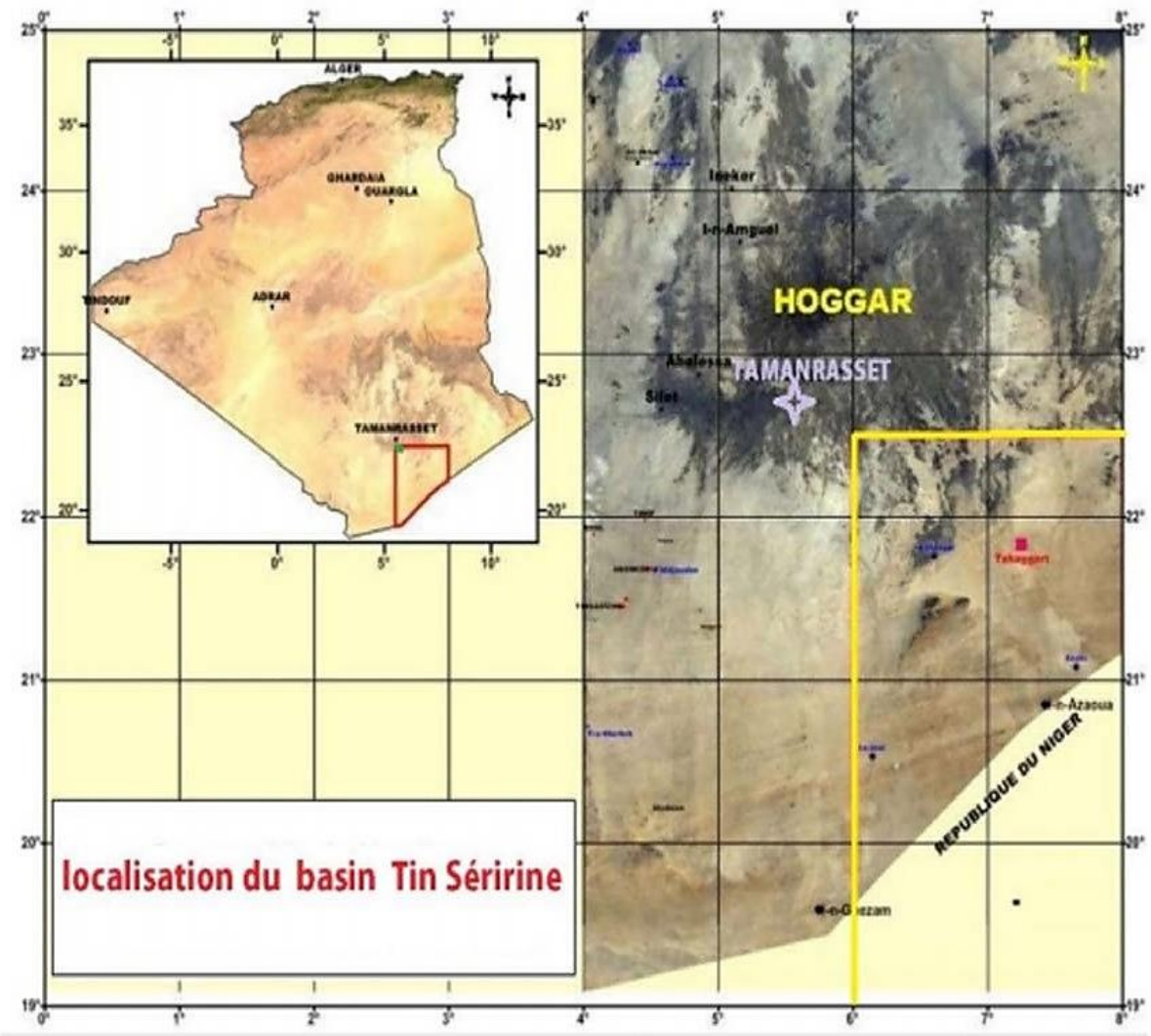

Figure IV-2 : Location of the Tin Séririne basin

II.2 Climate and Seismicity of the Study Area:

According to the various climatic parameters (1987–2018) provided by the National Meteorological Office in 2019 (temperature, precipitation, wind, evaporation, humidity, etc.), the climate is hyperarid and is characterized by low and irregular rainfall, with an average of approximately 30 mm/year. Temperatures are high during the summer season, potentially exceeding 45°C, while in winter they are generally mild, with average temperatures of 10 to 20°C. Winds are relatively frequent and irregular, playing an important role in the formation of ergs and regs. Their speed is significant from April to July, triggering during this period the sirocco and sandstorms, accompanied by a very high evaporation rate (approximately 6,621 mm/year).

The seismic hazard map established by the Applied Research Center in Earthquake Engineering shows that the investigated site belongs to "Zone 0", where seismicity is negligible (Algerian Seismic Regulations 99/version 2003).

II.3. Geological Context of the Tin Séririne Basin

The region has been the subject of extensive geological research, particularly that conducted by the Center for Research and Exploitation of Materials (1988–2003) of the High Commission for Research. The geology of the area is divided into three distinct domains.

First, the basement, present in the terrains of Laouni, Azrou-n-fad, Serouenout, and Issalane, comprises two Paleo-Proterozoic metamorphic assemblages.
The Lower Proterozoic is characterized by intensely metamorphosed gneisses, located east of the major fault at 8°30', belonging to the structure of the "Issalane massif". The Middle Proterozoic reveals varied formations such as biotite-amphibole gneisses, micaschists, and quartzites. Finally, the Terminal Proterozoic occupies nearly the entire region, composed mainly of syntectonic and post-tectonic granites. The Pharusian series present various types of granites, including heterogeneous migmatitic granites, calc-alkaline mixed biotite granites, and intrusive granites or "Taourits". The associated dykes and intrusions comprise different compositions, acidic (rhyolite, microgranites) or intermediate (andesitic microgranites), as well as dioritic or granodioritic rock intrusions cutting through the basement. In the Suggarien series, a significant portion consists of granites, such as the syntectonic migmatitic granites of Tafedest and the mixed granites of Atakor, both post-tectonic and of limited extent.

II.4. Main Water Resources

The peripheral region of the Hoggar features intra-mountain depressions that constitute the main hydrogeological basins, forming alluvial depressions that collect runoff water. Infiltration during floods leads to subsurface flows in the region's main wadis. The resulting underflow resources are poorly controlled, with significant groundwater losses. The aquifer system of the Tin Zaouatine Basin includes formations ranging from the Primary to the Quaternary periods. The Primary formations, affected by tectonic activity, are water-bearing near outcrops. The Secondary, Tertiary, and Quaternary formations form extensive aquifers extending as far as Mali. Groundwater in these formations is classified into four zones, including the basement aquifer, the Cambro-Ordovician sandstone aquifer, the Continental Intercalary sandstone aquifer, and the underflow aquifer. Static water levels in boreholes and wells range from 5.51 to 6.70 m. Quaternary deposits act as a drainage zone for the Cambro-Ordovician aquifer. The various aquifers are exploited through wells, and the underflow aquifer is supplied at the surface during floods, characterizing a porous physical environment with continuous flow.

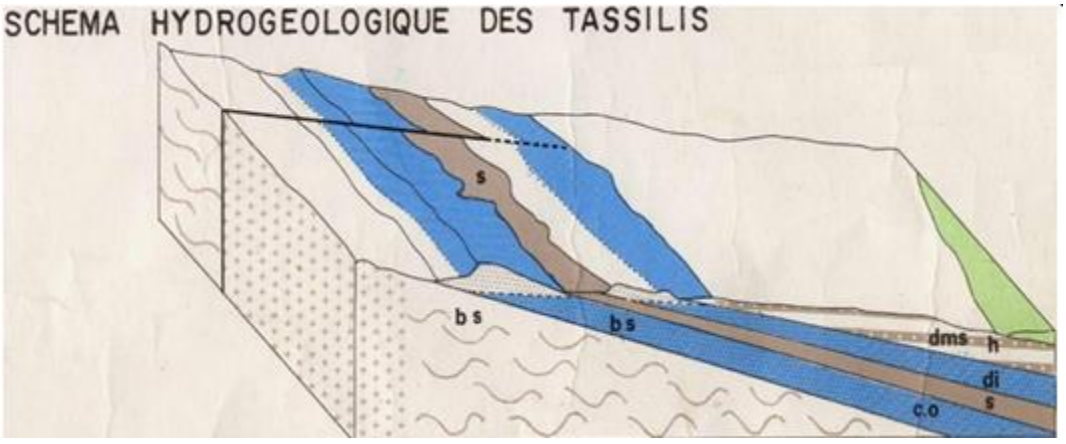

Figure IV-3 : Hydrogeological diagram of the Tassilis

Existing and Planned Production Sites

The production sites in the regions of In Guezzam and Tin Zaouatine, completed or planned by the DRE. Currently, three operational boreholes exist, namely Abelkane bis and Tafassasset bis in In Guezzam, producing 18 l/s (1,555 m^{33}/day) and 13 l/s (1,123 m^{33}/day)

respectively. Two planned boreholes in the same region, Tafassasset 2 and In ghassane 2, are not yet in operation. In the Tin Zaouatine region, the existing borehole In ghassane 1 produces 5 l/s (432 m^{3}/day), while the planned borehole In ghassane 2 is currently under development.

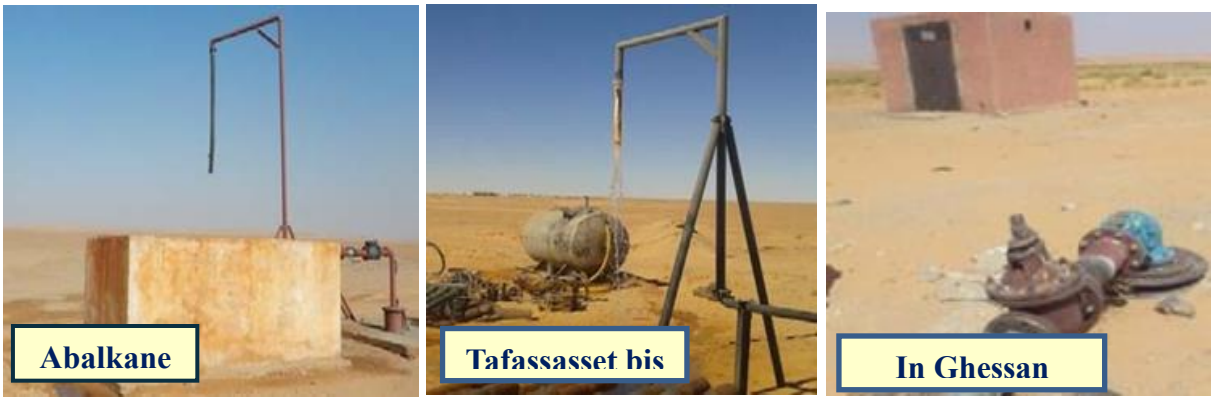

Figure IV-4 : Existing boreholes



Figure IV-5 : Location of existing and planned boreholes (In Guezzam Region)

III. Drinking Water Supply System for the Units

III.1. Estimation of Current Consumption

The exact quantity currently consumed by each unit is not clearly defined due to various factors, namely:

- Supply via tanker trucks,
- Irregular water supply,
- Absence of a Drinking Water Supply (DWS) system.

Furthermore, due to the distance from production sites and the absence of DWS systems, actual consumption is lower than the "normal" consumption that would be observed with a regular water supply. The current effective consumption of each unit is estimated on the basis of one to two tanker trucks with a capacity of 14 m^3 ³ per day, as indicated in Table 1.

Tableau IV-1 : Actual current consumption of existing units

Region	The unit a supplied		Quantity (m^3/j)
In Guazzem	Tafassasset	Tafassasset 1	**14**
		Tafassasset 2	**14**
		Tiririne 2	**14**
		Tiririne 3	**14**
	Kbar El Mait		**14**
	Djabal lahdid **(*)**		**14**
	Abelkane	Abelkane 1	**28**
		Abelkane 2	**14**
		Abelkane 3	**14**
Tin zaouatine	**El Khangua**		**14**

III.2. Water Supply Mode eau

Each unit is served by tanker trucks with a capacity of 14 m^{3}³. Inside the unit, the drinking water supply system consists of metal tanks placed on the ground, positioned behind the Saharan cabins (chalets, canteen, and sanitary facilities), to which they are connected.

The small metal tanks are regularly filled by the tanker trucks, and they supply the chalets, canteen, and sanitary facilities through pumps fitted with pressure boosters. An explanatory diagram is presented below.

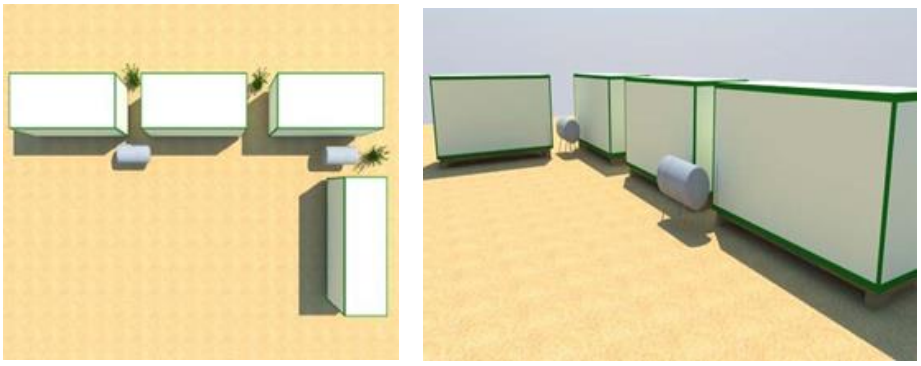

Figure IV-6 : Water supply mode within the units

III.3. Evolution of Consumers

The various users identified on site during the field survey are listed in Table 2.
Tableau IV-2 : Inventory of current and planned consumers

Region	Unit à alimenter		Nombre	
			Actuel	Future
In Guezzem	Tafassasset	Tafassasset 1	350	**1000**
		Tafassasset 2	300	**1000**
		Total	**750**	2000
	Hassi el Mardoum (*)		**300**	1000
	Tiririne	Tiririne 1 **(*)**	300	**1000**
		Tiririne 2	300	**1000**
		Tiririne 3	350	**1000**
		Total	**950**	3000
	Djabal lahdid **(*)**		**350**	1000
	Kbar El Mait		**350**	1000
	Timoultine **(*)**		**300**	1000
	Abelkane	Abelkane 1	700	**1000**
		Abelkane 2	300	**1000**
		Abelkane 3	300	**1000**
		Total	**1300**	3000
Tin zaouatine	**El Khangua**		300	1000

(*) Units planned

This study focuses exclusively on the intermediate segment SR2–SR3, with a length of approximately 18.6 km, for two reasons: first, this segment represents the section most susceptible to water hammer due to its varied topography and operating conditions; second, the first and last segments exhibit a different hydraulic behavior that does not call for the targeted comparative analysis.

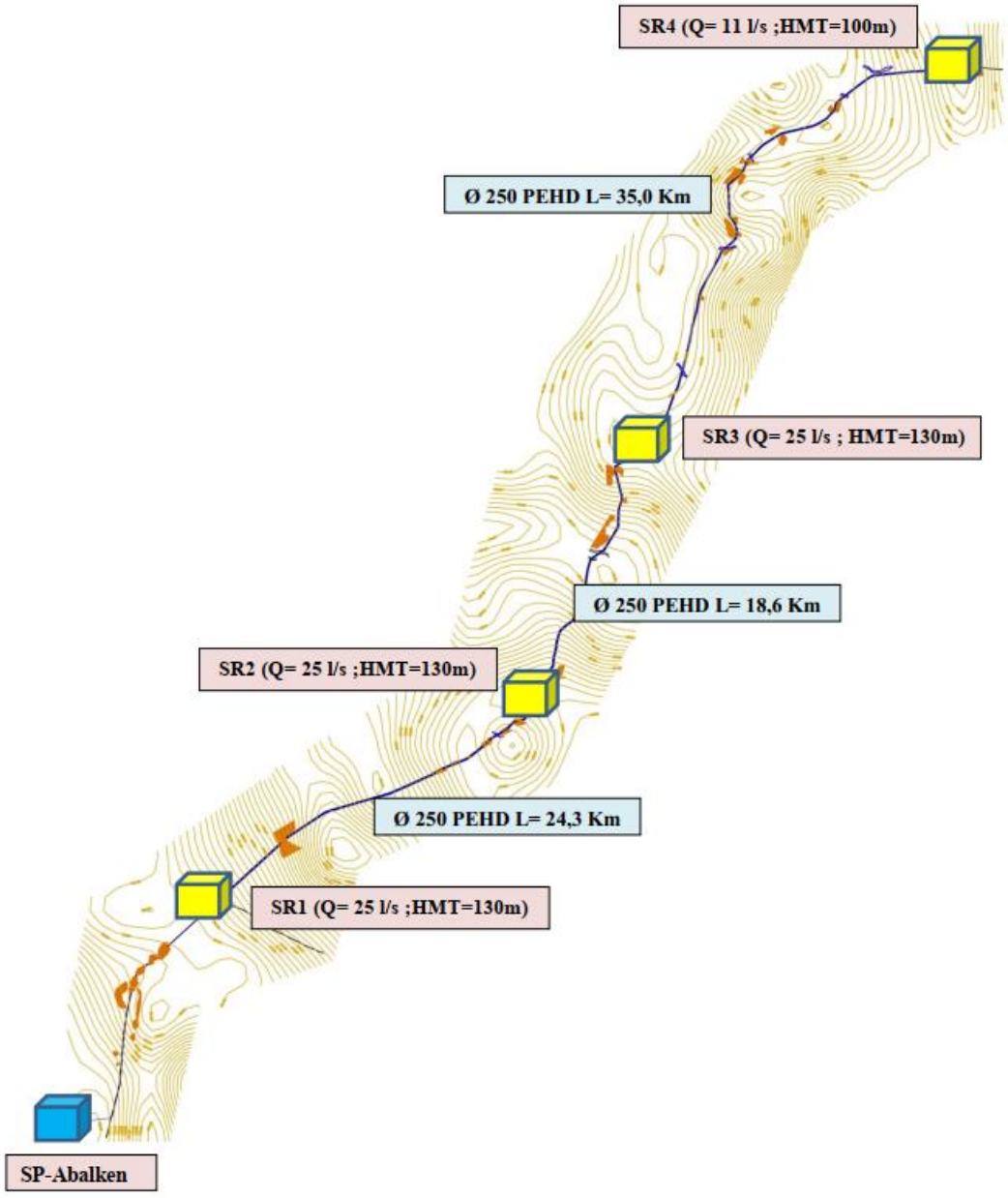

[Figure VI-6 Route Map of the Abalkan–Djebel Hadid Transmission Pipeline (SR1 to SR4)]

The studied system consists of the following principal components:

- Pipeline: Ductile Iron with an internal diameter of 251 responses to hydraulic transients. pipe types belong to pressure class PN16, rated for a nominal operating pressure of 16 bar, which defines the reference ceiling when evaluating the pressure envelope in the simulation results.

The route traverses varied terrain combining plateaus and elevated formations, producing significant elevation changes that enhance the potential for negative pressures and cavitation phenomena.

IV.1.2 Data and Assumptions

The model was constructed using data extracted from the project's technical study. Table 4-1 summarizes the principal geometric characteristics of the system.

Table 4-3 Geometric Characteristics of Segment SR2–SR3

Parameter	Value	Unit
Studied Segment	SR2 – SR3	
Total Length	18.635	km
Number of Pipes	40	pipe
Number of Nodes	38	node
Pipe Material	Ductile Iron	
Internal Diameter (DI)	251	mm
Internal Diameter (HDPE)	257.8	mm
Pressure Class	PN16	
Pump Type	Grundfos CR 95-6	
Nominal Flow Rate	25	L/s
Total Manometric Head (HMT)	140	m

The following simplifying assumptions were adopted:

- The pipeline is treated as a single continuous pipe of uniform diameter for each material separately.

- The initial simulation condition is assumed to be the full steady state (nominal flow rate of 25 L/s).

- Minor friction losses at fittings and bends are neglected given the pipe length relative to these elements.

- The reservoir at the end of the segment is treated as a fixed-pressure boundary condition.

IV.1.3 Steady-State Calibration

Prior to initiating transient simulations, the system's hydraulic integrity under steady-state conditions was verified using EPANET, by matching:

- The nominal flow rate (25 L/s) at all network nodes.

- The pressure distribution along the pipeline according to the Darcy–Weisbach equation. - The total hydraulic energy head consistent with HMT = 140 m.

The steady-state simulation results demonstrated sound and normal hydraulic operation of the system, confirming the validity of the entered data and establishing a reliable foundation for transitioning to dynamic simulation using HAMMER and AFT Impulse.

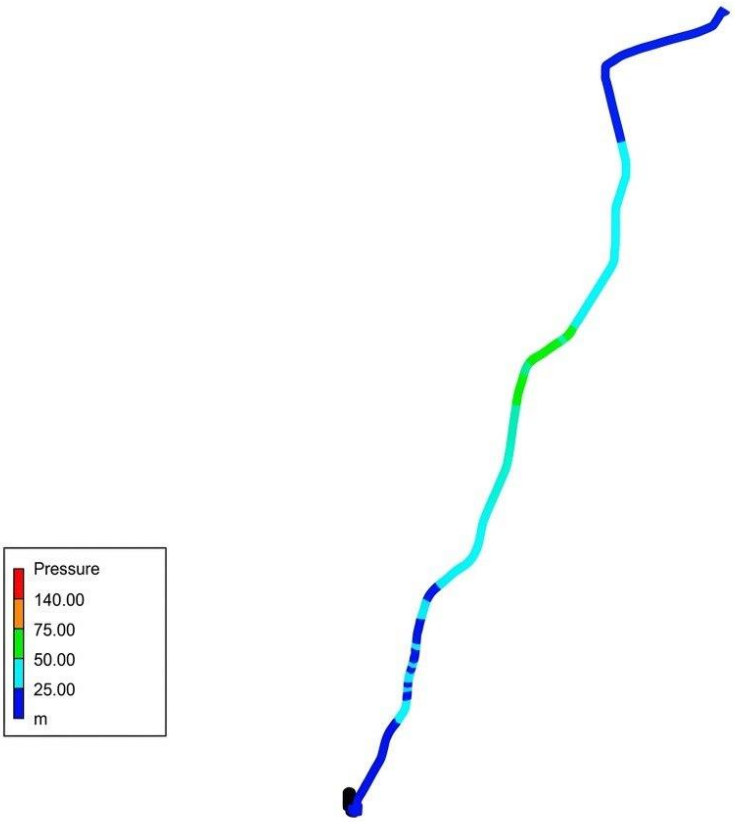

[Figure IV-7 Steady-State Pressure Distribution along the SR2–SR3 Pipeline]

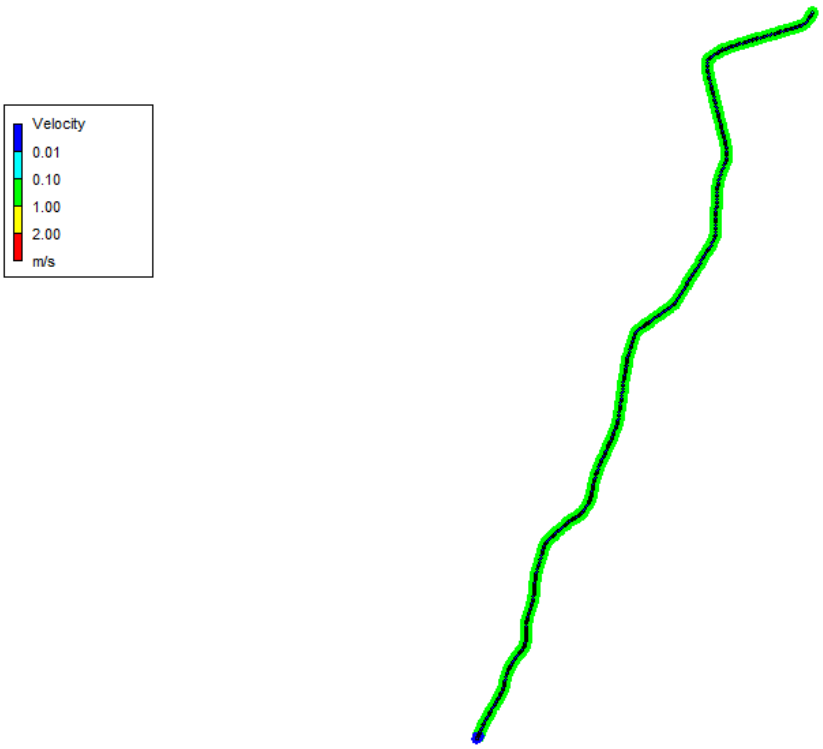

[Figure IV-8: Steady-State Velocity Distribution along the SR2–SR3 Pipeline SR2-SR3]

Table 4-4: Simulation Results at the Node Level (SR2–SR3)

	Altitude	Demande	Charge	Pression
ID	**m**	**LPS**	**m**	**m**
1	636.38	0	650.68	14.3
100	627.16	0	648.97	21.81
200	622.58	0	647.4	24.82
300	616.48	0	645.62	29.14
400	604.11	0	644.13	40.02
500	592.46	0	642.14	49.68
600	588.55	0	640.13	51.58
700	601.14	0	637.88	36.74
800	608.91	0	635.83	26.92
900	628.67	0	633.54	4.87
995	631.39	0	631.61	0.22
996	631.58	0	631.58	0

Table 4-5: Simulation Results at the Section Level (SR2–SR3)

N Amant	N aval	Longueur	Diamètre	Rugosité	Débit	Vitesse	Perte de Charge
		m	**mm**	**mm**	**LPS**	**m/s**	**m/km**
1	2	35	250	0.1	25	0.51	1.02
100	101	11.22	250	0.1	25	0.51	1.03
200	201	2	250	0.1	25	0.51	1.04
300	301	31.42	250	0.1	25	0.51	1.03
400	401	9.26	250	0.1	25	0.51	1.03
500	501	29.55	250	0.1	25	0.51	1.03
600	601	1.15	250	0.1	25	0.51	0.97
700	701	50	250	0.1	25	0.51	1.03
800	801	5.81	250	0.1	25	0.51	1.02
900	901	15.27	250	0.1	25	0.51	1.03
995	996	34.5	250	0.1	25	0.51	1.02

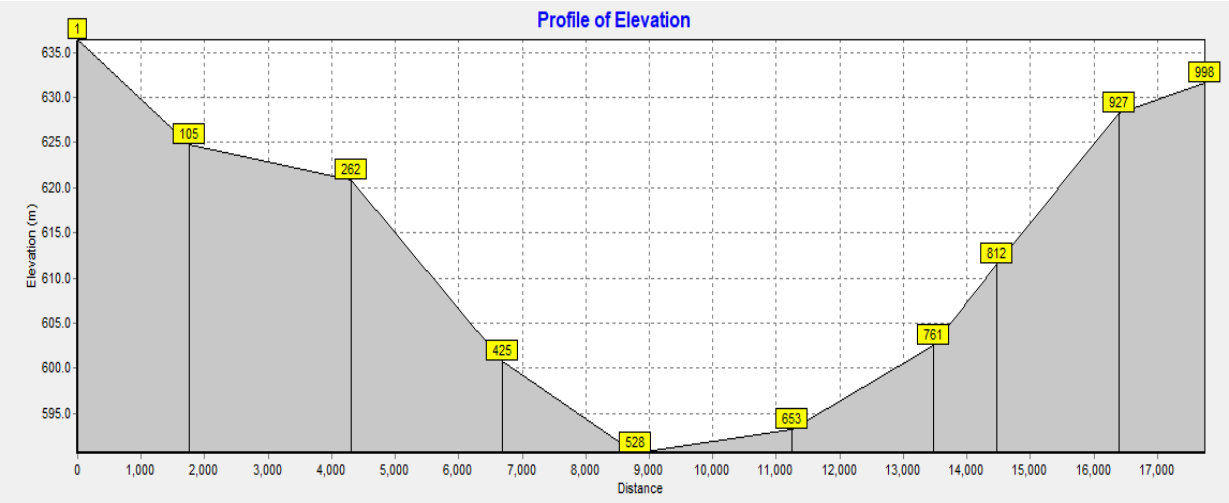

Figure IV-9 : Vertical Water Transfer Diagram (SR2–SR3) – Elevation Profiles

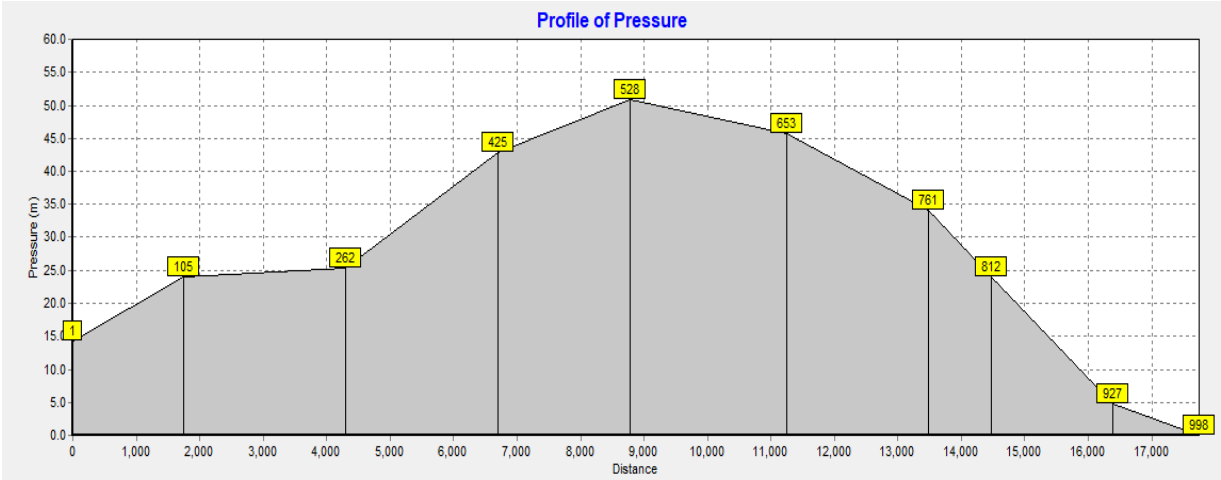

Figure IV-10 : Vertical Water Transfer Diagram (SR2–SR3) – Pressure Profiles

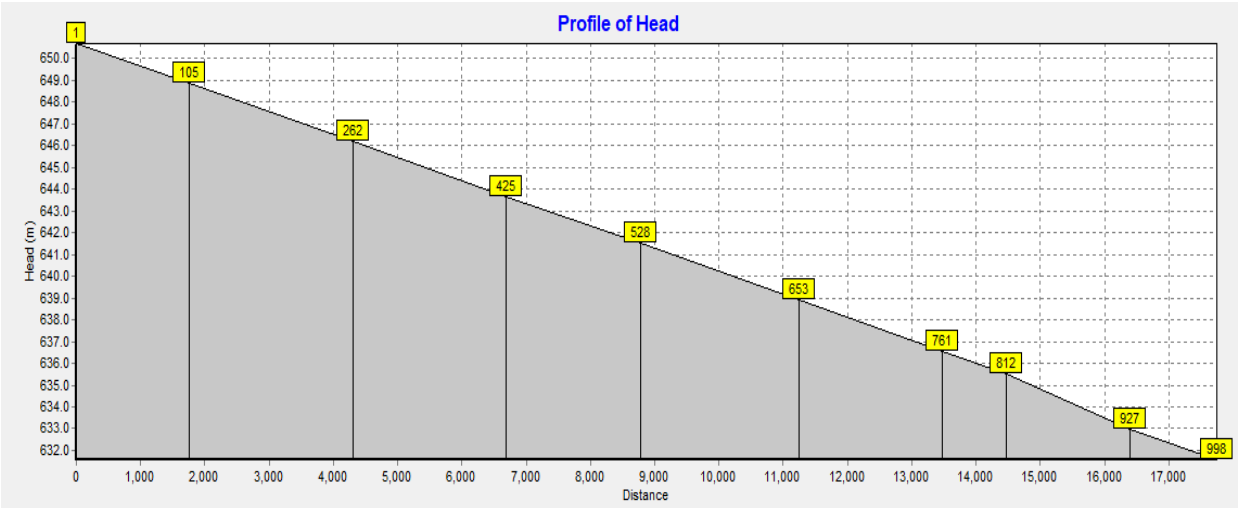

Figure IV-11 : Vertical Water Transfer Diagram (SR2–SR3) – Head Profiles

IV.2 Scenarios and Simulation Setup

IV.2.1 Scenario One Sudden Power Failure

This scenario simulates the instantaneous shutdown of the Grundfos CR 95-6 pump resulting from a sudden power outage one of the most common sources of water hammer in long-distance transmission systems. Upon sudden shutdown, the energy supplied to the fluid ceases instantaneously, generating a negative pressure wave that propagates from the pump toward the terminal reservoir, followed by a reflection that may produce surge pressures at certain points along the pipeline.

This scenario is simulated using both HAMMER and AFT Impulse for Ductile Iron pipe, covering both pre- and post-protection conditions, with the aim of assessing the degree of convergence between the two programs.

IV.2.3 Simulation Parameters

The following unified simulation parameters were adopted in both programs to ensure comparability:

Total simulation duration: 320 s

Time step: determined automatically according to the Courant condition (Courant ≤ 1)

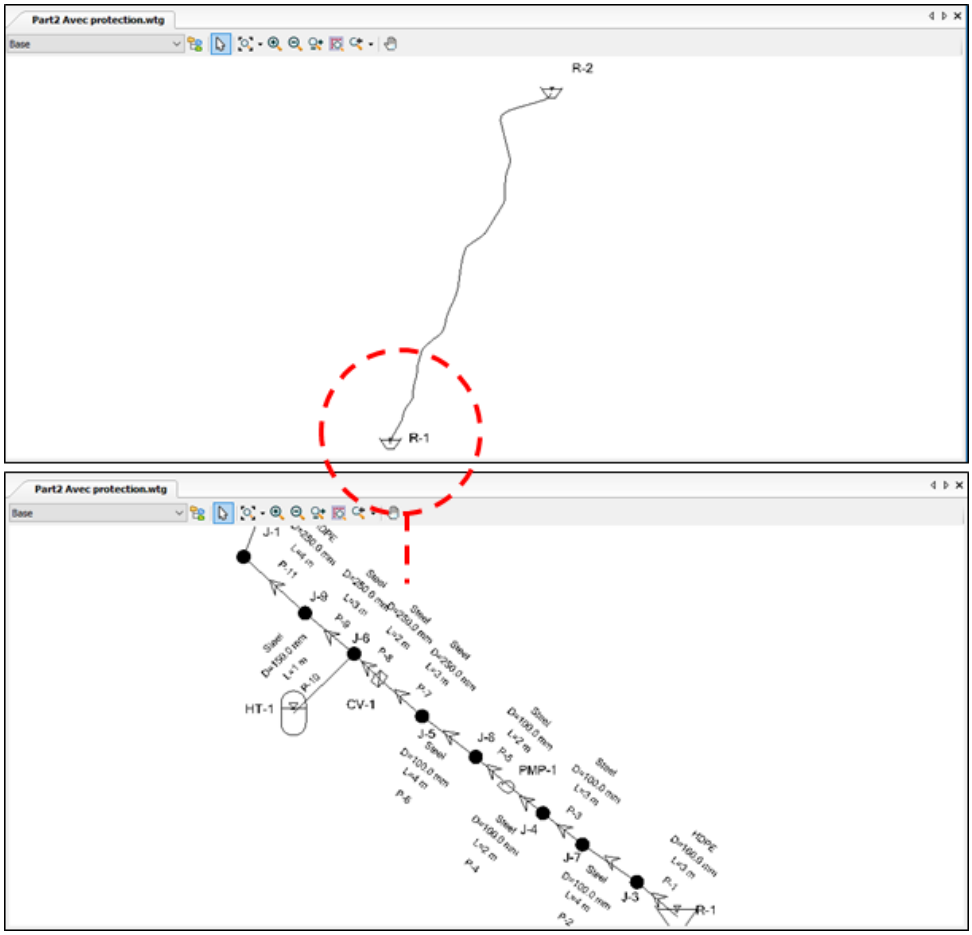

Figure IV-12 : Hydraulic Model Diagram in Bentley HAMMER (SR2–SR3)

IV.3 Results and Protection Device Evaluation

IV.3.1 Pre-Protection Results Pressure Envelopes and Critical Locations

Simulation results are presented prior to the addition of any protection device, with the aim of diagnosing critical locations and identifying the prevailing nature of the risk.

These results are obtained from both HAMMER and AFT Impulse for Ductile Iron pipe.

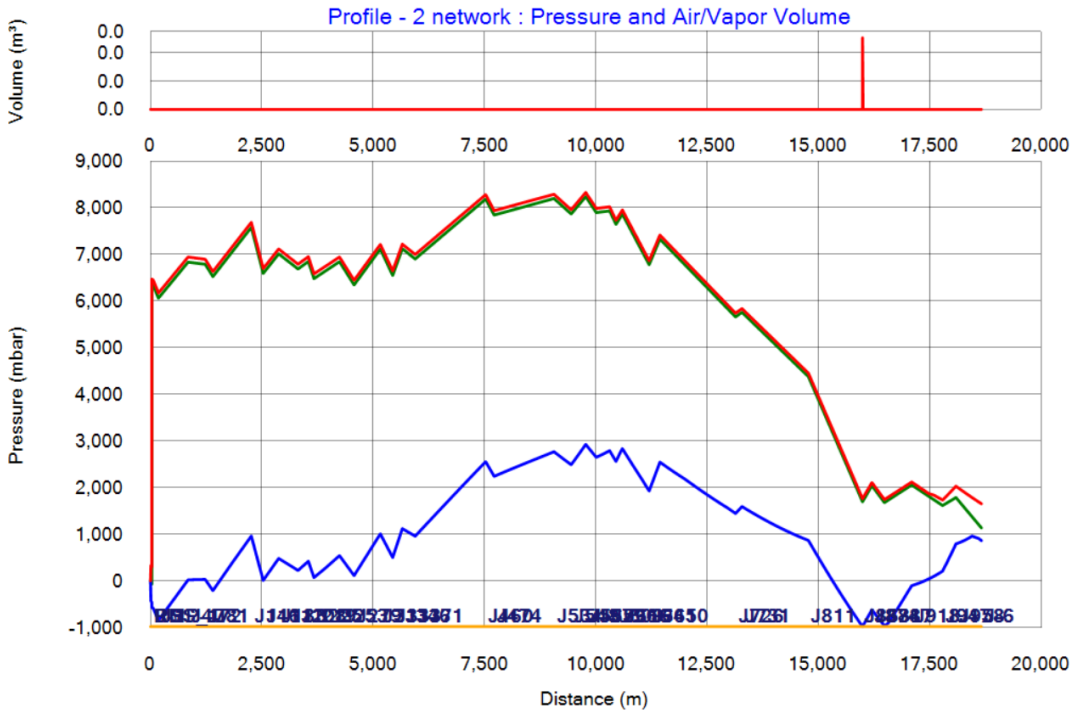

[Figure IV-13 Pressure Envelope Scenario 1 (Sudden Power Failure) — Ductile Iron — Pre-Protection —bently HAMMER]

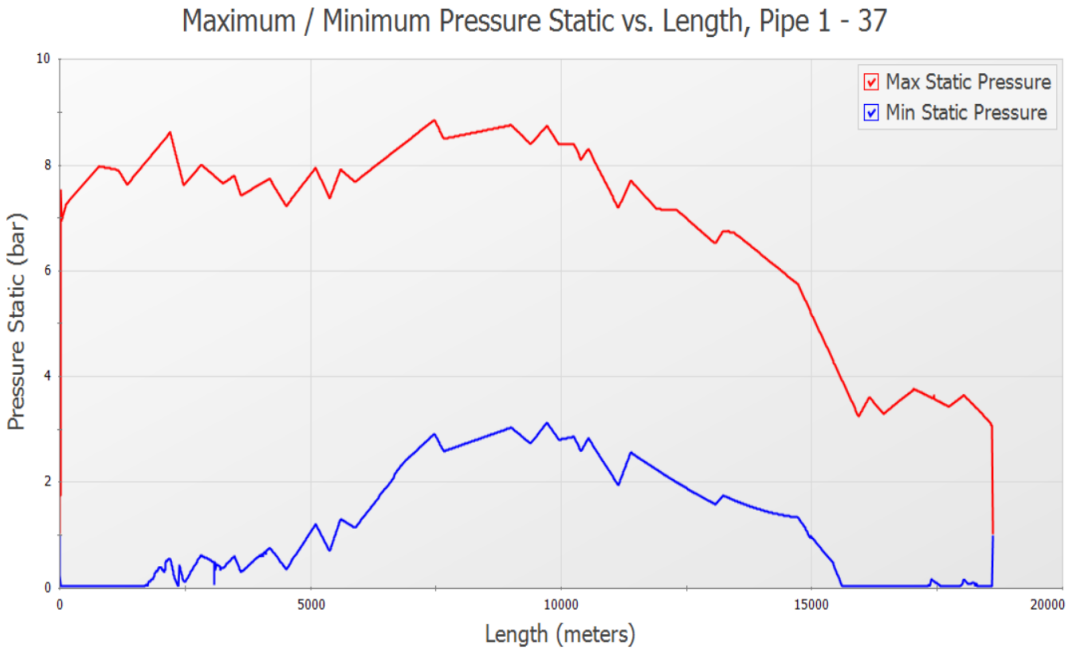

[Figure IV-14- Pressure Envelope — Scenario 1 (Sudden Power Failure) — Ductile Iron — Pre-Protection — AFT Impulse]

Hydraulic Model Inventory: Part2 Avec protection.wtg

Title	
Engineer	
Company	
Date	12/27/2023
Notes	

Scenario Summary

ID	1
Label	Base
Notes	
Active Topology	Base Active Topology
Physical	Base Physical
Demand	Base Demand
Initial Settings	Base Initial Settings
Operational	Base Operational
Age	Base Age
Constituent	Base Constituent
Trace	Base Trace
Fire Flow	Base Fire Flow
Energy Cost	Base Energy Cost
Transient	Base Transient
Pressure Dependent Demand	Base Pressure Dependent Demand
Failure History	Base Failure History
SCADA	Base SCADA
User Data Extensions	Base User Data Extensions
Steady State/EPS Solver Calculation Options	Base Calculation Options
Transient Solver Calculation Options	Base Calculation Options

Network Inventory

Pipes	1007	-Constant Speed - Four-Quadrant Characteristics	0
Laterals	0	-Constant Speed - Pump Definition	0
Junctions	1003	-Shut Down After Time Delay	1
Hydrants	0	-Variable Speed/Torque	0
Tanks	0	-Pump Start - Variable Speed/Torque	0
Reservoirs	2	Pump Stations	0
Customer Meters	0	Variable Speed Pump Batteries	0
Taps	0	PRV's	0
SCADA Elements	0	PSV's	0
Pumps	1	PBV's	0
-Constant Power	0	FCV's	0
-Custom Extended	0	TCV's	0
-Design Point (1 Point)	1	GPV's	0
-Multiple Point	0	Isolation Valves	0
-Standard (3 Point)	0	Spot Elevations	0
-Standard Extended	0		

Transient Network Inventory

Turbines	0	-Away from Wye	0
Periodic Head-Flows	0	Rupture Disks	0
Air Valves	0	Discharges to Atmosphere	0
Hydropneumatic Tanks	1	Orifices Between Pipes	0
Surge Valves	0	Valves With Linear Area Change	0
Check Valves	1	Surge Tanks	0
-Towards Wye	1		

Pressure Pipes Inventory

100.0 (mm)	14 m	250.0 (mm)	18,649 m
150.0 (mm)	1 m	All Diameters	18,667 m
160.0 (mm)	3 m		

IV.3.2 Protection Device Selection and Design

Based on the nature of the critical locations identified above particularly the negative pressures resulting from power failure air vessels (hydropneumatic tanks) are deemed the most appropriate protection device for this system,

for the following reasons:

- Their effectiveness in long pipelines with varying elevations.
- Their capacity to attenuate both positive and negative waves.
- Their suitability for remote areas where periodic maintenance is difficult, compared to alternatives such as surge tanks.

The vessel is positioned at the pumping station (upstream end) as the most effective location for intercepting the negative wave at its source.

Bladder hydropneumatic tank:

- Total volume V_T= 2 m³
- Air volume V_a= 0.8 m³
- Water volume V_w= 1.2 m³
- Pre-charge pressure P= 1 bar.

IV.3.3 Post-Protection Results

Simulations were repeated following the addition of the air vessel for both programs, and the pressure envelope before and after the intervention is compared. Results show the pressure envelope contained within the acceptable range [0 – PN16] across all combinations following the addition of the protection device.

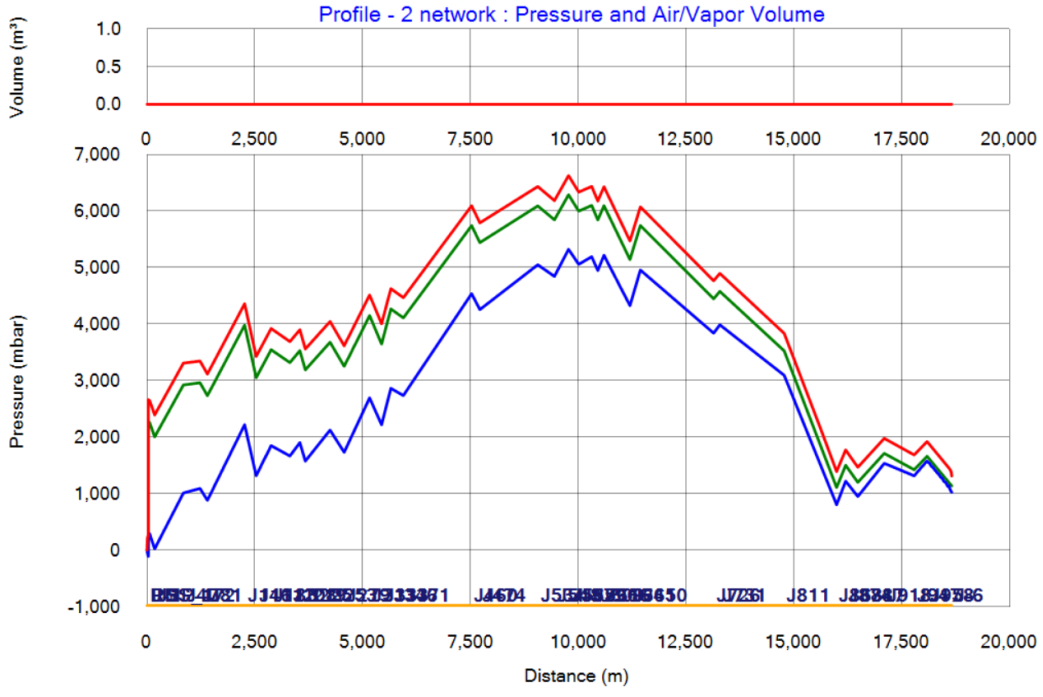

[Figure IV-15 Pressure Envelope Scenario 1 (Sudden Power Failure) — Ductile Iron — After-Protection — bently HAMMER]

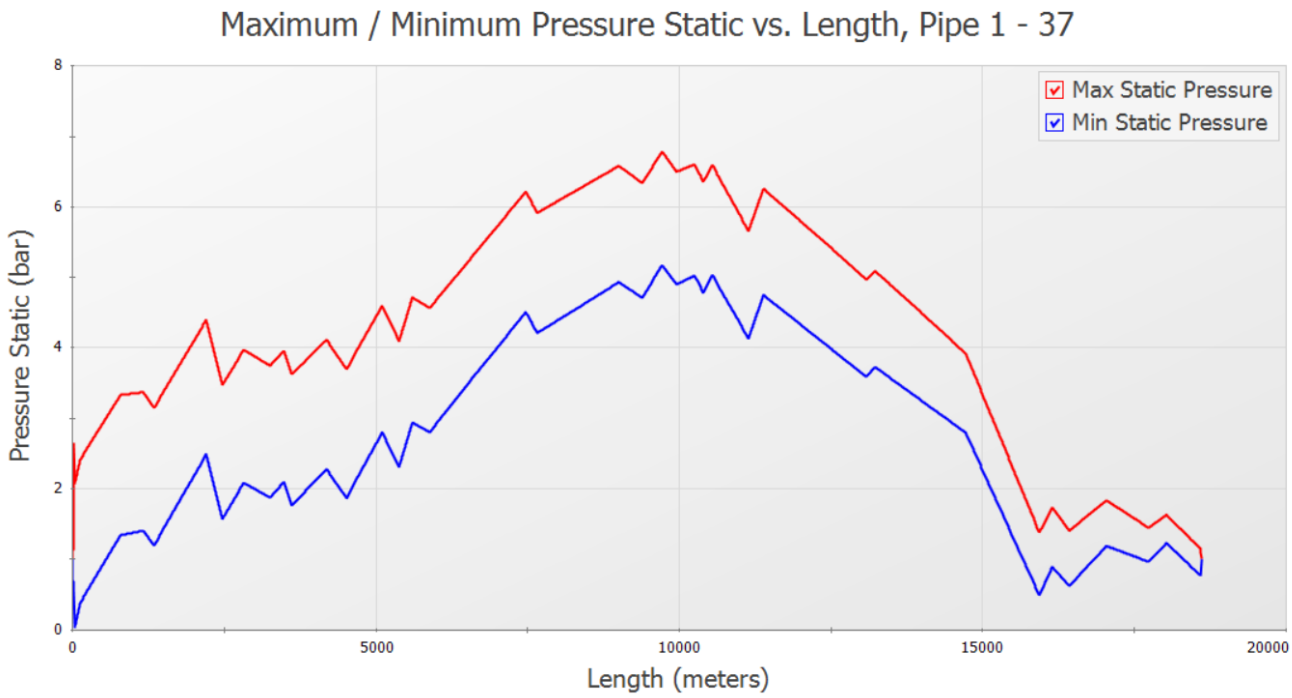

[Figure IV-16- Pressure Envelope — Scenario 1 (Sudden Power Failure) — Ductile Iron — Post-Protection — AFT Impulse]

IV.4 Comparison

This section presents a side-by-side comparison of the results obtained from HAMMER and AFT Impulse for Scenario One (sudden power failure) with Ductile Iron pipe, covering both pre- and post-protection conditions. The objective is to assess the degree of convergence between the two programs and to interpret any observed discrepancies.

IV.4.1 Maximum Pressure Peaks

Both programs produce comparable maximum transient pressures under pre-protection conditions, with HAMMER recording a global maximum of 8.33 bar and AFT Impulse recording 8.86 bar. The slight difference, amounting to approximately 6%, is attributable to differences in the internal time step and wave interpolation schemes adopted by each program, rather than a fundamental divergence in the underlying Method of Characteristics formulation used by both.
Following the addition of the air vessel, both programs confirm the effectiveness of the protection device: HAMMER records a post-protection maximum of 6.63 bar and AFT Impulse records 6.79 bar, both well within the PN16 pressure class ceiling of 16 bar.

IV.4.2 Minimum Pressure and Cavitation

The most notable difference between the two programs appears in the estimation of minimum pressures. Under pre-protection conditions, HAMMER reports minimum pressures reaching -0.98 bar at certain elevated nodes, while AFT Impulse constrains the minimum pressure to the vapor pressure threshold of 0.023 bar, activating its Discrete Vapor Cavity Model (DVCM) at multiple pipe stations. Both observations are physically consistent: they indicate the occurrence of cavitation at elevated points along the pipeline, but each program treats sub-vapor pressures differently by convention.
Post-protection results show significant improvement in both programs. HAMMER records a

minimum of 0.023 bar, while AFT Impulse records the same vapor pressure threshold locally at the pump station only, with minimal vapor volume, indicating that the air vessel has effectively suppressed the propagation of negative waves across the pipeline.

IV.4.3 Recommendations and Conclusions

The results of the inter-program comparison lead to the following conclusions: Regarding convergence, both HAMMER and AFT Impulse demonstrate satisfactory agreement in estimating maximum transient pressures, with a relative difference not exceeding 6% under pre-protection conditions and 2.4% under post-protection conditions. This level of convergence is consistent with what is expected from two programs sharing the same Method of Characteristics foundation, and confirms the reliability of the simulation results regardless of the program used. Regarding minimum pressures, the observed difference in negative pressure estimation reflects a fundamental difference in the friction model adopted by each program: HAMMER employs an unsteady friction model (Instantaneous Acceleration-Based, IAB) that attenuates wave energy more rapidly, while AFT Impulse adopts a quasi-steady friction model that retains higher wave energy, resulting in deeper negative pressure estimates. This is consistent with the findings of Wéber and Hős (2021), who established that discrepancies between the two friction models are more pronounced in negative waves than in positive ones.
Regarding protection effectiveness, both programs confirm that the air vessel installed at the pumping station successfully restores the pressure envelope to within the acceptable operational range, with maximum pressures remaining well below the PN16 ceiling and minimum pressures maintained above the cavitation threshold across the pipeline.

IV.5 Supplementary Case: Closed-End Boundary Condition

In transient hydraulic analysis, the choice of boundary condition at the terminal end of a pipeline is not a mere modelling formality it fundamentally governs the nature of pressure wave reflections and, consequently, the severity of the transient event. Throughout the comparative analysis presented in Section 4.4, the terminal reservoir with a fixed pressure head was adopted as the boundary condition. This choice was deliberate: it represents the most favorable operating configuration and is fully supported by both HAMMER and AFT Impulse, thereby ensuring a valid and meaningful inter-program comparison. However, it does not represent the most critical condition that a hydraulic engineer must consider in practice.
The closed-end boundary condition in which the terminal end of the pipeline is sealed with no outflow represents the worst-case configuration from a transient perspective. When a pressure wave reaches a closed end, it reflects entirely without any energy dissipation at the boundary, theoretically doubling the wave amplitude at the point of reflection. In contrast, a reservoir boundary partially absorbs the incoming wave by maintaining a fixed pressure head, thereby attenuating the reflected wave. This fundamental difference in wave reflection behavior makes the closed-end condition the reference scenario for any conservative hydraulic protection design. From a professional standpoint, simulating the closed-end condition is therefore not an optional refinement but an engineering obligation: it defines the upper bound of transient severity that the protection system must be capable of handling. Accordingly, all combinations of Scenario One were simulated under the closed-end boundary condition using HAMMER, covering both pipe materials Ductile Iron and HDPE and both pre- and post-protection states.
AFT Impulse, however, could not complete the post-protection simulations under this boundary condition. The program successfully executed the pre-protection cases but encountered convergence

limitations in the post-protection configurations, which precluded a full inter-program comparison in this setting. This limitation was the primary motivation for redirecting the comparative analysis toward the fixed-head reservoir condition, where both programs operate without restriction, as detailed in Section 4.4. The results obtained under the closed-end condition using HAMMER are therefore presented here as a supplementary reference, illustrating the upper bound of transient severity for this system and contextualizing the conservative basis upon which the protection design was established.

The results confirm that the closed-end condition produces significantly higher maximum pressures and more severe negative pressure troughs than the reservoir condition across both materials, reinforcing the conservative nature of the protection design adopted in this study. The air vessel sized and validated under the reservoir condition therefore provides a minimum protection baseline; a complete protection design addressing the closed-end scenario would require either re-sizing of the vessel or supplementary protective measures, and is identified as a direction for future investigation.

Conclusion

This chapter presented the practical application of a comparative hydraulic transient analysis through a real case study represented by the intermediate segment SR2–SR3 of the water transmission pipeline between Abalkan and Djebel Hadid, approximately 18.6 km in length, using Ductile Iron pipe classified under pressure class PN16.

The computational model was constructed in both HAMMER and AFT Impulse, and its steady-state convergence was verified using EPANET before proceeding to dynamic simulation. Scenario One sudden power failure at the pump was selected as the basis for the analysis, representing one of the most common and critical sources of water hammer in long-distance transmission systems. Pre-protection results revealed critical locations where minimum pressures drop to the cavitation threshold, particularly at elevated points along the pipeline profile. Based on these findings, an air vessel installed at the pumping station was selected as the most appropriate protection device, given its effectiveness in attenuating both positive and negative pressure waves in long pipelines with variable topography.

Post-protection simulations confirmed the effectiveness of the air vessel in restoring the pressure envelope to within the acceptable operational range in both programs, with maximum pressures remaining well below the PN16 ceiling and minimum pressures maintained above the cavitation threshold across the pipeline.

The inter-program comparison, conducted under the fixed-head reservoir boundary condition the configuration fully supported by both programs revealed satisfactory convergence in the estimation of maximum transient pressures, with a relative difference not exceeding 6%. The observed discrepancy in minimum pressure estimation was attributed to the difference in friction models adopted by each program, consistent with the findings reported in the literature.

Finally, the closed-end boundary condition was examined as a supplementary case, representing the worst-case transient scenario from a design perspective. Results obtained using HAMMER confirmed that this configuration produces significantly more severe pressure transients than the reservoir condition, establishing the upper bound of transient severity for this system and identifying the complete treatment of this scenario as a direction for future investigation.

Conclusions & Recommendations



Conclusions & Recommendations

This part presents the conclusions drawn from the comparative hydraulic transient analysis conducted in Chapter Four, along with practical recommendations addressed to both engineers and researchers working in the field of water hammer simulation and surge protection. The findings are grounded in the simulation results obtained through HAMMER and AFT Impulse, and informed by the practical experience accumulated throughout the execution of this study. The chapter is organized across three thematic areas: the water hammer phenomenon as observed in the studied segment, the selection and design of surge protection measures, and the comparative assessment of the two simulation tools.

Summary of Achievements

This study conducted a systematic comparative analysis of two hydraulic transient simulation programs HAMMER and AFT Impulse applied to a real long-distance water transmission pipeline in the Alhaggar region of southern Algeria. The work was organized across three main components.

The theoretical framework, developed in Chapter Two, established the physical and mathematical foundations of the water hammer phenomenon, covering the governing equations, wave celerity, cavitation mechanisms, and the Method of Characteristics as the common numerical basis shared by both programs.

The software analysis, presented in Chapter Three, provided a structured comparison of the two programs in terms of their architecture, modeling capabilities, friction models, and domain of application laying the groundwork for interpreting the differences observed in the simulation results.

The field application, detailed in Chapter Four, applied both programs to the SR2–SR3 pipeline segment under Scenario One sudden pump power failure using Ductile Iron pipe under both pre- and post-protection conditions, with a supplementary analysis conducted under the closed-end boundary condition using HAMMER.

Main Conclusions

Conclusions Related to the Water Hammer Phenomenon in the Studied Segment

The simulation results confirm that the topographic profile of the pipeline is the primary factor governing both the nature and severity of water hammer. The SR2–SR3 segment, characterized by significant elevation changes over an 18.6 km course, exhibited exclusively negative pressure transients under the power failure scenario, with no positive pressure peaks exceeding the PN16 ceiling recorded prior to protection. This behavior indicates that the dominant risk in this system is cavitation rather than overpressure, and that critical locations are concentrated at topographic high points along the profile.

This finding reinforces a fundamental principle in hydraulic transient engineering: two pipelines operating under identical hydraulic conditions may exhibit entirely different transient behaviors if their elevation profiles differ. The protection strategy must therefore be derived from site-specific simulation results rather than generic guidelines.

Conclusions Related to Surge Protection

The results demonstrate that a single air vessel installed at the pumping station proved sufficient to restore the pressure envelope to within the acceptable operational range for the SR2–SR3 segment under the fixed-head reservoir boundary condition. This outcome, however, is a direct consequence of the specific hydraulic and topographic characteristics of this segment and should not be generalized.

The supplementary analysis conducted under the closed-end boundary condition revealed that more severe transient conditions demand a combination of protective measures: an air vessel at the pumping station, air release valves at critical high points, and a controlled valve closure time. This multi-device approach combining active protection elements such as air vessels and air release valves with passive measures such as controlled valve closure timing proved necessary to achieve full pressure envelope containment under worst-case conditions.

This observation leads to a practical conclusion: in pipelines with multiple high points, significant elevation changes, or high flow velocities, a single protection device rarely provides complete coverage. The appropriate protection strategy must always be derived from the pre-protection transient simulation results and tailored to the specific characteristics of the system.

Conclusions Related to the Comparison Between HAMMER and AFT Impulse

Table V.1 — Comprehensive Comparative Assessment: Bentley HAMMER vs. AFT Impulse

Parameter / Criterion	Bentley HAMMER	AFT Impulse	Notes / Difference
Core numerical method	MOC — fixed-grid explicit	MOC — fixed-grid explicit	Identical
Friction model	Brunone–Vítkovský IAB (unsteady acceleration-based)	Quasi-Steady (Darcy–Weisbach extended)	Fundamental difference
Wave attenuation accuracy	Higher — IAB damps oscillations more realistically in long pipes	Conservative — retains higher wave energy across cycles	Diverges with pipe length and Re number
Cavitation model	DVCM (Discrete Vapor Cavity Model)	DVCM (Discrete Vapor Cavity Model)	Identical
Fluid-Structure Interaction (FSI)	Not included — uncoupled model (justified for buried pipelines)	Not included — uncoupled model	Identical assumption
CFL stability criterion	$\Delta t = \Delta x / a$ (Courant ≤ 1) ±15 % celerity rounding allowed	CFL ≤ 1 — stricter internal time-step enforcement	Similar — minor implementation difference
Learning curve	Gentle — suitable for beginners and non-specialist engineers	Steep — requires dedicated specialist training	Major difference

Parameter / Criterion	Bentley HAMMER	AFT Impulse	Notes / Difference
Computation speed	Fast — low internal overhead	Slow — high internal discretization demand	Major difference
Hardware requirements	Mid-high	High	Major difference
Fluid library	Water-focused	Extensive — water, chemicals, gases, steam, non-Newtonian	AFT Impulse advantage (irrelevant for water projects)
Ecosystem integration	Native — WaterCAD, WaterGEMS, EPANET, AutoCAD	Standalone (companion: AFT Fathom only)	HAMMER advantage
GIS and reporting	Full GIS via Bentley platform; pressure envelopes, wave animation	Tabular reports only; no native GIS integration	HAMMER advantage
Input strictness	Tolerant — flexible boundary condition handling	Rigid — strict input requirements; errors can block simulation entirely	Operational risk for AFT
Protection device library	Air vessel, surge tank, PRV, air inlet valve, VFD	Air vessel, PRV, check valve, rupture disc	HAMMER broader for water systems
Primary user base	Water utilities and municipal engineers worldwide	Industrial and process engineers	Different target sectors
Municipal water supply networks	Optimal	Acceptable	HAMMER preferred
Long-distance transmission pipelines	Optimal	Acceptable	HAMMER preferred
Industrial pipeline systems	Acceptable	Optimal	AFT Impulse preferred
Chemical / petrochemical plants	Not recommended	Optimal	AFT Impulse only
Nuclear facility cooling systems	Not recommended	Optimal	AFT Impulse only
Academic training — beginner level	Strongly recommended	Not recommended	HAMMER only
Research requiring high wave attenuation accuracy	Preferred — IAB model better validated in literature	Conservative baseline may overestimate oscillations	HAMMER preferred

The comparative analysis yields a practical and nuanced assessment of both programs.

In terms of numerical accuracy, both programs demonstrated equivalent performance in estimating maximum transient pressures, with a relative difference not exceeding 6 under pre-protection conditions and 2.4 of convergence confirms the reliability of the Method of Characteristics as implemented in both tools and establishes that either program is numerically adequate for water hammer analysis in water network applications.

The more significant finding, however, lies in the operational domain. HAMMER offers seamless integration with WaterCAD, WaterGEMS, EPANET, and AutoCAD, eliminating redundant data entry between steady-state and transient analyses. It is computationally fast, places minimal demands on hardware resources, and is accessible to engineers without specialized transient analysis expertise. These characteristics make it the natural choice for water supply and distribution network projects.

AFT Impulse, by contrast, offers higher internal discretization precision and a significantly richer fluid library. However, in the context of water network projects, these advantages become liabilities: the program's strict input requirements and detailed modelling approach consume considerably more computation time and hardware resources than the problem demands, and its stricter boundary condition handling can restrict or block the simulation entirely under certain configurations as was observed in this study. When the precision offered by AFT Impulse is not required by the nature of the project, its operational constraints represent a net disadvantage.

The central conclusion of this comparison is therefore the following: for water supply and distribution network projects, HAMMER is the more efficient, accessible, and practical tool, with a level of accuracy that is fully adequate for this domain. AFT Impulse's capabilities are better suited to industrial pipeline systems involving non-water fluids or high-precision process requirements, where its additional investment in time and expertise is justified.

Limitations of the Study

The present study is subject to three limitations that should be acknowledged in the interest of scientific transparency:

1. The inter-program comparison was confined to a single scenario sudden pump power failure with a single pipe material Ductile Iron under the fixed-head reservoir boundary condition. This configuration was deliberately selected as the common ground fully supported by both programs, but it represents only a subset of the full simulation matrix originally envisaged.

2. The protection design was validated under the fixed-head reservoir boundary condition only. The closed-end boundary condition, representing the worst-case transient scenario for this system, was simulated exclusively using HAMMER. The adequacy of the current air vessel sizing under this condition has therefore not been fully established.

3. The study is based on a single pipeline segment. The conclusions drawn regarding program performance and protection strategy selection reflect the specific characteristics of the SR2–SR3 segment and should be validated against additional case studies before being generalized.

Recommendations and Research Perspectives

Operational and Engineering Recommendations

Regarding simulation tool selection:

- For water supply and distribution network projects, HAMMER is recommended as the primary simulation tool. Its integration with the Bentley engineering ecosystem, computational efficiency, and accessibility to non-specialist users make it the most practical choice for this domain, with a level of accuracy that is fully adequate for water hammer analysis in water network applications.

- For industrial pipeline systems involving non-water fluids, complex equipment configurations, or high-precision process requirements, AFT Impulse is the more appropriate tool. Its extensive fluid library and rigorous modelling approach make it well-suited to applications where the additional investment in computation time and user expertise is justified by the complexity of the system.

- For engineers at the early stages of their training in hydraulic transient analysis, HAMMER is strongly recommended as the entry point, given its intuitive interface and forgiving approach to boundary condition definition.

Regarding protection design:

- Engineers are advised against relying on a single protection device as a universal solution. The appropriate protection strategy must always be derived from pre-protection transient simulation results and tailored to the specific topographic and hydraulic characteristics of the system.

- In pipelines with multiple high points, significant elevation changes, or high flow velocities, a combination of active protection measures such as air vessels and air release valves with passive measures such as controlled valve closure timing should be considered as the baseline design approach.

Recommendations for Future Research

Two directions are identified as priorities for future research:

1. The boundary condition handling behavior of both programs warrants dedicated investigation. The technical limitations encountered with AFT Impulse under the closed-end boundary condition in this study represent an underexplored area in the published literature, and a systematic analysis of how both programs respond to different boundary configurations would contribute meaningfully to the field.

2. The comparative framework established in this study should be extended to additional pipe materials particularly HDPE and to additional scenarios, once the boundary condition limitations are better understood. A dedicated inter-program comparison covering a wider simulation matrix would provide a more complete basis for tool selection guidance in hydraulic transient analysis.

GENERAL CONCLUSION

Water hammer remains one of the most critical challenges in the design and operation of long-distance pressurized pipeline systems. This study addressed this challenge through a dual objective: a systematic comparative analysis of HAMMER and AFT Impulse as hydraulic transient simulation tools, and the application of this comparative framework to a real engineering case study in the Alhaggar region of southern Algeria.

The field application demonstrated that the SR2–SR3 segment is exclusively susceptible to negative pressure transients under the power failure scenario, owing to its varied topographic profile. A single air vessel installed at the pumping station proved sufficient to restore the pressure envelope to within safe operational limits, confirming both the adequacy of the protection design and the convergence of the two simulation tools under these conditions.

The inter-program comparison established a maximum relative difference of 6 pressure estimation a margin that is negligible for practical engineering purposes. The more significant finding lies in the operational domain: HAMMER's integration, computational efficiency, and accessibility establish it as the more practical tool for water network applications, while AFT Impulse's precision and fluid library depth position it as the preferred choice for complex industrial systems. Crucially, the study demonstrated that the advantages of AFT Impulse can become operational liabilities in water network projects, where its strict input requirements and heavy computational demands are disproportionate to the nature of the problem.

The supplementary analysis under the closed-end boundary condition established the upper bound of transient severity for this system and confirmed that single-device protection strategies are insufficient under worst-case conditions reinforcing the principle that surge protection design is inherently site-specific.

The findings of this study offer practical guidance for engineers selecting between HAMMER and AFT Impulse, and identify boundary condition behavior as a critical and underexplored dimension of inter-program comparison that warrants dedicated future investigation.

Bibliographical References

[1] Ghidaoui, M.S., Zhao, M., McInnis, D.A. and Axworthy, D.H. (2005). A review of water hammer theory and practice. *Applied Mechanics Reviews*, ASME, 58(1), pp. 49–76.

[2] Tijsseling, A.S. and Anderson, A. (2007). Johannes von Kries and the history of water hammer. *Journal of Hydraulic Engineering*, ASCE, 133(1), pp. 1–8.

[3] Bergant, A., Simpson, A.R. and Tijsseling, A.S. (2006). Water hammer with column separation: a historical review. *Journal of Fluids and Structures*, 22(2), pp. 135–171.

[4] Wylie, E.B. and Streeter, V.L. (1993). *Fluid Transients in Systems*. Prentice-Hall, Englewood Cliffs, NJ.

[5] Urbanowicz, K., Stosiak, M., Towarnicki, K. and Bergant, A. (2021). An overview of the numerical approaches to water hammer modelling: the ongoing quest for practical and accurate numerical approaches. *Water*, MDPI, 13(11), 1597.

[6] Chaudhry, M.H. (2014). *Applied Hydraulic Transients*, 3rd ed. Springer, New York.

[7] Boulos, P.F., Karney, B.W., Wood, D.J. and Lingireddy, S. (2005). Hydraulic transient guidelines for protecting water distribution systems. *Journal AWWA*, 97(5), pp. 111–124.

[8] Wéber, R. and Hős, C. (2021). Analysis of unsteady friction models used in engineering software for water hammer analysis: implementation case in WANDA. *Water*, MDPI, 13(4), 495.

[9] Gasiaa, F.S. (2009). *Pressure Transient in Networks, Simulation and Analysis*. M.Sc. Thesis, Al-Fateh University, Tripoli, Libya.

[10] Vargas, L. et al. (2025). Water hammer mitigation using hydro-pneumatic tanks: a multi-criteria evaluation of simulation tools and machine learning modelling. *Water*, MDPI, 17(13), 1883

[12] Toumi, S. and Remini, B. (2024). Numerical modeling and simulation of water hammer phenomena using the MacCormack method. *Water Practice and Technology*, IWA, 19(6), pp. 2333–2350.

[13] Zhang, X. et al. (2024). Water hammer in pipelines based on different friction models. *Scientific Reports*, 14, Article 51409. https://doi.org/10.1038/s41598-024-51409-9

[14] Urbanowicz, K., Bergant, A., Stosiak, M., Deptuła, A., Karpenko, M., Kubrak, M. and Kodura, A. (2022). Water hammer simulation using simplified convolution-based unsteady friction model. *Water*, MDPI, 14(19), 3151. https://doi.org/10.3390/w14193151

[15] Neyestanaki, M.K. et al. (2024). Unveiling the impact of pipe materials on water hammer in pressure pipelines: an experimental and numerical study. *Scientific Reports*, 14, Article 30599. https://doi.org/10.1038/s41598-024-80853-w

[16] Meniconi, S. et al. (2024). Mapping pressure surge source in urban water networks: integrating low- and high-frequency pressure data with an illustrative real case study. *Water Resources Research*, 60, e2023WR036773. https://doi.org/10.1029/2023WR036773

[17] Tang, Y. et al. (2024). Analysis of the effectiveness of water hammer protection programs for complex long-distance and high-head water supply projects. *Water*, MDPI, 16(11), 1582. https://doi.org/10.3390/w16111582

[18] Bakhshipour, A.E. et al. (2025). Leak detection in water supply networks using inverse transient analysis in time and frequency domain: a comparative investigation. *Frontiers in Water*, 7, 1661148. https://doi.org/10.3389/frwa.2025.1661148
[19] Yan, H. et al. (2025). A hybrid model coupling data and hydraulic transient laws for water distribution systems. *Water Resources Research*, 61, e2023WR036641. https://doi.org/10.1029/2023WR036641